UNLIMITED

RSRE
MEMORANDUM No. 4083

ROYAL SIGNALS & RADAR ESTABLISHMENT

A MONTE CARLO PERFORMANCE ANALYSIS OF ACCELERATED SVD-BASED HIGH DISCRIMINATION ALGORITHMS

Author: J L Mather

PROCUREMENT EXECUTIVE,
MINISTRY OF DEFENCE,
R S R E MALVERN,
WORCS.

RSRE MEMORANDUM No. 4083

UNLIMITED

ROYAL SIGNALS AND RADAR ESTABLISHMENT

Memorandum 4083

TITLE: A MONTE CARLO PERFORMANCE ANALYSIS OF ACCELERATED SVD-BASED HIGH DISCRIMINATION ALGORITHMS

AUTHOR: J L Mather

DATE: July 1988

SUMMARY

High discrimination algorithms are increasingly being considered for the task of processing data from arrays of sensors and in the form of time series. Many such algorithms rely on singular value decomposition of a data matrix or eigen analysis of the corresponding covariance estimate, thereby imposing a heavy computational requirement. However, if the data is oversampled, or if the solution vector may be constrained, in terms of its angular extent or frequency range for example, it is often possible to pre-process the data matrix in such a way as to reduce its size. This may be carried out by means of a fixed matrix pre-multiplication, and can lead to a substantial acceleration of the subsequent analysis. The method is described, and its use exemplified in combination with a number of well-known high discrimination algorithms. A number of results from a Monte Carlo analysis are given which show that the new technique can lead to significantly improved parameter estimates being obtained from the high discrimination algorithms.

CONTENTS

1. INTRODUCTION

There is currently a substantial and growing interest in high discrimination (or high "resolution") algorithms for processing the data collected from arrays of sensors and in the form of time series. Particular attention has been devoted to algorithms employing singular value decomposition (svd) of a data matrix, or equivalently, eigenvector decomposition of the estimated covariance matrix [1]. It is thought that such algorithms hold great potential for the interpretation of signals collected in radar and sonar phased array systems, since, under suitable conditions, they are able to locate multiple independent sources of signal within the conventional correlation filter beamwidth limitations.

However, such algorithms have serious shortcomings which must be dealt with before their full potential for high discrimination may be realised in practical systems. Principal among these is the huge data processing burden imposed by the singular value decomposition or eigen analysis in problems of realistic size.

In order to tackle the requirement to process data quickly, whilst using inherently computer intensive algorithms, attempts have been made to increase the available processing rate through the design of parallel svd and eigen decomposition algorithms and special purpose systolic processing architectures [2]. Under some special conditions, it is possible to reduce the dimension of the data matrix by employing the spatial averaging or sub-aperture technique [1], more commonly encountered as a pre-processing stage if coherent multipath is suspected [3]. Methods have also been described [4,5] by which the processing requirement of multi-domain data may be reduced below that of naive extensions of previously available algorithms. One of these [5] makes use of the sub-aperture technique to pre-process domains of the data subsequent to the first (for example, to process time domain data, following a spatial analysis), and could be carried out still more rapidly by processing multiple channels of sub-aperture data in parallel.

In general, the approaches referred to above make use of additional prior knowledge about the form of the problem in order to provide a suitable framework for the subsequent straightforward use of the normal singular and eigen vector based algorithms. Following an introduction to our data model in section 2, and a review of traditional methods of analysis in section 3, we give details of a further novel stage of pre-processing, in section 4, which reduces the size of the data matrix. It does this by making use of prior knowledge concerning the degree of oversampling of the data, or the boundaries of the required solution. The reduction is achieved in such a way that the maximum practical number of signals may still be detected, given some knowledge of the signal to noise ratio. Section 4.2 describes the application of the new technique, which we refer to as an eigenvector projection method (EPM), to a number of well-known high discrimination algorithms, such as MUSIC [6,18]. Section 4.3 is a more detailed discussion of the effect of EPM pre-processing. Section 5 presents examples of our computer simulations, and, in particular, discusses typical results from a Monte Carlo analysis of the performance of the EPM modified algorithms. A larger number of Monte Carlo results are collated for reference in the Appendices, together with some discussion regarding their consistency and the possibility of a more economical representation of such data.

2. THE DATA MODEL

The usual data model employed [1] is as follows

$$\underline{d}(t) = \mathbf{M}\,\underline{f}(t) + \underline{w}(t) \qquad (1)$$

where $\underline{f}(t)$ is a vector representing the input which is to be reconstructed, $\mathbf{M}$ is a linear transformation matrix, $\underline{w}(t)$ is a vector sample of zero mean Gaussian white noise, and

$\underline{d}(t)$ is the resulting data vector, or snapshot, at time t. We will assume for simplicity that the matrix M (often referred to as the array manifold [6]) is known to within a negligible calibration error [1]. For example, in the case of an array of n sensors expected to receive signals from independent point sources, M will be an $(n \times N)$ matrix, whose N columns (denoted $\underline{m}(\theta_i)$, i = 1 to N) represent the independent spatial transformations of *calibration* signals from N possible discrete angles, θ_i. Thus, M contains a representative subset of the continuum of *possible* received waveforms: it provides calibration information about the array manifold rather than details of specific signal sources. If $\underline{f}(t)$ represents the complex amplitudes of the signals associated with m independent point sources, as measured at a given instant, $\underline{d}(t)$ will be given by the linear combination of m corresponding columns of M, scaled by the signal amplitudes and perturbed by additive noise. From a reconstruction of $\underline{f}(t)$, we hope to locate the m sources and estimate their powers.

3. METHODS OF DATA ANALYSIS

The usual method of solution is to use the calibration matrix, M, to form a set of correlation filters which are "matched" to each of the potential signal directions, θ_i, and to evaluate

$$P(\theta_i,t) = |f'(\theta_i,t)|^2 = \underline{m}^H(\theta_i)\ \underline{d}(t)\ \underline{d}^H(t)\ \underline{m}(\theta_i) \ /\ \{\underline{m}^H(\theta_i)\ \underline{m}(\theta_i)\}\ ,\quad i = 1 \text{ to } N, \qquad (2)$$

where the superscript H denotes the complex conjugate (Hermitian) transpose, and $|\underline{x}|^2$ denotes the squared magnitude of the individual elements of the vector, $\underline{x}$, and $\underline{m}^H(\theta_i)$ is a row of the matrix M^H. This is a simple estimate of the spatial power distribution of the input, $\underline{f}(t)$. Such processing may be considered as "scanning" the data with the beamforming weight vector, $\underline{m}^H(\theta_i)$. $P(\theta,t)$ has the familiar broad multiple lobed pattern of classical analysis, with consequent poor discrimination of multiple signals, resulting from the wide beamwidth and high sidelobes.

Traditional least squares techniques [7] suggest a possible alternative solution of the form

$$|\underline{f}'(t)|^2 = |(M^H M)^{-1} M^H \underline{d}(t)|^2 \quad , \qquad (3)$$

where $(M^H M)^{-1} M^H$ is known as the pseudo-inverse of M. However, in order to solve for $|\underline{f}'(t)|^2$, limits to the angular extent of the required reconstruction, θ_- and θ_+, are necessarily implied [1], since the matrix M must be fully defined before its pseudo-inverse can be evaluated. Thus, it is not sensible to "scan" the data beyond these pre-defined limits. In addition, the resulting reconstruction is extremely sensitive both to the accuracy of the implied angular bounds, and also, as written in equation (3), to the additive noise within the data [1].

The solution in equation (3) may be rewritten in terms of the singular value decomposition of M [7]. Thus,

$$|\underline{f}'(t)|^2 = |V\ S^{-1}\ U^H\ \underline{d}(t)|^2 \quad , \qquad (4)$$

where U and V are unitary matrices containing the left and right singular vectors of M respectively, and S is the diagonal matrix of singular values of M. That the decomposition depends on the limits, θ_- and θ_+, is illustrated by Fig. 1, which shows the singular value spectra calculated for each of four M matrices corresponding to different angular coverages. Fig. 2 demonstrates the similarity between an angular limitation for a 0.5 wavelength spaced linear array, as defined by $\theta_- = -14.5^\circ$ and $\theta_+ = +14.5^\circ$, and spatial oversampling using an array with 0.25 wavelength inter-element spacing, $\theta_- = -30^\circ$ and $\theta_+ = 30^\circ$. By setting both the smallest singular values (those for which $(s_1/s_i)^2$, the squared ratio of the first to i^{th} singular values, is greater than the signal to noise ratio) and their corresponding inverses to zero, and thus forming a reduced rank pseudo-inverse of M, the sensitivity to noise, referred to in the previous paragraph, may be reduced [8].

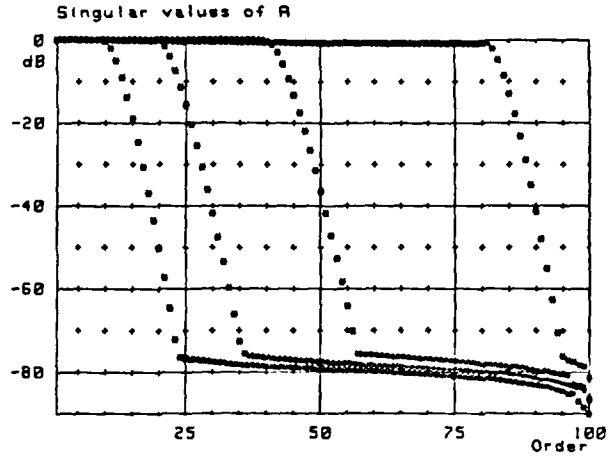

Fig. 1. The singular value spectra of four different M matrices, each of which is a calibration matrix for the same 100 element 0.5 wavelength spaced phased array, but corresponding to different angular constraints, θ_- and θ_+. (a) $\sin(\theta_+) = -\sin(\theta_-) = 0.1$; (b) $\sin(\theta_+) = -\sin(\theta_-) = 0.2$; (c) $\sin(\theta_+) = -\sin(\theta_-) = 0.4$; (d) $\sin(\theta_+) = -\sin(\theta_-) = 0.8$. The uppermost portion of each curve indicates that, within the spaces defined by the related singular vectors, signals may be transformed virtually without attenuation. The steeply sloping portion of each curve indicates rapidly increasing attenuation of the corresponding singular vectors as they are transformed via M. The lower, almost horizontal section indicates the presence a "noise" component resulting from accumulated numerical errors in the computation: transformation of the data via M^{-1} (as in equation (4)) would be significantly affected by these numerical errors, if they were not removed by setting the inverted singular values to zero. In each of the cases, a to d, the change of angular constraints leads to an approximate doubling of the unattenuated degrees of freedom.

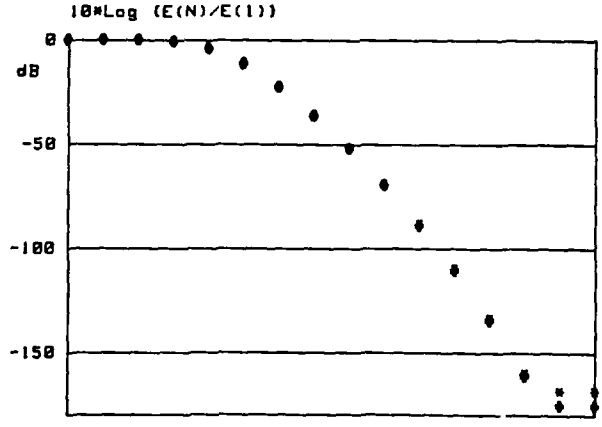

Fig. 2. A comparison of the singular value spectra for two 16 element linear arrays:
(*) element spacing 0.25 wavelengths; $\sin(\theta_+) = -\sin(\theta_-) = 0.5$
(#) element spacing 0.5 wavelengths; $\sin(\theta_+) = -\sin(\theta_-) = 0.25$.

4. AN EIGENVECTOR PROJECTION METHOD (EPM)

4.1. REDUCTION OF THE DATA MATRIX

The reduction in the sensitivity to noise of the method defined by equation (4), is achieved by projecting the data onto the subspace defined by those k vectors, denoted below by U_k, which are contained in the matrix U and are associated with the remaining k non-zero singular values. It can be seen from equation (4) that the validity of this processing rests on the assumption that the signal components in the data may be sufficiently accurately represented by the vector

$$\underline{c}(t) = U_k^H \, \underline{d}(t) \quad . \tag{5}$$

By this we mean that the components of the data which are suppressed by this projection are assumed to be indistinguishable from the noise. The vector $\underline{c}(t)$ has dimension $k \leq n$, which depends on the assumed signal to noise ratio, the limits θ_- and θ_+, and the degree of spatial oversampling or redundancy in the array.

Under conditions of low signal to noise ratio, the single snapshot pseudo-inverse reconstruction technique of equation (4) achieves little better discrimination performance than the classical matched filter, despite the additional implied constraint on the spatial extent of the input [1]. However, it is under these very conditions that the dimension of the vector $\underline{c}$ is most significantly reduced. Furthermore, the singular transformation of equation (5) may also be applied to multiple snapshots of data, stored in a matrix D of dimensions $(n \times P)$, where P is the number of snapshots. Thus,

$$C = U_k^H \, D \quad , \tag{6}$$

where C is a matrix of dimensions $(k \times P)$. This forms the basis of our eigenvector projection method (EPM).

4.2. APPLICATION OF EPM TO HIGH DISCRIMINATION ALGORITHMS

The widely quoted MUSIC method [6] makes use of the left singular vectors, E, of the data matrix, D (which are the same as the eigenvectors of the $(n \times n)$ covariance matrix, $(D \, D^H)$), to form the angular estimate

$$P(\theta_i) = \frac{\underline{m}^H(\theta_i) \, E_N \, E_N^H \, \underline{m}(\theta_i)}{\underline{m}^H(\theta_i) \, \underline{m}(\theta_i)} \quad , \quad i = 1 \text{ to } N \tag{7}$$

where E_N is the matrix of so-called "noise-subspace" singular vectors corresponding to the $(n - m)$ smallest singular values of D. The normalisation term in the denominator of equation (7) is included (as in equation (2)) to allow for non-uniform weighting of the gain vectors represented by the array manifold. The locations of the minima of this function are used to estimate the positions of the signal sources.

Clearly, finding E for a large sensor array dimension n imposes a heavy processing burden. However, if the corresponding singular vectors, F, of the reduced data matrix C are evaluated, a bounded solution may be calculated, via the MUSIC algorithm, as

$$P(\theta_i) = \frac{\underline{m}^H(\theta_i) \, U_k \, F_N \, F_N^H \, U_k^H \, \underline{m}(\theta_i)}{\underline{m}^H(\theta_i) \, U_k \, U_k^H \, \underline{m}(\theta_i)} \quad , \quad i = 1 \text{ to } N, \quad \theta_- \leq \theta_i \leq \theta_+ \, . \tag{8}$$

where F_N is the matrix of noise-subspace singular vectors of C, and U_k transforms these vectors back into the n-space of the array manifold. Correct normalisation is retained by using the "modified" array manifold vectors, $U_k^H \, \underline{m}(\theta_i)$, in the denominator.

Normalisation of the angular spectrum is of particular importance in the extension of EPM to certain other high discrimination algorithms, such as Burg's MEM [11] and the method of Kumaresan and Tufts [9]. Without correct normalisation, the methods fail to

perform correctly. MEM, in normalised form, may be written as

$$P(\theta_i) = \frac{\underline{m}^H(\theta_i)\ \underline{w}\ \underline{w}^H\ \underline{m}(\theta_i)}{\underline{m}^H(\theta_i)\ \underline{m}(\theta_i)} \quad , \quad i = 1 \text{ to } N, \tag{9}$$

where

$$\underline{w} = R^{-1}\ \underline{e}_1 \ , \tag{10}$$

and $\underline{e}_1$ is the first column of the identity matrix.

Therefore, EPM/MEM may be written as

$$P(\theta_i) = \frac{\underline{m}^H(\theta_i)\ \underline{w}_1\ \underline{w}_1^H\ \underline{m}(\theta_i)}{\underline{m}^H(\theta_i)\ \underline{w}_2\ \underline{w}_2^H\ \underline{m}(\theta_i)} \quad , \quad i = 1 \text{ to } N, \quad \theta_- \leq \theta_i \leq \theta_+ \ , \tag{11}$$

where

$$\underline{w}_1 = U_k\ (C\ C^H)^{-1}\ U_k^H\ \underline{e}_1 \ , \quad \underline{w}_2 = U_k\ U_k^H\ \underline{e}_1 \ . \tag{12}$$

The Kumaresan and Tufts algorithm (KT) may also be written in normalised form as in equation (9), but with the weight vector, $\underline{w}$, now given by

$$\underline{w} = \frac{E_N\ \underline{e}_N^H}{\underline{e}_N\ \underline{e}_N^H} \ , \tag{13}$$

where $\underline{e}_N$ is the first row of the noise subspace matrix of singular vectors, E_N.

Thus, EPM/KT, the EPM pre-processed version of the KT algorithm, has the same form as equation (11), but in this case,

$$\underline{w}_1 = \frac{(U_k\ F_N)(\underline{g}^H)}{\underline{g}\ \underline{g}^H} \quad , \quad \text{and} \quad \underline{w}_2 = \frac{U_k\ \underline{u}_k^H}{\underline{u}_k\ \underline{u}_k^H} \tag{14}$$

where $\underline{u}_k$ is the first row of U_k, and $\underline{g}$ is the first row of $(U_k\ F_N)$.

EPM may also be applied to the MLM method of Capon [10], which is then written as

$$P(\theta_i) = \frac{\underline{m}^H(\theta_i)\ U_k\ C^{-1}\ U_k^H\ \underline{m}(\theta_i)}{\underline{m}^H(\theta_i)\ U_k\ U_k^H\ \underline{m}(\theta_i)} \ . \tag{15}$$

Variants of the above algorithms, specifically designed for regularly spaced linear arrays, and involving the location of complex polynomial roots in the z-plane [15], may also benefit from the accelerated calculation of the singular vectors and matrix inversions made possible by EPM. The numerator terms of the algorithms given above in equations (7) to (15) may be written in the general form

$$P(\theta_i) = \underline{m}^H(\theta_i)\ X\ \underline{m}(\theta_i) \tag{16}$$

where, for example, $X = (E_N\ E_N^H)$ in the MUSIC algorithm, and $X = (U_k\ F_N\ F_N^H\ U_k^H)$ in the EPM/MUSIC algorithm, etc. We may now define the polynomial,

$$D(z) = \sum_{j=-n+1}^{n-1} x_j\ z^{-j} \tag{17}$$

where each of the coefficients, x_j, is calculated as the sum of the values along the j^{th} diagonal of X. Locating the roots of this polynomial is approximately equivalent, in the case of data from a regularly spaced, uniformly weighted linear array, to finding the peaks of the spatial spectral estimate given by equation (16). Barabell et al [15] have shown that root-finding variants of such algorithms have enhanced signal location performance over the more usual "spectral" versions that we have concentrated on in this report.

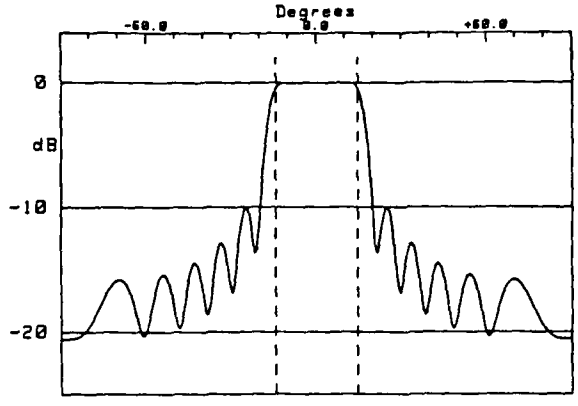

(a)

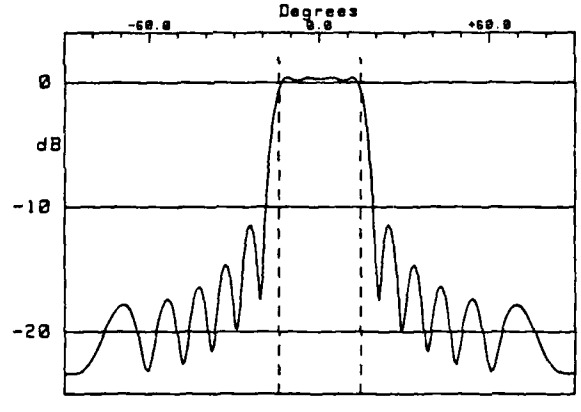

(b)

Fig. 3. (a) Spatial frequency filter function applied by EPM(k=5), assuming angular constraints given by $\sin(\theta_+) = -\sin(\theta_-) = 0.25$ *(indicated by vertical broken lines) for a 16 element 0.5 wavelength spaced linear array. (b) Spatial filter function obtained using 5 equally weighted conventional beams, directed at -1.78, -0.89, 0, 0.89, and 1.78 beamwidths away from boresight.*

Again for the case of regular linear or planar arrays, sub-aperture processing may still be utilised to combat coherent multipath or to analyse time series information, provided that it is applied to the corresponding original data and reference matrices, D and M, prior to EPM. The matrix U_k will then be that corresponding to the sub-aperture array manifold.

Signal powers and time-domain behaviour may be extracted [1,6] simply by replacing M in the usual equations by $A = (U_k^H M)$. Each identified signal direction is referenced to a particular column of the matrix A. Thus if these columns are collected together and stored in a matrix, A_s, the time series associated with each direction is a row of the matrix, T, given by [1]

$$T = (A_s^H A_s)^{-1} A_s^H C \quad , \tag{18}$$

and the signal powers may be estimated as the diagonal elements of the matrix

$$P = T T^H \quad . \tag{19}$$

As the Monte Carlo simulation results described in section 5 show, EPM pre-processing leads to improved angular estimates as a result of noise reduction. The fidelity of the extracted time series, and the accuracy of the estimated powers will be improved over results from the equivalent "conventional" high discrimination processing principally at low signal to noise ratio, by virtue of the enhanced probability of resolution.

4.3. PROPERTIES OF EPM

EPM is equivalent to a spatial beamforming process, using the conjugate transpose of the principal eigenvectors, U_k^H, of M in place of the more usual beam steering vectors. The effect is similar to directing a limited number of conventional beams into the angular region of interest [14]. This may be illustrated by plotting the effective beam pattern, which may be considered as a spatial filter transfer function. Fig. 3a shows a typical function applied to the data space by EPM, generated by assuming a 4 beamwidth angular region of interest, using a 16 element 0.5 wavelength spaced linear array, and $k = 5$. Fig. 3b shows the function obtained using five equally weighted conventional beams, directed at -1.78, -0.89, 0, 0.89 and 1.78 beamwidths away from boresight. The beam positions have been chosen such that the resulting pattern approximately resembles that of the eigenvector processor. In filter terms, the choice of beam positions gives a trade-off between in-band ripple and out-of-band rejection. We have not explored the effect of using differently weighted beams or irregularly spaced beams, for example. EPM provides a secure basis for choosing the optimal maximum number of "beams", based on knowledge of signal to noise, and automatically places those "beams" so as to give a good trade-off as described above.

Although the angular estimates of signals located within the region of interest, derived following EPM pre-processing are not sensitive to the validity of the assumed angular frequency constraints, θ_- and θ_+, the same is not true of the signal extraction and power estimation stages (equations (18) and (19)). If significant signal amplitudes exist at unknown angles beyond these boundaries, the estimates of power and time behaviour may degrade [1]. The same is true for any of the high discrimination algorithms if they fail to locate one or more signals accurately. For example, the signal estimation performance based on the output of MUSIC would deteriorate in a similar manner if the $P(\theta_i)$ of equation (7) was also to be limited to $\theta_- \leq \theta_i \leq \theta_+$. This sensitivity arises because the inversion required by equation (18) is sensitive to power leakage into sidelobes which fall beyond beyond θ_- and θ_+. This is illustrated by an example in Fig. 4, which shows a typical filter function, as applied by equation (18) to a three target scenario, where we have assumed that only two of the targets have been detected, the third being located slightly beyond the assumed angular window delimited by the vertical dotted line at θ_+. The third target falls within the main "lobe" of the filter response, but has not been

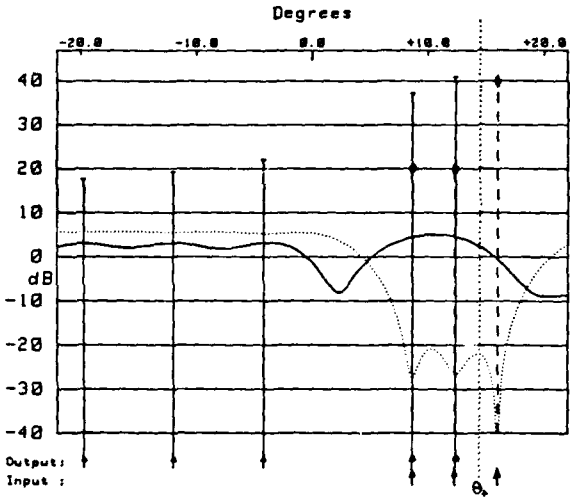

Fig. 4. A three source scenario is defined by the vertical broken lines surmounted by diamond shapes, indicating the positions and powers of the signals. The MUSIC spectral estimate, represented by the dotted line, locates all three signals. However, assuming that θ_+ is indicated by the vertical dotted line, estimation of signal powers using equations (18) and (19) ignores one signal position and is in error, as shown by the solid vertical lines surmounted by short horizontal bars. The continuous line in the diagram shows the spatial filter function applied by the incorrectly supported pseudo-inverse in equation (18).

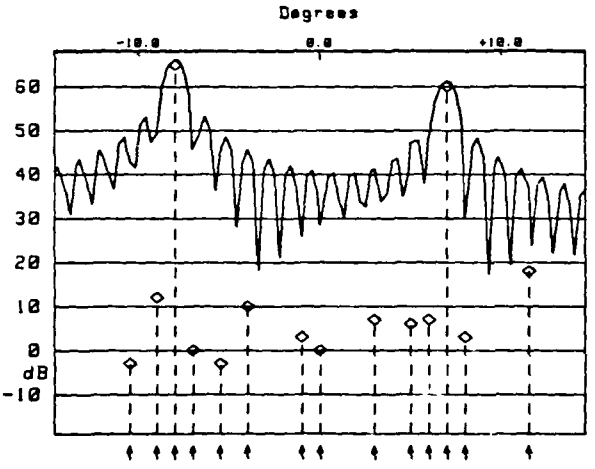

Fig. 5. The continuous line shows the result of processing the data from a 100 element sensor array, corresponding to a 14 source scenario, by forming an average of the 100 single snapshot matched filter reconstructions of equation (2). Vertical lines surmounted by diamond shapes indicate the actual source powers and positions. In this reconstruction it is not possible to locate the majority of the signals with confidence.

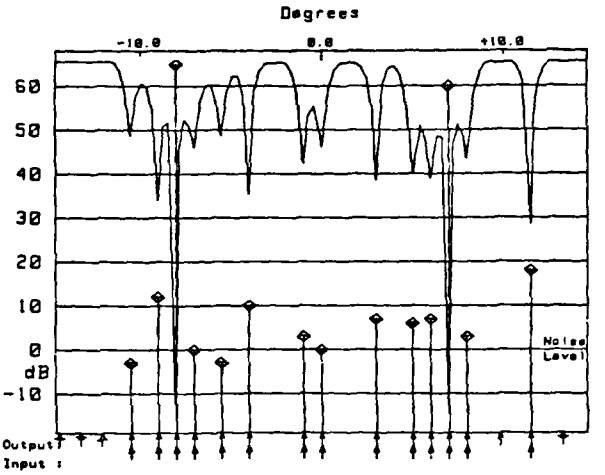

Fig. 6. The continuous line shows the result of processing the same data as in Fig. 5, using the MUSIC algorithm (equation (7)) acting on the 86 noise-space eigenvectors of the full 100×100 data covariance matrix. Vertical lines surmounted by diamond shapes indicate the actual source powers and positions. Vertical lines surmounted by horizontal bars indicate the power and position estimates derived from the null positions in the MUSIC result. The estimated signal parameters are very close to the actual input values.

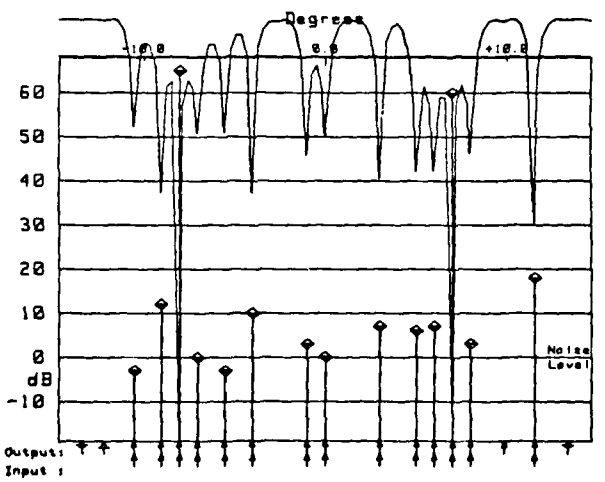

Fig. 7. The continuous line shows the result of analysing the same data as in Figs. 5 and 6 by EPM/MUSIC (equation (8)), processed in order to reduce the total number of eigenvectors to 26, and the computation time by a factor of 56. As in Fig. 6, the source positions and power estimates are well matched to the actual source parameters. The minima of the MUSIC scan in this case are deeper than those of Fig. 6 by approximately 10dB as a result of the enhanced noise immunity conferred by the EPM pre-processing.

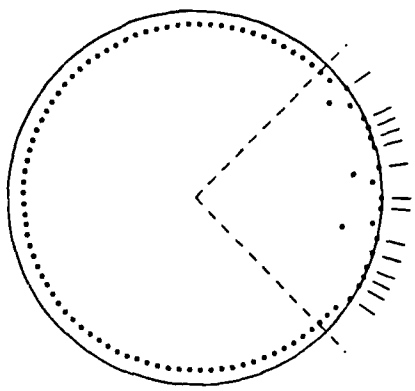

Fig. 8. A plot of the locations of the zeros of the polynomial generated by equation (17) applied to the MUSIC noise space eigenvectors used in Fig. 6. True signal locations are indicated by the short lines close to the unit circle and the assumed angular constraints (which denote the limits of Figs. 6 and 7) by the broken radial lines.

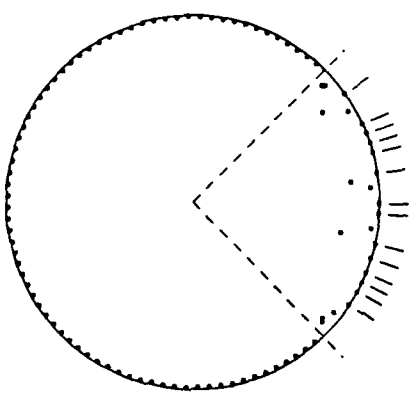

Fig. 9. A plot of the locations of the zeros of the polynomial generated by equation (17) applied to the EPM(k=5)/MUSIC noise space eigenvectors used to create Fig. 7. True signal locations are indicated by the short lines close to the unit circle and the assumed angular constraints (which denote the limits of Figs. 6 and 7) by the broken radial lines.

detected. Thus the power estimate is higher than if only two targets were present, the excess being falsely attributed to the two identified angles and any spurious noise-related detections. It may be possible to reduce such sensitivity by the application of multiple constraint adaptive canceller techniques to null signals in the sidelobes of the EPM filter during the power estimation step.

5. EXPERIMENTAL RESULTS

As a demonstration of the EPM technique, we present the results of processing a set of simulated snapshots of data corresponding to a multiple source scenario, using EPM in combination with the MUSIC algorithm. This is followed by a discussion of the results of Monte Carlo analyses of data from a variety of two source scenarios, in which results obtained from high discrimination algorithms acting on the normal covariance matrix are compared to those obtained from the same algorithms acting on the reduced size covariance matrix output from EPM. The actual Monte Carlo results are more comprehensively presented for reference in the Appendices.

5.1. MULTIPLE SOURCE SCENARIO

The data matrix for the multiple source scenario consisted of 100 simulated snapshots of complex data from a linear array of 100 omnidirectional elements separated with 0.5 wavelength spacing, receiving signals from 14 independent point sources distributed between $\pm 15^{\circ}$ in the far field. Independent samples of zero mean Gaussian noise were added at each sensor and time instant.

As a basis for comparison, Fig. 5 shows the conventional matched filter response (an average of the 100 single snapshot reconstructions given by application of equation (2)) to this scenario. This plot displays the broad multiple lobed structure characteristic of this method. It also serves to demonstrate that the discrimination problem is often more related to a difficulty in the detection of low power signals which have been obscured by the sidelobes of the high power signals, rather than simply a lack of resolution per se.

To demonstrate the performance of the new technique, we have derived two further reconstructions of the same multiple source scenario, as analysed in each case by MUSIC. In Fig. 6 the data has been processed in the normal manner, involving the eigen decomposition of the full 100×100 complex valued covariance matrix. In Fig. 7, the data has been pre-processed using EPM, taking into account the assumed maximum angular distribution of the targets of $\pm 15^{\circ}$, and a dynamic range (signal to noise) estimate of only 6dB, to form a reduced (26×26) complex covariance matrix for input to the eigenvector decomposition. The result, running typical serial Householder reduction and QL diagonalisation routines [12], was a reduction in the time taken for this stage by a factor of approximately 56, as would be expected. The reconstructions of Figs. 6 and 7 are virtually indistinguishable, apart from the fact that the nulls in the pre-processed result are deeper than those in the usual MUSIC plot by some 10dB. This has occured as a result of discarding noisy degrees of freedom in the data via the EPM processing, and indicates an improvement in the ability of the algorithm to extract signals from noise, as is further demonstrated by the results of section 5.2.

To demonstrate the applicability of EPM to the z-plane root variants of high discrimination algorithms, Fig. 8 shows the z-plane locations of the zeros of the polynomial given by equation (17) in the root version of MUSIC. The data used was the same as that for Figs. 5, 6 and 7. Fig. 9 shows the corresponding plot of roots from the EPM pre-processed MUSIC algorithm. Root positions beyond the assumed field of view (indicated by the radial lines) may be ignored.

DATA COLLECTION AND ANALYSIS ALGORITHM

```
1. RECORD DATA:
    FOR each emitter separation
        FOR each signal to noise ratio
            FOR each repeat
                generate new data matrix
                FOR each algorithm
                    RECORD angle and power estimates onto disc
                    RECORD null depths
                NEXT algorithm
            NEXT repeat
            RECORD average of covariance eigenvalue spectra
        NEXT signal to noise ratio
    NEXT emitter separation


2. ANALYSE DATA:
    FOR each separation
        FOR each signal to noise ratio
            FOR each repeat
                FOR each algorithm
                    FOR each angle estimate
                        test against thresholds in angle and power
                        assign targets to estimates
                        record positions and powers of resolved pairs
                    NEXT angle estimate
                    count total false alarms
                    count total resolutions
                NEXT algorithm
            NEXT repeat
            FOR each algorithm
                average probability of resolution
                average false alarm rate
            NEXT algorithm
        NEXT signal to noise ratio
        FOR each signal to noise ratio
            FOR each algorithm
                FOR each emitter
                    IF resolved THEN
                        calculate mean position
                        calculate bias of mean from true position
                        calculate standard deviation of angle estimates
                    END IF
                NEXT emitter
            NEXT algorithm
        NEXT signal to noise
    NEXT separation
```

Fig. 10. Monte Carlo data collection and analysis procedures.

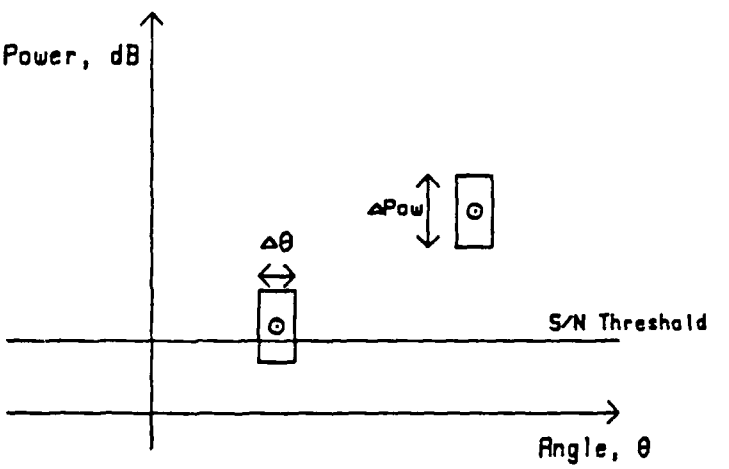

Fig. 11. Two signals are indicated by ⊙ symbols. During data analysis, a power threshold may be set, below which all estimates are assumed to be related to noise and are therefore ignored. All estimates above this signal to noise threshold are then counted as either false alarms or true target detections. Signals are assumed to be detected if the (angle, power) coordinates fall within the boxes defined by the true signal coordinates, and $\Delta\theta$ and ΔPow. Throughout the analyses presented in the present report, $\Delta\theta$ = 1 beamwidth, and ΔPow = 6dB.

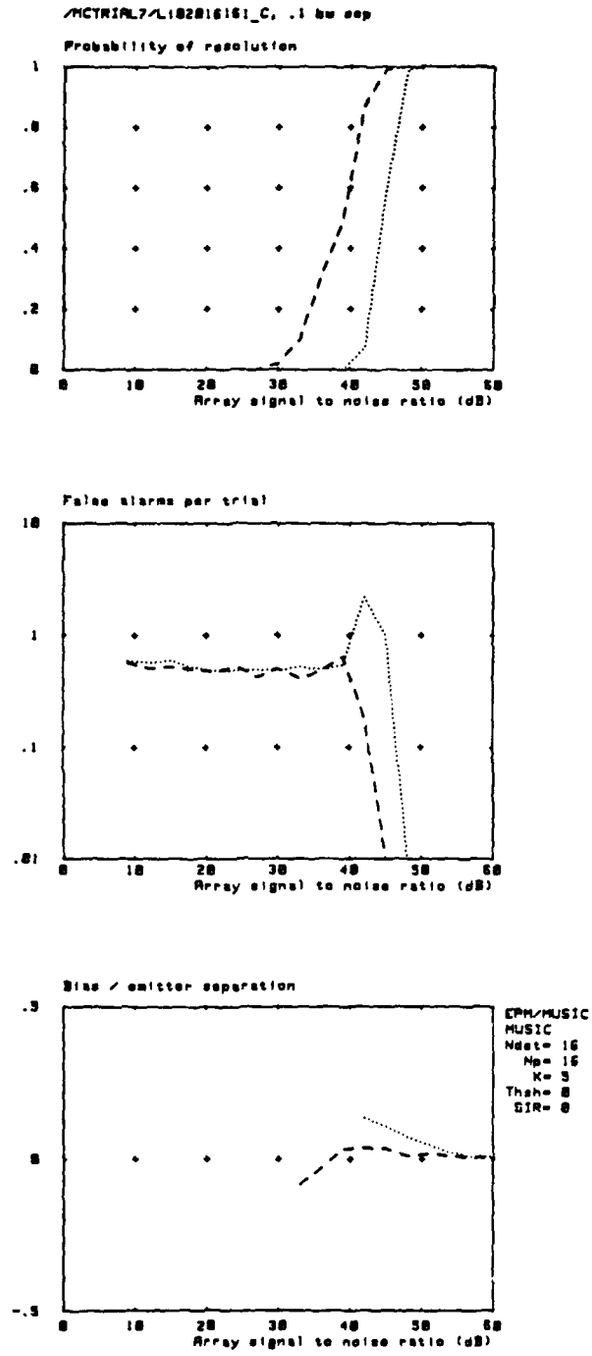

Fig. 12. Performance statistics as a function of array signal to noise ratio (ASNR) for two signals, located at 0 and 0.1 beamwidths from broadside. Results are based on 100 trials at each ASNR, taking 16 snapshots of data from the 16 element 0.5 wavelength spaced linear array. Dotted l. es show the results of processing using the MUSIC algorithm (equation (7)) and dashed lines show the results obtained using EPM(k=5)/MUSIC. Assumed angle of view from -2 to +2 beamwidths.

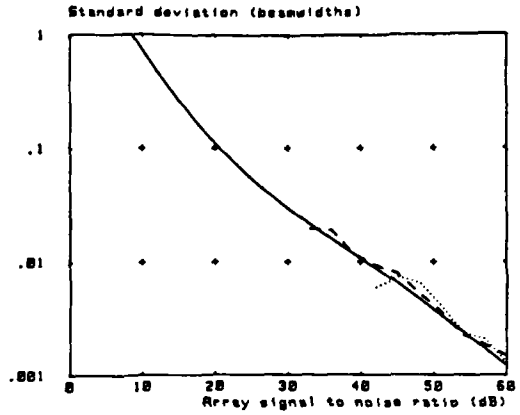

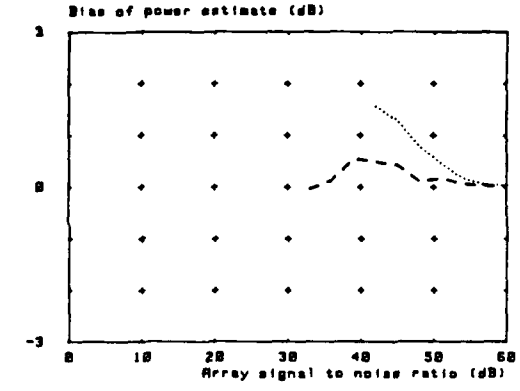

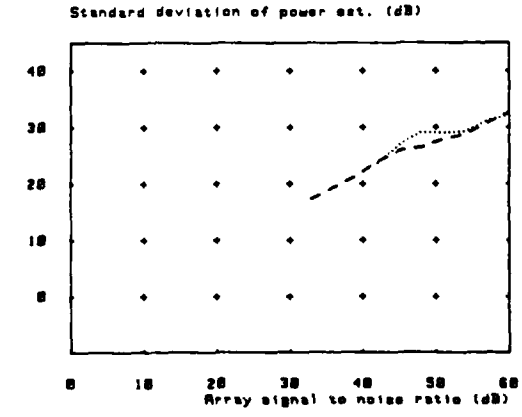

Fig. 12 (cont). Performance statistics as a function of array signal to noise ratio (ASNR) for two signals, located at 0 and 0.1 beamwidths from broadside. Results are based on 100 trials at each ASNR, taking 16 snapshots of data from the 16 element 0.5 wavelength spaced linear array. Dotted lines show the results of processing using the MUSIC algorithm (equation (7)) and dashed lines show the results obtained using EPM(k=5)/MUSIC. The continuous line in the plot of angular standard deviation is the Cramér Rao bound.

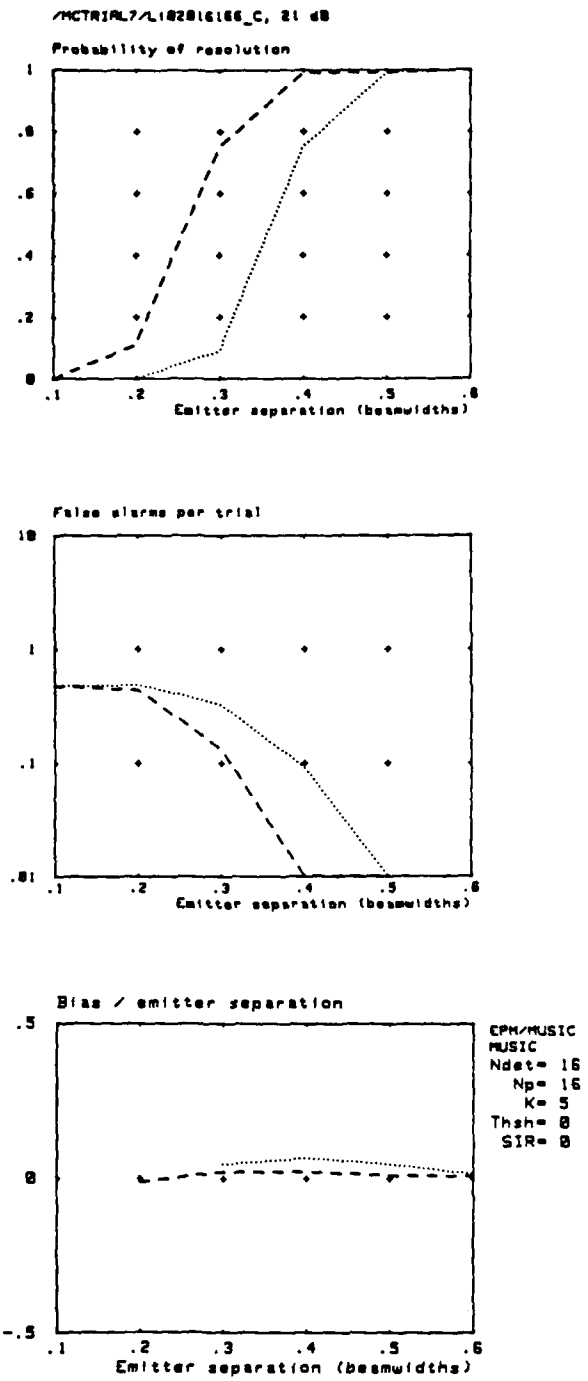

Fig. 13. Performance statistics as a function of emitter separation (beamwidths) for two signals, one located at broadside, and each having an ASNR of 21dB. Results are based on 100 trials at each separation, taking 16 snapshots of data from the 16 element 0.5 wavelength spaced linear array. Dotted lines show the results of processing using the MUSIC algorithm (equation (7)) and dashed lines show the results obtained using EPM(k=5)/MUSIC. Assumed angle of view from −2 to +2 beamwidths.

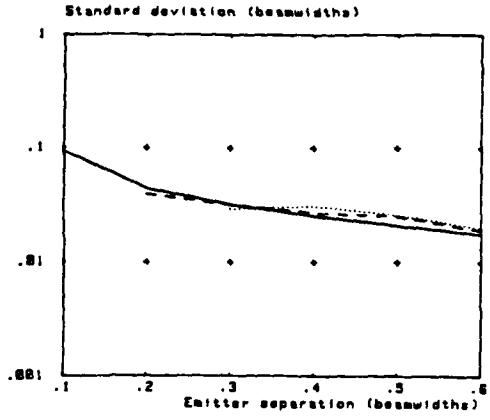

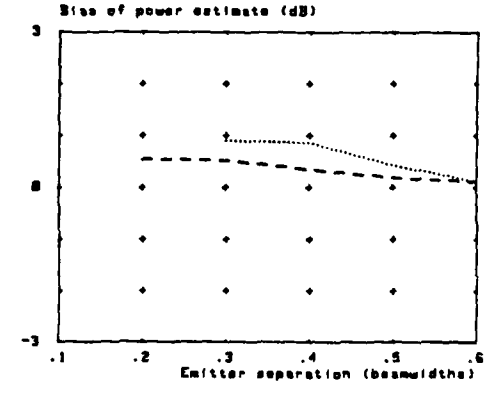

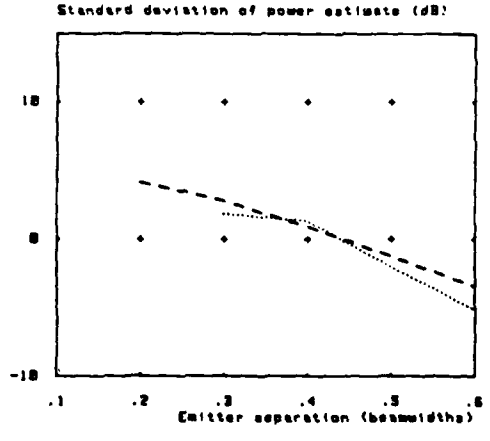

Fig. 13 (cont). Performance statistics as a function of emitter separation (beamwidths) for two signals, one located at broadside, and each having an ASNR of 21dB. Results are based on 100 trials at each separation, taking 16 snapshots of data from the 16 element 0.5 wavelength spaced linear array. Dotted lines show the results of processing using the MUSIC algorithm (equation (7)) and dashed lines show the results obtained using EPM(k=5)/MUSIC. The continuous line in the plot of angular standard deviation is the Cramér Rao bound.

5.2. MONTE CARLO ANALYSIS

5.2.1. DATA COLLECTION AND ANALYSIS

A more complete investigation of the performance of algorithms incorporating EPM has been carried out via a series of Monte Carlo simulations. These enable comparison of the performance of algorithms, with and without EPM, over many trials. The results are collected in terms of such parameters as the bias and standard deviation of the angle and power estimates, the probability of resolution and false alarm rate. Statistics have been collected, based on 100 trials of each algorithm at each of a number of discrete angular separations and signal to noise ratios. The results are presented in a similar format to those of Barabell et al [13].

Fig. 10 is a summary of the procedure used in the collection and analysis of the statistical data. During the Monte Carlo trials, the positions of all minima of $P(\theta)$ and their depths are recorded, together with the corresponding powers estimated using equations (18) and (19), and an average of the eigenvalue spectrum of the covariance matrix at each signal to noise ratio. During analysis, thresholds may be set in angle, power or null depth in order to distinguish between correctly identified signals, false alarms, and estimates which may be ignored. For example, Fig. 11 shows how thresholds may be set in power and angle. First of all a noise level power threshold is set, all signals falling below this line being rejected. Signals above this threshold are assigned as detections if the estimate of (angle, power) falls within the window defined by an angular uncertainty, $\Delta\theta$, and a power uncertainty, ΔP, each centred on the appropriate true signal coordinate. All other detections are counted as false alarms. The statistical results presented in the following sections (and in Appendices A1 to A4 and A6) are all conditioned on resolution (detection of both targets), as indicated in Fig. 10.

In the following sections, signal to noise ratio is measured in terms of the "array signal to noise ratio" (ASNR) of one of the two targets. This is defined as ((signal to noise at each element of the array, per snapshot) $- 10 \log_{10}(n)$).

5.2.2. TARGETS CLOSE TO BROADSIDE

The results presented in Figs. 12 to 17 relate to the analysis of 16 snapshots of data from a 16 element linear array with 0.5 wavelength element spacing, and with θ_+ and θ_- set to $\pm 14.5^\circ$ (± 4 beamwidths). Using a dynamic range of 6dB in the selection of the significant basis vectors, U_k, has resulted in the dimension k being equal to 5, unless otherwise stated. The target scenario simply consists of two equal powered random phase signal sources in the far field, the first located at the broadside position (perpendicular to the line of the array), and the second at a fractional beamwidth to one side. The beamwidth referred to here is the angle from the peak of the main lobe of a matched filter (equation (2)) placed on the first target location, to the position of the first null.

Fig. 12 shows the variation of the performance statistics as a function of ASNR (the theoretical integrated signal to noise power ratio for each of the two emitters) for an emitter separation of 0.1 beamwidths. The results, taken at 3dB signal to noise ratio increments, are shown for the MUSIC algorithm acting on the 16×16 covariance matrix (dotted lines) and for MUSIC acting on the EPM processed 5×5 covariance matrix (dashed lines). The solid line in the plot of standard deviation is the Cramér Rao bound [16] for the problem, assuming uncorrelated emitters. A noise power threshold of $10 \log_{10}(n)$ has been used, together with $\Delta\theta = 1$ beamwidth and $\Delta P = 6$dB. In both cases, as the ASNR rises, the probability of resolution increases (associated with a peak in the false alarm rate), bias of the angle and power estimates tend to zero, and the variance of the angle estimates, $\mathrm{var}(\hat{\theta}_i)$, tend towards the Cramér Rao bound. The bias and variance results are plotted for the "left-hand" signal, and thus negative angular bias

indicates that the nulls of $P(\theta)$ corresponding to the signals have moved further apart.

Unexpectedly perhaps, the variance of the power estimate, $\text{var}(\hat{p}_i)$, *increases* with rising ASNR. Examining the results given in Fig. 13 and Appendix 1, we see that $\text{var}(\hat{p}_i)$ decreases with increasing angular separation. This fluctuation of the power estimate is likely to arise from mismatch between the derived direction vectors, as used in $\mathbf{A}_s$, and the actual signal direction vectors. A mismatch in the direction vector of the "desired" signal is likely to be correlated both with the noise background, and also with any residue arising from poor cancellation of the second signal (as a result of an inaccurate angle estimate), and would thus contribute to $\text{var}(\hat{p}_i)$, in manner similar to that observed for constrained adaptive cancellers [17]. The primary root cause may thus be assumed to be time domain correlation of the signals and noise. In support of this, we note that the algorithm which delivers the values of $\text{var}(\hat{\theta}_i)$ closest to the Cramér Rao bound is generally also associated with the lowest $\text{var}(\hat{p}_i)$, and that both variances decrease as angular separation and the number of snapshots increase (Appendix 1). Plotting $\text{var}(\hat{p}_i)$ as a percentage of the true power results in a curve which tends towards a constant variance as ASNR increases.

We see that, for this scenario, in addition to reducing the time taken for the computation of the eigenvectors by a factor of approximately 32, processing by EPM has an effect on performance which is roughly equivalent to a 5–10dB increase in array signal to noise ratio. If the noise was distributed equally amongst all the available degrees of freedom (and the signal was concentrated in the k primary degrees of freedom) before processing by EPM, we might expect an improvement of approximately 5dB in this case, and so the observed change seems reasonable.

Fig. 13 shows a similar set of performance curves, plotted now as a function of emitter separation (in 0.1 beamwidth increments) for an array signal to noise ratio of 21 dB. The results again show that the performance of the EPM/MUSIC combination consistently equals or improves upon that of MUSIC alone.

Further results, similar to those of Fig. 12, but demonstrating the behaviour of MUSIC, KT, MEM, MLM, their z-plane root counterparts, and the EPM pre-processed equivalents for a range of signal separations, are given in Appendix 1. Also included in that Appendix are results obtained from analyses of only 5 snapshots of data. The degree of improvement in performance is seen to depend on the choice of basic algorithm, reflecting the different emphasis given by each of them to the covariance eigen components. Generally, some improvement in performance is apparent, in addition to a reduction of computation time, until the limits imposed by the chosen thresholds are reached. Whilst the z-plane algorithm variants have enhanced performance over the "spectral" versions when the array is perfectly regular, the application of EPM tends only to lead to further improvements in probability of resolution at the expense of increased angle estimation bias. Bias increases as the estimates become increasingly contaminated by noise, and the z-plane roots move away from the unit circle.

In order to investigate the effect of choosing a particular threshold, we have analysed Monte Carlo data so as to measure the variation of resolution probability and of false alarm rate as a function of the noise level threshold. Thus, for a given signal separation, plots such as those of Figs. 14 to 16 for EPM(k=5)/MUSIC may be produced, the multiple curves corresponding to different array signal to noise ratios. Examination of false alarm rate as a function of noise level threshold (Fig. 16) shows that false alarms may be rapidly reduced at signal to noise ratios which are much higher or lower than the range in which resolution is first achieved. This suggests that such false alarms are largely related to the noise background. In the range for which resolution probability is increasing, many false alarms are likely to result from the situation in which only one target has been detected within the $(\Delta\theta,\Delta P)$ window, and a second detection falls beyond

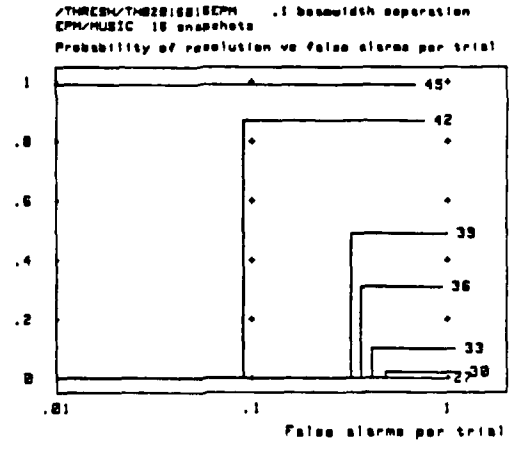

Fig. 14. Probability of resolution as a function of false alarm rate, parameterised by ASNR, as derived by varying the signal to noise power threshold, for EPM(k=5)/MUSIC. Signals at 0 and 0.1 beamwidths from broadside.

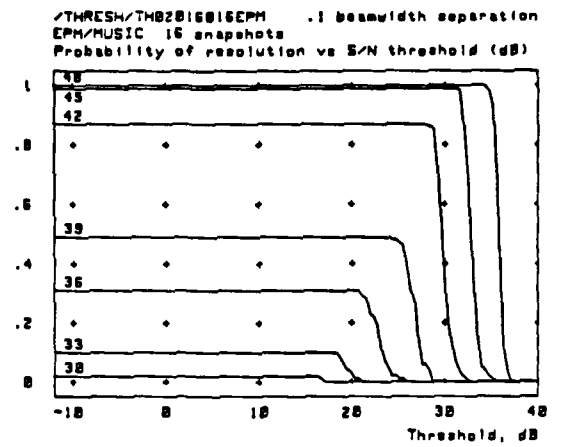

Fig. 15. Probability of resolution as a function of signal to noise threshold, parameterised by ASNR, for EPM(k=5)/MUSIC. Signals at 0 and 0.1 beamwidths from broadside.

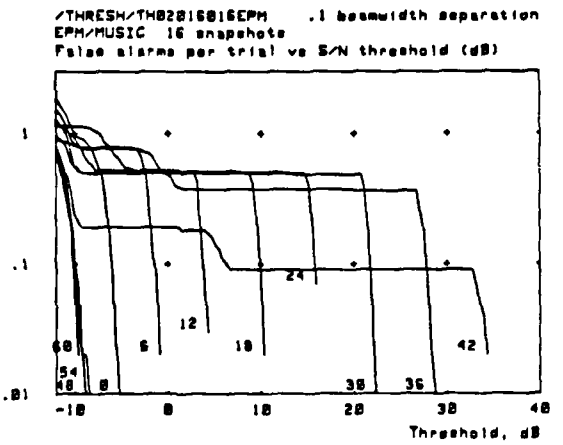

Fig. 16. False alarm rate as a function of signal to noise threshold, parameterised by ASNR, for EPM(k=5)/MUSIC. Signals at 0 and 0.1 beamwidths from broadside.

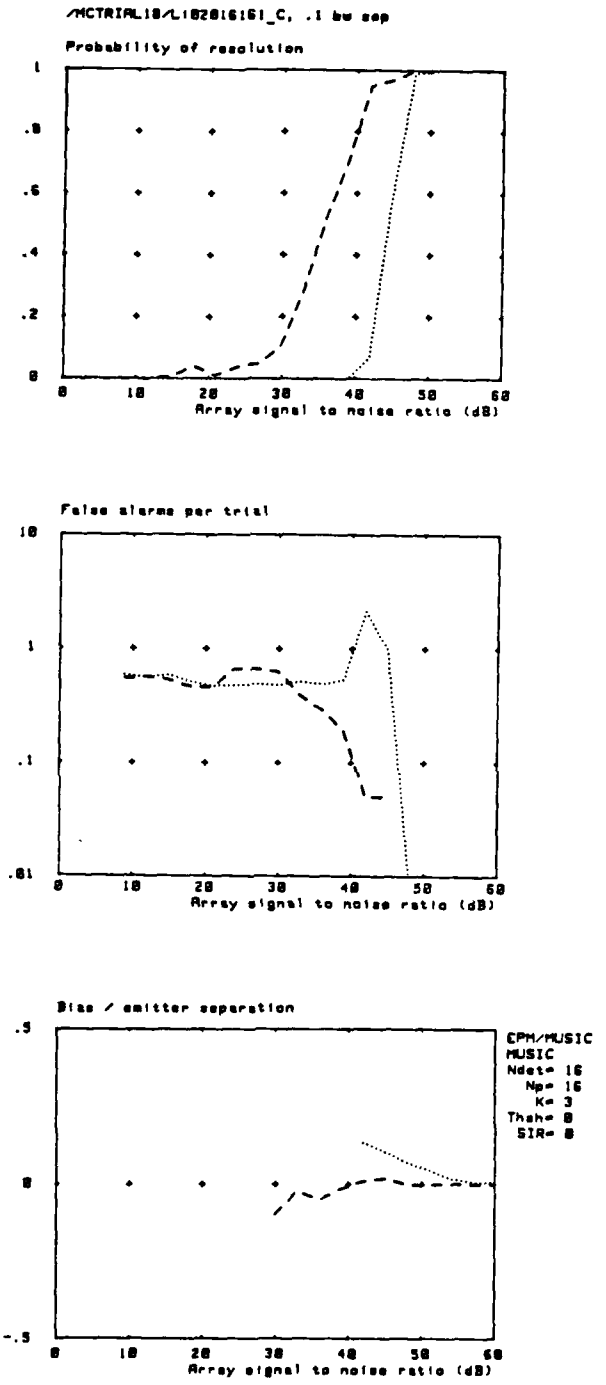

Fig. 17. Performance statistics as a function of array signal to noise ratio (ASNR) for two signals, located at 0 and 0.1 beamwidths from broadside. Results are based on 100 trials at each ASNR, taking 16 snapshots of data from the 16 element 0.5 wavelength spaced linear array. Dotted lines show the results of processing using the MUSIC algorithm (equation (7)) and dashed lines show the results obtained using EPM(k=3)/MUSIC. Assumed angle of view from −2 to +2 beamwidths.

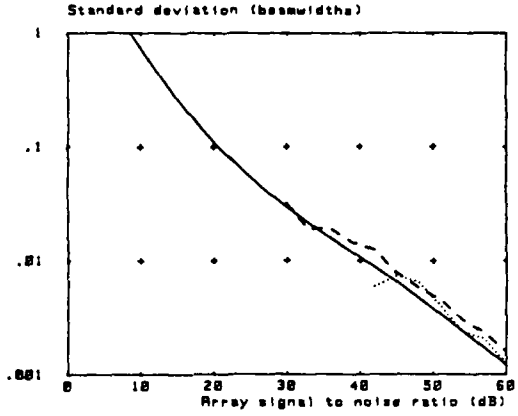

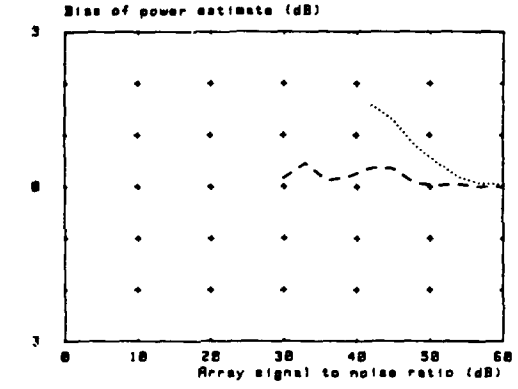

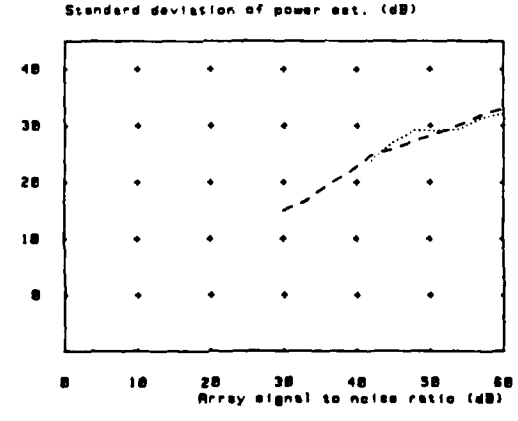

Fig. 17 (cont). Performance statistics as a function of array signal to noise atio (ASNR) for two signals, located at 0 and 0.1 beamwidths from broadside. Results are based on 100 trials at each ASNR, taking 16 snapshots of data from the 16 element 0.5 wavelength spaced linear array. Dotted lines show the results of processing using the MUSIC algorithm (equation (7)) and dashed lines show the results obtained using EPM(k=3)/MUSIC. The continuous line in the plot of angular standard deviation is the Cramér Rao bound.

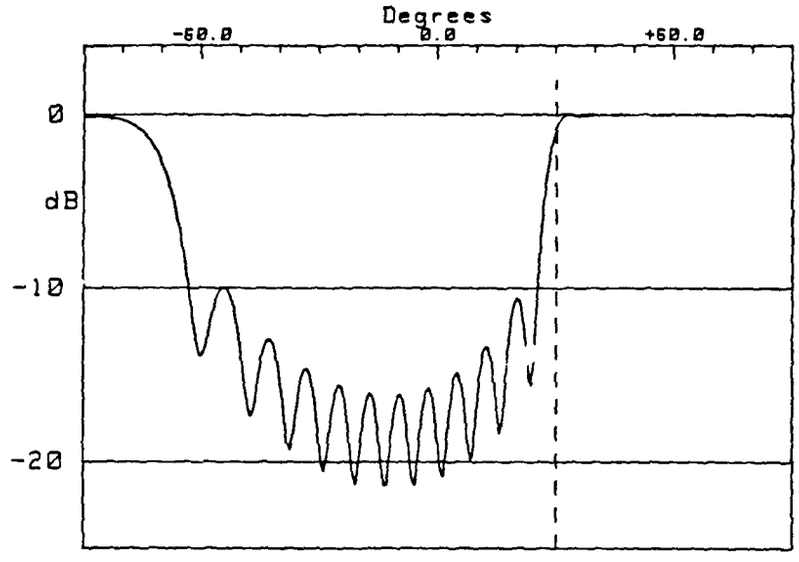

Fig. 18. Spatial frequency filter function applied to data by EPM(k=5), assuming angular constraints given by $\sin(\theta_-) = 0.5$ and $\sin(\theta_+) = 1.0$ (indicated by vertical broken lines) for a 16 element 0° [illegible]-wavelength spaced linear array.

one or both of the thresholds. Such a second detection is most likely to be "signal related" rather than "noise related" when the resolution threshold is approached.

Finally in this section, Fig. 17 again compares the results of normal MUSIC processing with that of EPM/MUSIC, for a signal separation of 0.1 beamwidths, and 16 snapshots of data from the 16 element linear array. In this case however, the dimension k assumed for EPM was 3, the minimum necessary for resolution of the two targets using MUSIC. Computation time is further reduced, and the ASNR required for resolution lowered. Thus, (within certain angular limits which we have not explored - see the following section) if the number of targets, m, is known a priori, k may be reduced to $m+1$ for maximum enhancement of performance.

5.2.3. TARGETS FAR FROM BROADSIDE

Because of the similarity of the assumption made in the previous section regarding the extent of the field of view (ie, signals confined to a region about the broadside position) with an assumption of spatial oversampling, it is perhaps strange to consider being able to use EPM for a field of view in which such oversampling cannot be assumed. However, the rank reduction which forms the basis of the method is related to a more general assumption of "redundancy" in the array which includes the possibility of oversampling. Thus, having created a calibration matrix, $\mathbf{M}$, corresponding to $\theta_- = 30^\circ$ and $\theta_+ = 90^\circ$ for example, its singular values decline in a similar way to those of the previous M, based on the oversampling assumption. Once again, the maximum number of "significant" basis vectors, $\mathbf{U}_k$, can be determined from knowledge of the overall signal to noise ratio, and an EPM filter defined. For the example of the 16 element linear array, Fig. 18 shows the EPM spatial filter function created by taking $k = 5$. The function is not as sharply confined to the region of interest as was the case in Fig. 3a, but spreading over a range of negative angles. However this will not be a problem, and the additional range may be ignored. (We further note that, in this example, choosing $k < 5$ leads to nulls of the spatial filter function being placed within the assumed angle of view, and a consequent loss of performance in the region of such nulls.)

Taking the above situation, with two equal power independent sources located at 7.8 and 7.9 beamwidths (77° and 81°) from boresight, Fig. 19 compares the performance of MUSIC acting on the full 16x16 covariance matrix with that achievable via the 5x5 EPM processed covariance estimate. Probability of resolution has improved as a result of the EPM pre-processing, although by the equivalent of only a 2-3dB shift along the ASNR axis, which is somewhat less than was the case for targets close to broadside. In this case, variance of the angle estimate has actually increased following EPM. Appendix 2 gives further results, for a range of algorithms, corresponding to targets placed well away from broadside. These results show a range of behaviour which depends on the basic algorithm. For example, the performance of the KT algorithm is virtually unchanged in the present case, whereas that of MEM is improved by the equivalent of an increase of up to 10dB in the power of each signal as measured by probability of resolution, and by approximately 5dB in terms of variance of the angle estimates.

5.2.4. TWO UNEQUAL POWER SIGNALS

High discrimination algorithms, of the type referred to in this report, have the important characteristics of enabling the detection of multiple signals within the beamwidth defined by the matched filter (equation (2)), and, perhaps even more importantly, of enabling the detection of targets whose powers fall below the sidelobes of the conventional beamformer. Combining these two features, we expect to be able to resolve signals of differing powers within the main beamwidth.

Fig. 20 compares the performance of MUSIC with that of EPM(k=5)/MUSIC for the

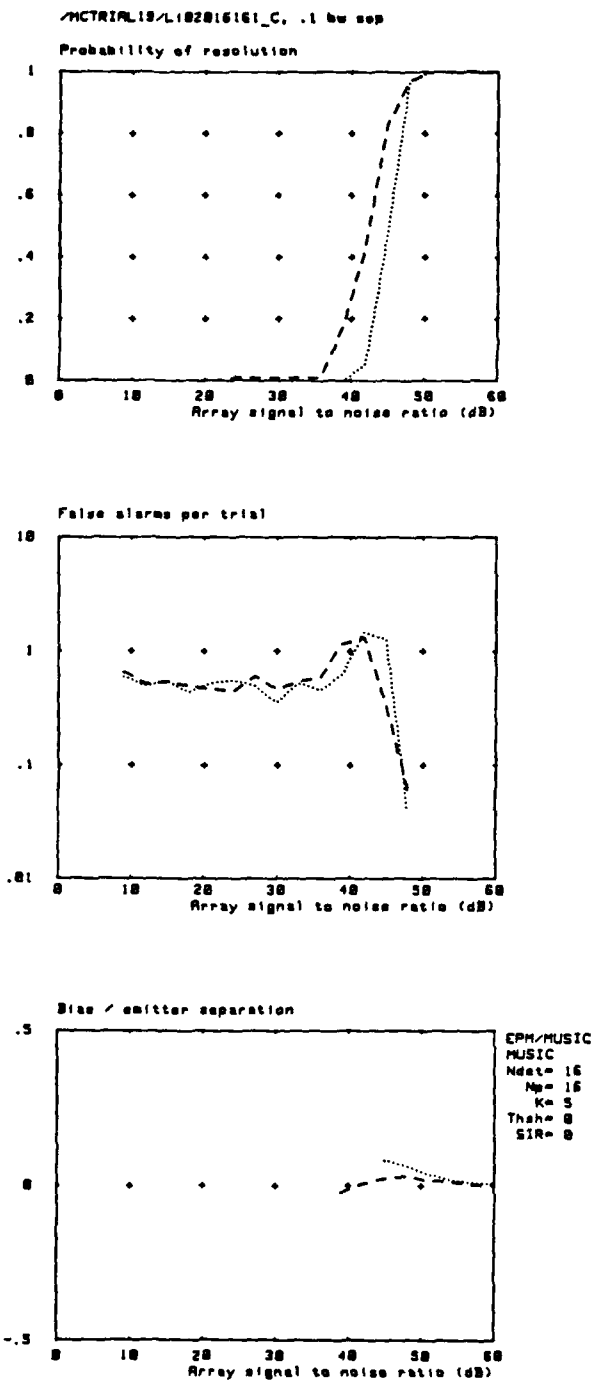

Fig. 19. Performance statistics as a function of array signal to noise ratio (ASNR) for two signals, located at 7.8 and 7.9 beamwidths from broadside. Results are based on 100 trials at each ASNR, taking 16 snapshots of data from the 16 element 0.5 wavelength spaced linear array. Dotted lines show the results of processing using the MUSIC algorithm (equation (7)) and dashed lines show the results obtained using EPM(k=5)/MUSIC. Assumed angle of view from +4 to +8 beamwidths.

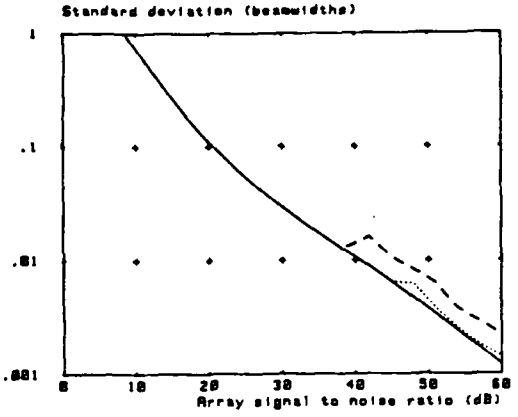

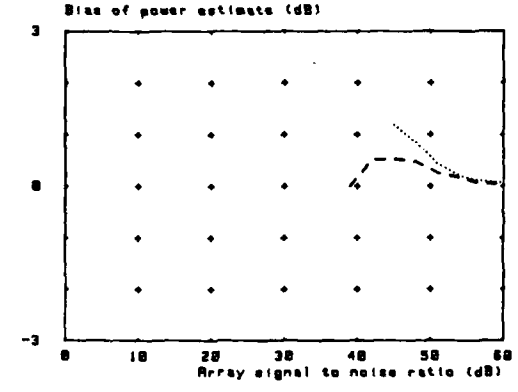

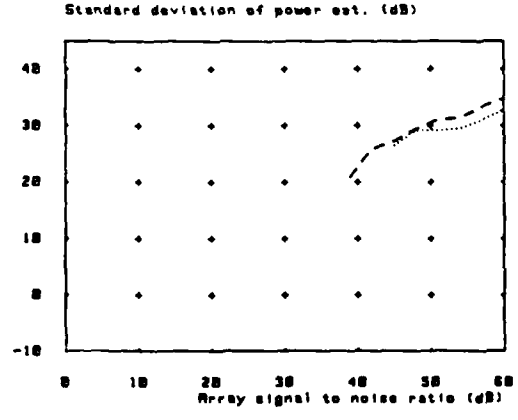

Fig. 19 (cont). Performance statistics as a function of array signal to noise ratio (ASNR) for two signals, located at 7.8 and 7.9 beamwidths from broadside. Results are based on 100 trials at each ASNR, taking 16 snapshots of data from the 16 element 0.5 wavelength spaced linear array. Dotted lines show the results of processing using the MUSIC algorithm (equation (7)) and dashed lines show the results obtained using EPM(k=5)/MUSIC. The continuous line in the plot of angular standard deviation is the Cramér Rao bound.

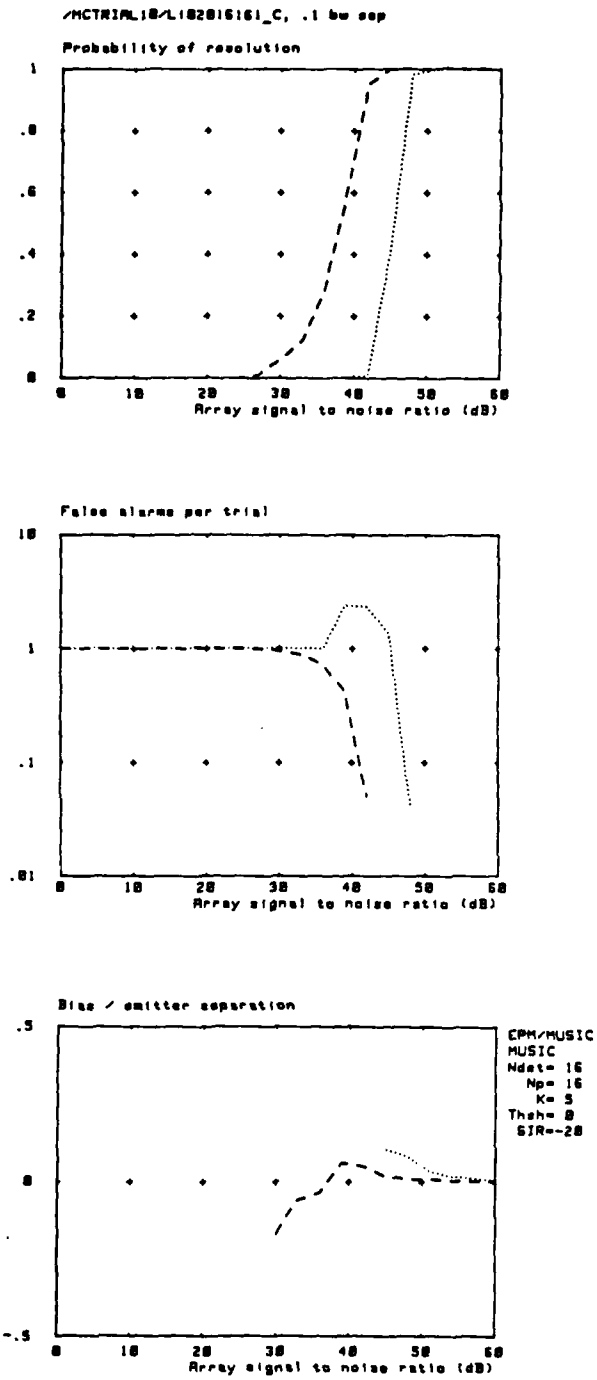

Fig. 20. Performance statistics as a function of array signal to noise ratio (ASNR) for the lower power signal of a pair located at 0 and 0.1 beamwidths from broadside. Signal to interference ratio (SIR) is -20dB. Results are based on 100 trials at each ASNR, taking 16 snapshots of data from the 16 element 0.5 w elength spaced linear array. Dotted lines show the results of processing using the MUSIC algorithm (equation (7)) and dashed lines show the results obtained using EPM(k=5)/MUSIC. Assumed angle of view from -2 to +2 beamwidths.

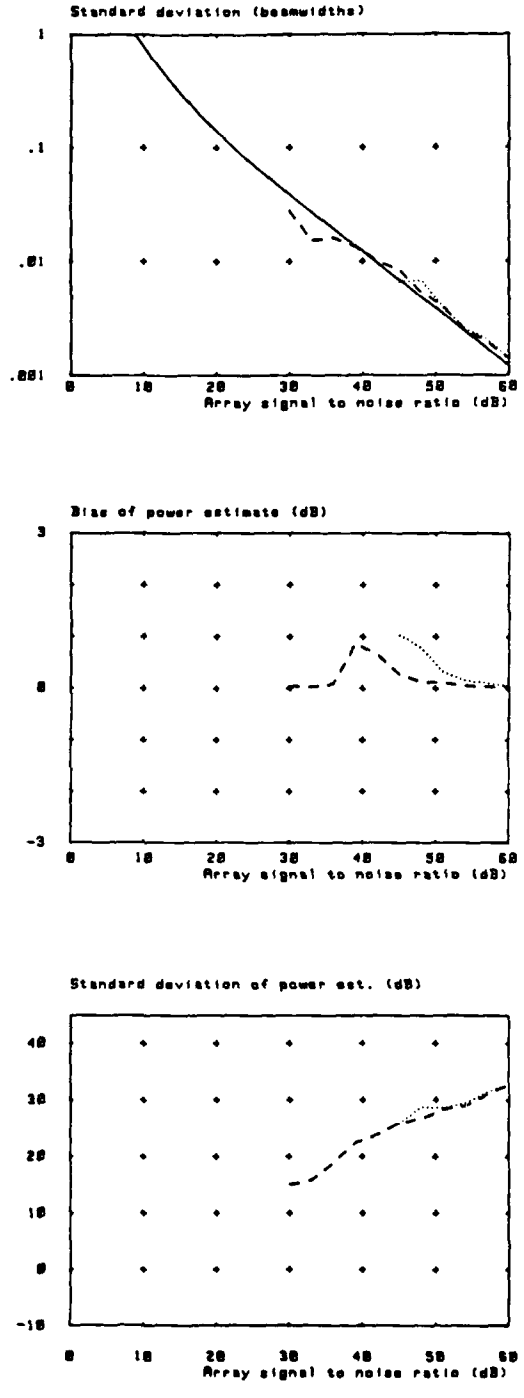

Fig. 20 (cont). Performance statistics as a function of array signal to noise ratio (ASNR) for the lower power signal of a pair located at 0 and 0.1 beamwidths from broadside. Signal to interference ratio (SIR) is -20dB. Results are based on 100 trials at each ASNR, taking 16 snapshots of data from the 16 element 0.5 wavelength spaced linear array. Dotted lines show the results of processing using the MUSIC algorithm (equation (7)) and dashed lines show the results obtained using EPM(k=5)/MUSIC. The continuous line in the plot of angular standard deviation is the Cramér Rao bound.

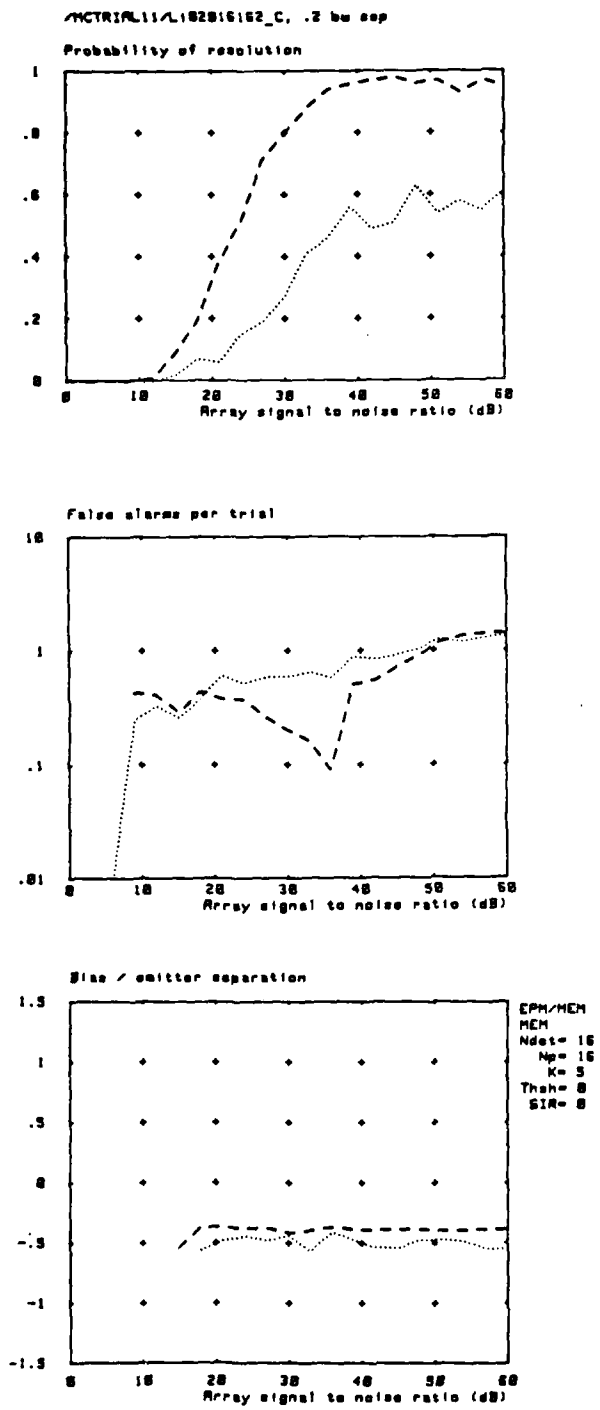

Fig. 21. Performance statistics as a function of array signal to noise ratio (ASNR) for a pair of signals located at 0 and 0.2 beamwidths from broadside. The array calibration is randomly perturbed in amplitude (by up to ±10%, and in phase (by up to ±1%). See Appendix 4 for further details. Results are based on 100 trials at each ASNR, taking 16 snapshots of data from the 16 element 0.5 wavelength spaced linear array. Dotted lines show the results of processing using the MEM algorithm (equation (9)) and dashed lines show the results obtained using EPM(k=5)/MEM (equation (11)). Assumed angle of view from -2 to +2 beamwidths.

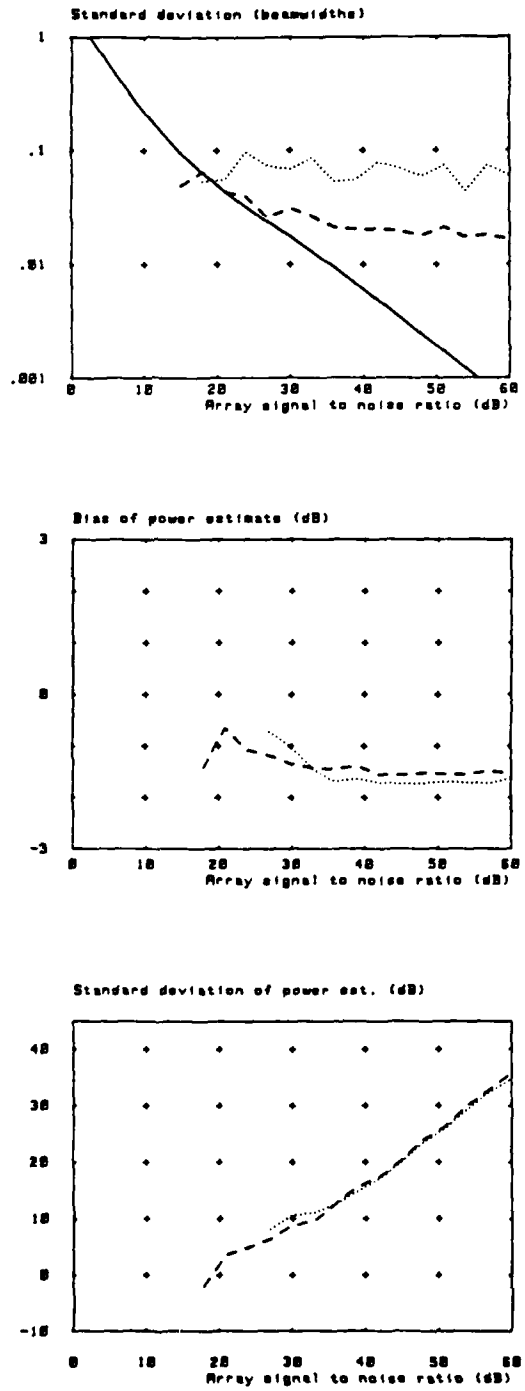

Fig. 21 (cont). Performance statistics as a function of array signal to noise ratio (ASNR) for a pair of signals located at 0 and 0.2 beamwidths from broadside. The array calibration is randomly perturbed, as described in Appendix 4. Results are based on 100 trials at each ASNR, taking 16 snapshots of data from the 16 element 0.5 wavelength spaced linear array. Dotted lines show the results of processing using the MEM algorithm (equation (9)) and dashed lines show the results obtained using EPM(k=5)/MEM (equation (11)). The continuous line in the plot of angular standard deviation is the Cramér Rao bound.

example of two signals, located at 0 and 0.1 beamwidths with respect to broadside. In this case, the ratio of the power of the signal at broadside to that of the signal at 0.1 beamwidths is -20dB, and the ASNR scales in Fig. 20 correspond to the lower power signal. Again, the performance of the basic algorithm is improved through the application of EPM, in this case by the equivalent of approximately 5 or 6dB ASNR. It is also interesting to compare this result with that of Fig. 12 for the case of equal power targets. It can be seen that there has been a slight deterioration in overall performance for both MUSIC and EPM/MUSIC in the present case, in that the false alarm rate is slightly higher and that the probability of resolution curve falls to zero at slightly higher ASNR.

Further results for a range of algorithms, including the z-plane variants, are given in Appendix 3.

5.2.5. ARRAY CALIBRATION ERRORS

The particular high discrimination algorithms referred to in this report are known to be sensitive to errors in the calibration of the antenna array, embodied in the matrix M. In order to investigate the effect of EPM pre-processing under such circumstances, simulations were carried out of 16 snapshots from a 16 element linear array, as used in previous sections, but with ±10% random amplitude weights and ±1% random phase weights across the elements. These weights were chosen from independent rectangular distributions. The particular set of weights used for these simulations is given in Appendix 4, together with results which compare the behaviour of different algorithms.

For illustration in the present section, Fig. 21 shows results obtained for two equal power signals, located at 0 and 0.2 beamwidths away from boresight (as measured on the basis of the assumed uniform calibration). The algorithms used on the data from the mis-calibrated array were MEM and EPM(k=5)/MEM, assuming a field of view extending from -14.5° to $+14.5^{\circ}$.

The presence of errors in the array calibration has caused the performance of MEM to deteriorate considerably. Probability of resolution reaches only around 0.6 for ASNR less than 60dB; false alarm rate is higher than in the accurately calibrated case (as can be seen from Figs. A1.8 and A1.9) and continues to rise with increasing ASNR; standard deviation of the angle estimates declines only gradually with increasing ASNR; and the particular choice of errors in this case has resulted in an almost constant bias of both the angle and power estimates. Pre-processing using EPM increases probability of resolution to greater than 0.9 by 40dB ASNR, reduces the false alarm rate for the same thresholding procedure (although the trend is still rising as ASNR increases), and reduces both standard deviation and bias. Power estimation variance remains virtually unchanged after EPM, following a curve which lies between those for the accurately calibrated case.

Further results, given in Appendix 4, show that the behaviour of MLM is similar to that of MEM under the same circumstances, whilst MUSIC and KT seem to be more robust. However, it is worth noting that these results have been collected for a single perturbed antenna calibration. More work needs to be carried out before general conclusions regarding the relative robustness of algorithms can be derived with certainty.

6. CONCLUSIONS

We have shown how the svd based rank reduction of the constrained calibration matrix, M, leads to a scheme for accelerating the data analysis required by modern high discrimination algorithms such as MUSIC. We have referred to this scheme as an "eigenvector projection method", or EPM. In the spatial resolution problem, the

achievable speed-up depends on the angular limits to the required reconstruction, the degree of spatial oversampling, and the assumed signal to noise ratio. In general, our experiments have indicated that the rank reduction may sometimes be taken to the extreme of choosing only $m+1$ significant basis vectors, where m is the number of signals to be detected, in order to obtain maximum processing economy without degradation of the source reconstruction. The choice of this limit will depend in practice on the number of high power signal sources to be reconstructed, and the range of spatial sampling rates corresponding to the chosen field of view. The simulation results presented here have shown that a substantial decrease in the processing time may be achieved. In addition, a large number of Monte Carlo results have been presented which have demonstrated significant improvements in the ability of a number of high discrimination algorithms to extract signal parameters from noisy data, following processing by EPM. Furthermore, EPM processing has been observed to have a beneficial effect on data taken from an array whose calibration was randomly perturbed. Following consideration of the consistency of our Monte Carlo results, we have concluded that the performance of svd-based algorithms, for a perfectly calibrated array, is limited primarily by the cross-correlation between the signals and the additive noise, as perceived through a limited number of snapshots. Finally, we note that, although demonstrated here using linear arrays, EPM is equally applicable to alternative array geometries.

REFERENCES

[1] Mather, J.L.
Least squares solutions in signal processing using the singular value decomposition.
Royal Signals and Radar Establishment Memorandum no. 3864, (1986).

[2] Brent, R.P., Luk, F.T., van Loan, C.F.
Computation of the singular value decomposition using mesh-connected processors.
J. VLSI and Comp. Sys. 1(3), 242-270, (1985).

[3] Gabriel, W.F.
Tracking closely spaced multiple sources via spectral estimation techniques.
NRL Report 8603, (1982).

[4] Clarke, I.J., de Villiers, G.D., Mather, J.L.
Resolution limits of a two dimensional antenna array.
Proc. SPIE, 564, 15-22, (1985).

[5] Mather, J.L., Clarke, I.J.
Sequential processing of multiple data domains using SVD.
Proc. Inst. Acoust. 7(4), 9-15, (1985).

[6] Schmidt, R.O.
Multiple emitter location and signal parameter estimation.
RADC Spectrum Estimation Workshop, 243-258, (1979).

[7] Lawson, C.L., Hanson, R.J.
Solving least squares problems
Englewood Cliffs, N.J., Prentice Hall, 1974.

[8] Varah, J.M.
On the numerical solution of ill-conditioned linear systems with applications to ill-posed problems.
SIAM J. Numer. Anal. 10(2), 257-267, (1973).

[9] Kumaresan, R., Tufts, D.W.
Estimating angles of arrival of multiple plane waves.
IEEE Trans. AES-19(1), 134-139, (1983).

[10] Capon, J., Greenfield, R.J., Kolker, R.J.
Multidimensional maximum likelihood processing of a large aperture seismic array.
Proc. IEEE 55(2), 192-211, (1967).

[11] Burg, J.P.
The relationship between maximum entropy spectra and maximum likelihood spectra.
Geophysics 37(2), 375-376, (1972).

[12] Wilkinson, J.H., Reinsch, C.
Linear Algebra Handbook for Automatic Computation, vol 2.
Springer Verlag, 1971.

[13] Barabell, A.J., Capon, J., DeLong, D.F., Johnson, J.R., Senne, K.D.
Performance comparison of superresolution array processing algorithms.
MIT Lincoln Lab. Project report TST-72, 9 May 1984.

[14] Mather, J.L.
Beamforming pre-processors for high discrimination algorithms: a Monte Carlo investigation.
Royal Signals and Radar Establishment Memorandum, in preparation.

[15] Barabell, A.J.
Improving the resolution performance of eigenstructure-based direction-finding algorithms.
IEEE Proc. Int. Conf. Acoustics Speech Signal Processing 1, 336-339, (1983).

[16] van Trees, H.L.
Detection, estimation, and modulation theory, I.
Wiley, N.Y., 1968.

[17] Hudson, J.E.
Adaptive array principles.
IEE Electromagnetic Waves Series 11, Peter Perigrinus, 1981.

[18] Gething, P.J.D.
Optimum solution for multiple emitter location.
IEEE Trans AP-35(7), 876, (1987).

APPENDIX 1. MONTE CARLO RESULTS: TWO TARGETS CLOSE TO BROADSIDE

Contained in this appendix are a number of results relating to the problem described in section 5.2.2. Data from a uniformly weighted 16 element 0.5 wavelength spaced linear array, receiving signals from two far-field random phase point sources, has been simulated and analysed by a variety of high discrimination algorithms and their EPM pre-processed counterparts. Results, in terms of probability of resolution, false alarm rate, and bias and variance of the resolved angle and power estimates, are plotted in a variety of ways as follows:

Section A1.1: all as a function of array signal to noise ratio (ASNR) for a variety of angular separations.
Section A1.2: probability of resolution as a function of the average ratio of second to third eigenvalue of the data covariance estimate.
Section A1.3: all as a function of angular separation for a given ASNR.
Section A1.4: probability of resolution and false alarm rate as a function of noise threshold, parameterised by ASNR.

Each set of plots corresponds to results from a particular group of algorithms, as follows:

A:	MUSIC -----	B:	EPM(k=5)/MUSIC	C:	EPM(k=3)/MUSIC
	KT ·····		EPM(k=5)/KT		EPM(k=3)/KT
	MEM -·-·-·-		EPM(k=5)/MEM		EPM(k=3)/MEM
	MLM —-—-—		EPM(k=5)/MLM		EPM(k=3)/MLM

D:	ROOT-MUSIC	E:	EPM(k=5)/ROOT-MUSIC
	ROOT-KT		EPM(k=5)/ROOT-KT
	ROOT-MEM		EPM(k=5)/ROOT-MEM
	ROOT-MLM		EPM(k=5)/ROOT-MLM

A1.1. RESULTS AS A FUNCTION OF ASNR

The results as a function of ASNR are plotted as follows:

Figure	Methods	Number of snapshots	Location of signals (beamwidths from boresight)
A1.1	A	16	0, 0.1
A1.2	B		
A1.3	C		
A1.4	D		
A1.5	E		
A1.6	A	5	
A1.7	B		
A1.8	A	16	0, 0.2
A1.9	B		
A1.10	C		
A1.11	D		
A1.12	E		
A1 13	A	5	
A1.14	B		

A1.15	A	16	0, 0.3
A1.16	B		
A1.17	C		
A1.18	A	5	
A1.19	B		
A1.20	A	16	0, 0.4
A1.21	B		
A1.22	A	5	
A1.23	B		

Comparing Figs. 1.1 and 1.7, for example, we see that EPM(k=5) pre-processing causes algorithms to perform at least as well for 5 snapshots in this situation as do the straightforward algorithms for 16 snapshots.

A1.2. RESULTS AS A FUNCTION OF EIGENVALUE RATIO

Since the high discrimination algorithms under consideration depend on the separation of signals as perceived from the point of view of the eigen basis of the estimated covariance matrix, it was thought that plotting against some measure based on the average eigenvalue spectrum might allow a more compact representation of the statistical results. Qualitatively, one might expect that the likelihood of successful resolution would depend on the separation of the signal subspace eigenvalues from those of the noise space [1]. In particular, for the case of two partially correlated signals investigated here, the magnitude of the second eigenvalue with respect to the noise background is clearly important. We have therefore plotted our results as a function of $E(2)/E(3)$, where E(2) and E(3) are, respectively, the averages of the second and third eigenvalues of the covariance matrix. In the case of the EPM pre-processed methods, the eigenvalues are those of the reduced size covariance matrix.

A selection of the probability of resolution results as a function of eigenvalue ratio are plotted as follows:

Figure	Methods	Number of snapshots	Location of signals (beamwidths from boresight)
A1.24	A	16	0, 0.1
A1.25	B		
A1.26	C		
A1.27	A	5	
A1.28	B		
A1.29	A	16	0, 0.2
A1.30	B		
A1.31	C		
A1.32	A	5	
A1.33	B		
A1.34	A	16	0, 0.3
A1.35	B		
A1.36	C		
A1.37	A	5	
A1.38	B		

For a given number of snapshots and angular separation MUSIC, for example, achieves a high probability of resolution for approximately the same eigenvalue ratio in both normal and EPM forms. However, in general, as can be seen from these plots, the eigenvalue ratio required for resolution is a function both of signal separation and number of snapshots, the latter corresponding to "separation" or decorrelation in the time domain (both between the signals themselves and the noise background - see Appendix 7). We therefore appear not to have a convenient means of compressing our statistical results.

A1.3. RESULTS AS A FUNCTION OF ANGULAR SEPARATION

A selection of results have been replotted as a function of angular separation for a given ASNR, as follows:

Figure	Methods	Number of snapshots	ASNR (dB)
A1.39	A	16	21
A1.40	B		
A1.41	A	5	
A1.42	B		

A1.4. RESULTS AS A FUNCTION OF NOISE THRESHOLD

Further to the example given in Figs. 12 to 14, described in section 5.2.2, we present a few plots of probability of resolution and false alarm rate as a function of noise power threshold and ASNR for a given angular separation. The results are as follows:

Figure	Method	Number of snapshots	Location of signals (beamwidths from boresight)
A1.43	MUSIC	16	0, 0.1
A1.44	EPM(k=5)/MUSIC		
A1.45	KT		
A1.46	EPM(k=5)/KT		
A1.47	MEM		
A1.48	EPM(k=5)/MEM		
A1.49	MLM		
A1.50	EPM(k=5)/MLM		

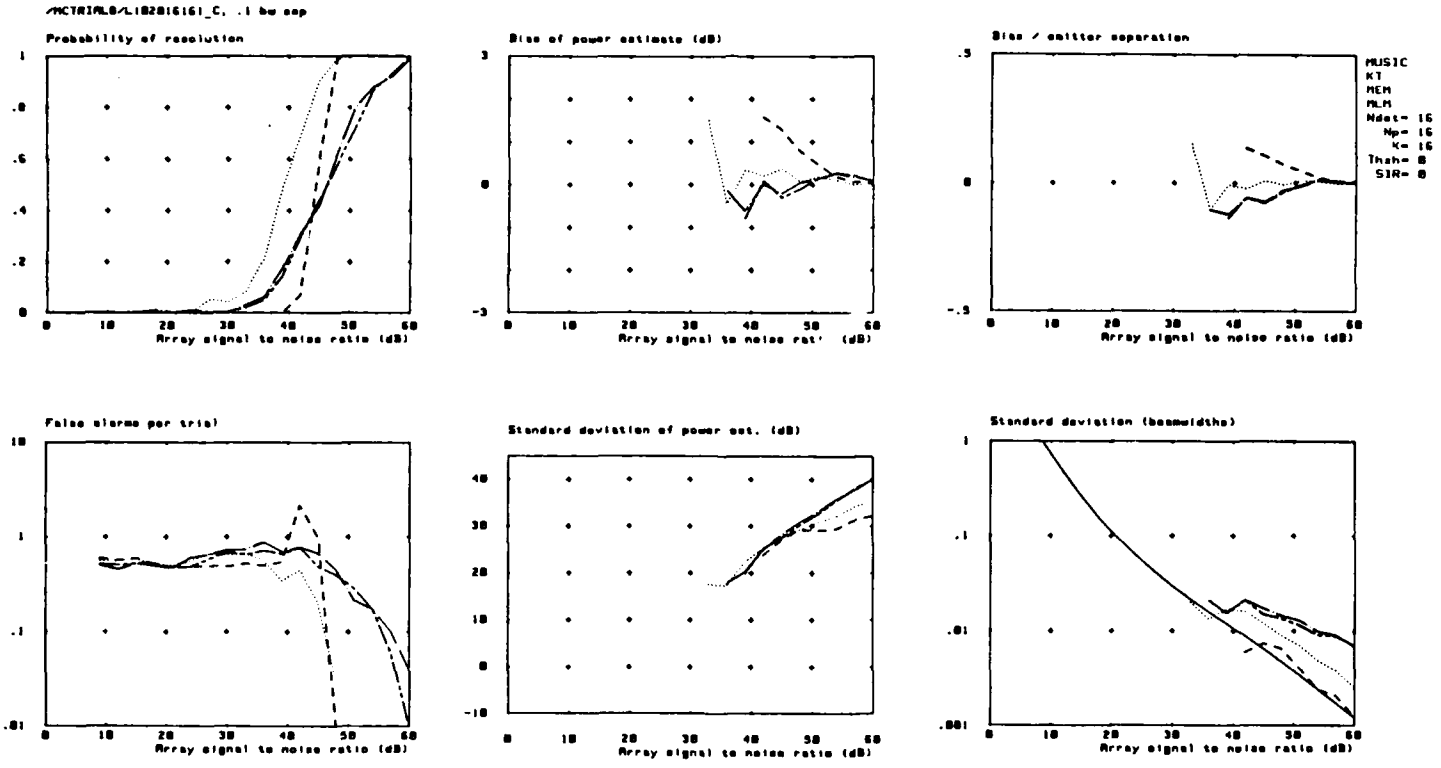
Probability of resolution
Bias of power estimate (dB)
Bias / emitter separation
MUSIC
KT
MEM
MLM
Ndet= 16
Np= 16
K= 16
Thsh= 0
SIR= 0
False alarms per trial
Standard deviation of power est. (dB)
Standard deviation (beamwidths)
Array signal to noise ratio (dB)

Fig. A1.1

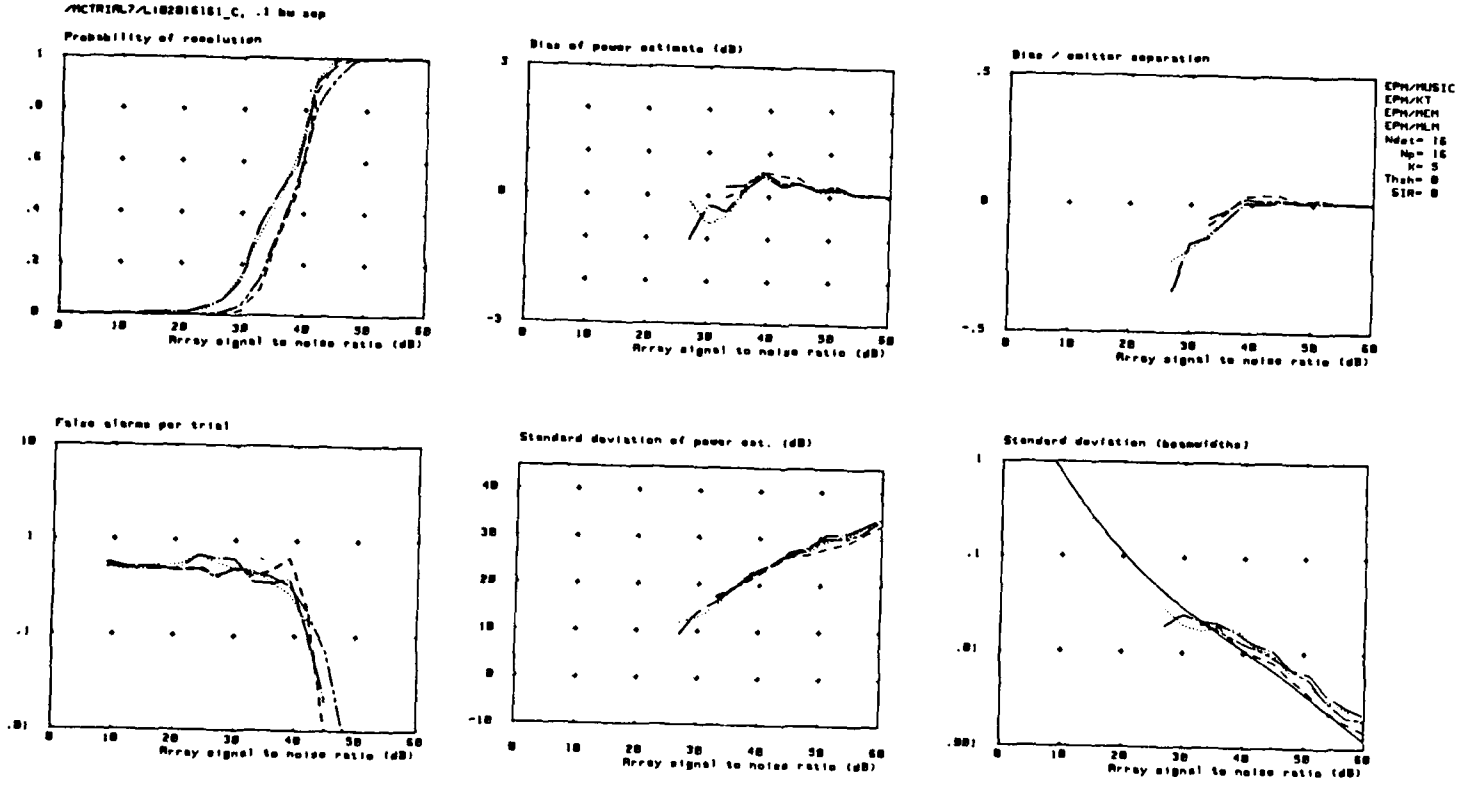
Probability of resolution
Bias of power estimate (dB)
Bias / emitter separation
EPH/MUSIC
EPH/KT
EPH/MEM
EPH/MLM
Ndat= 16
Np= 16
K= 5
Thsh= 0
SIR= 0
False alarms per trial
Standard deviation of power est. (dB)
Standard deviation (beamwidths)
Array signal to noise ratio (dB)

Fig. A1.2

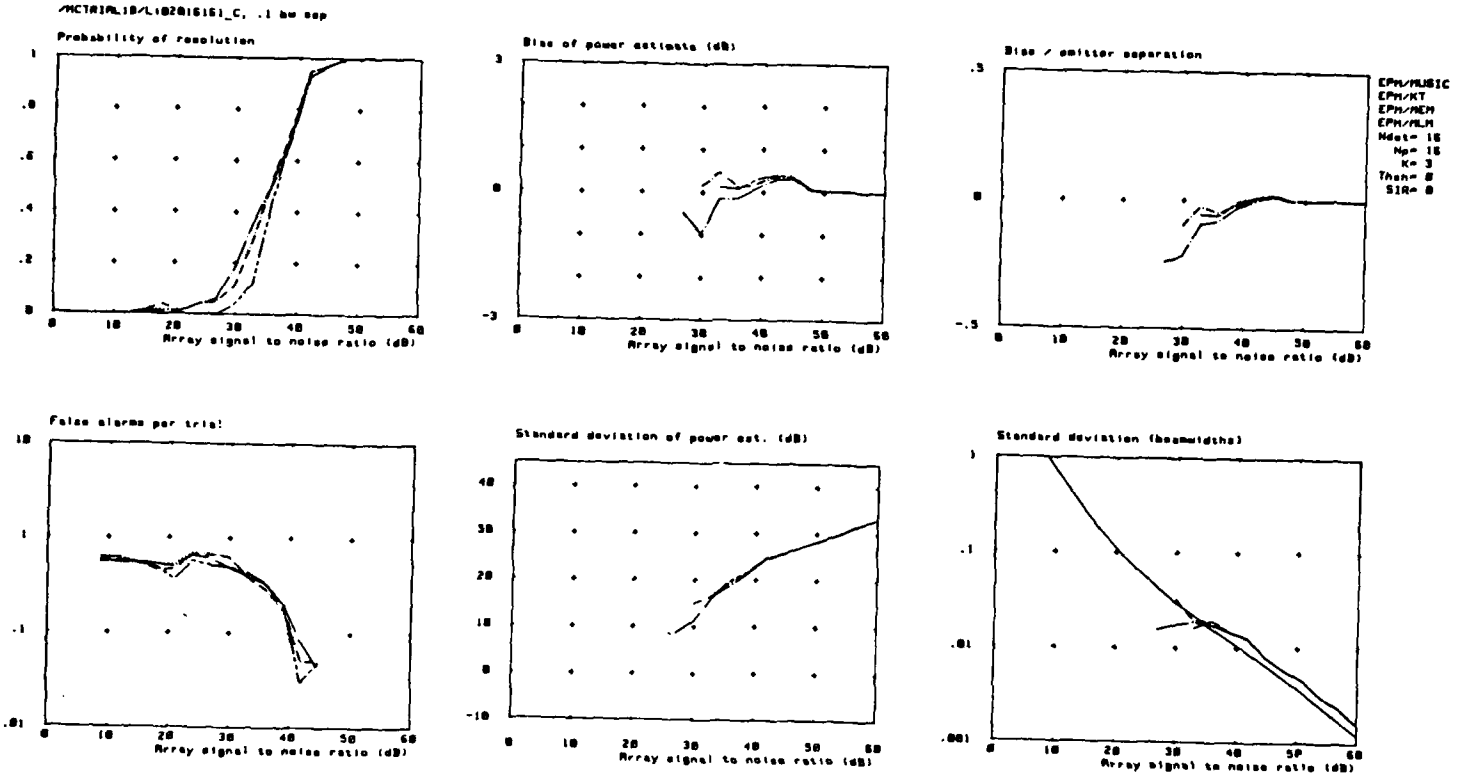
Probability of resolution
Array signal to noise ratio (dB)
Bias of power estimate (dB)
Array signal to noise ratio (dB)
Bias / emitter separation
Array signal to noise ratio (dB)
EPH/MUSIC
EPH/KT
EPH/MEM
EPH/MLM
Ndat= 16
Np= 16
K= 3
Thsn= 0
SIR= 0
False alarms per trial
Array signal to noise ratio (dB)
Standard deviation of power est. (dB)
Array signal to noise ratio (dB)
Standard deviation (beamwidths)
Array signal to noise ratio (dB)

Fig. A1.3

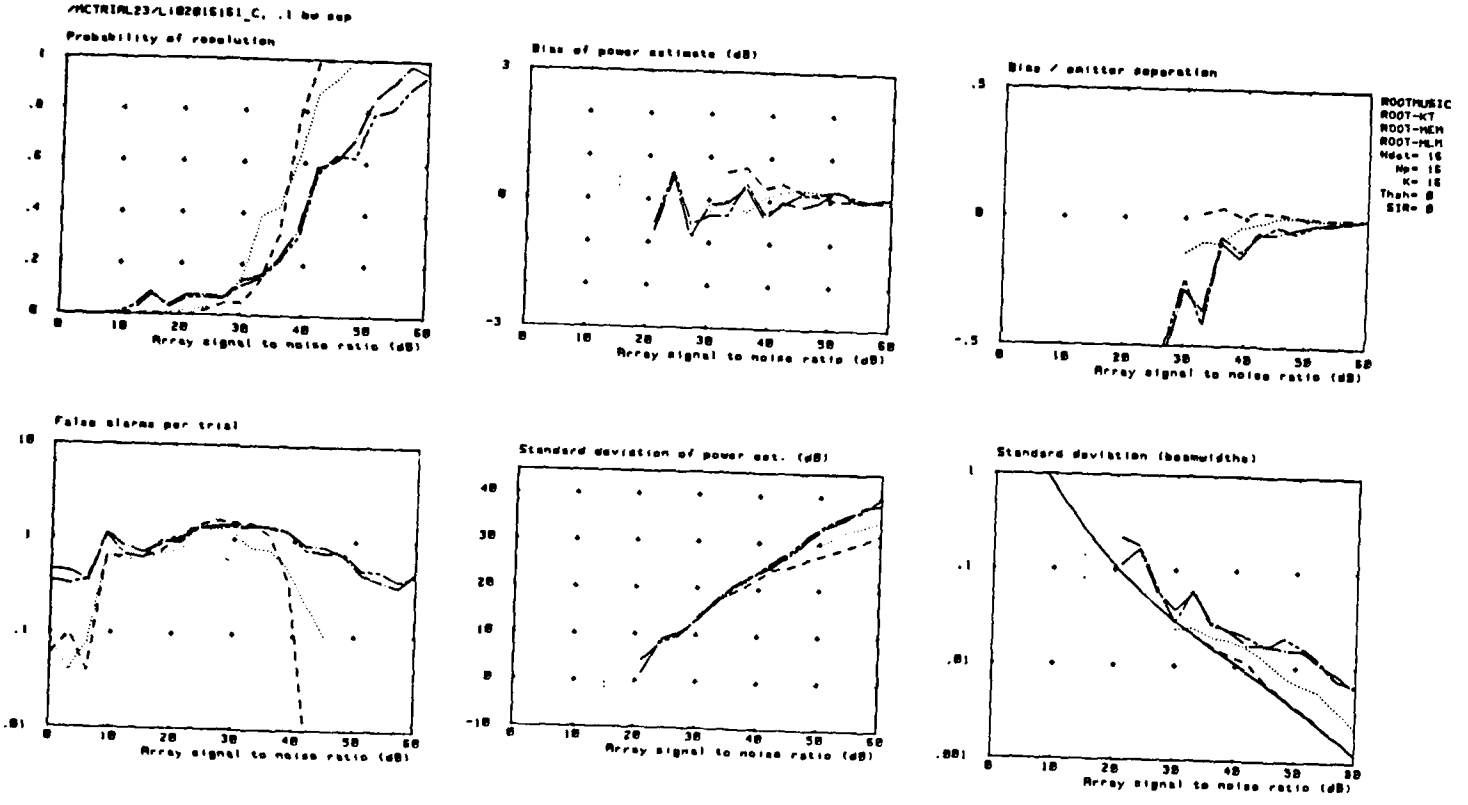
Probability of resolution
Bias of power estimate (dB)
Bias / emitter separation
ROOTMUSIC
ROOT-KT
ROOT-MEM
ROOT-MLM
False alarms per trial
Standard deviation of power est. (dB)
Standard deviation (beamwidths)
Array signal to noise ratio (dB)

Fig. A1.4

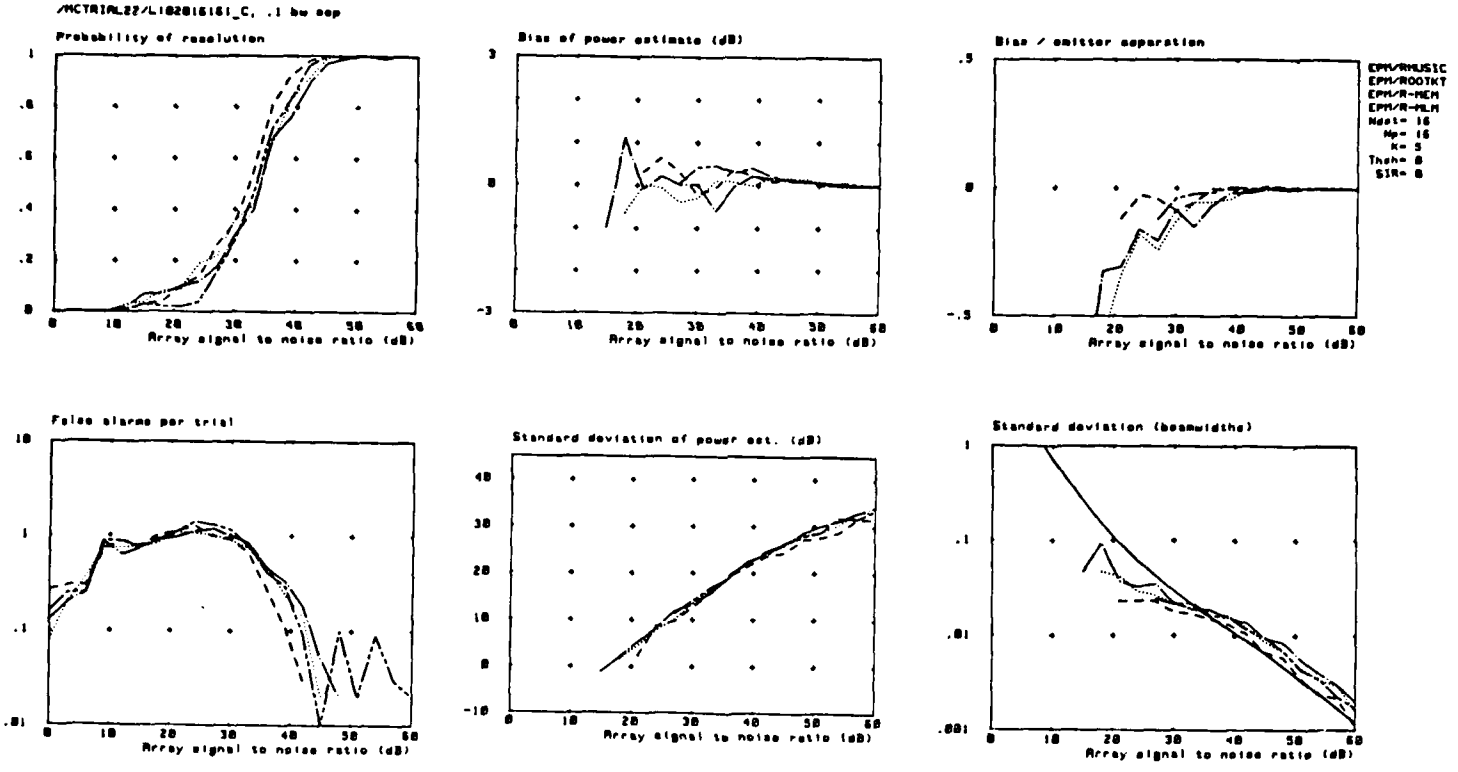
/MCTRIAL22/LI82816161_C, .1 bw sep
Probability of resolution
Bias of power estimate (dB)
Bias / emitter separation
EPM/MUSIC
EPM/ROOTKT
EPM/R-MEM
EPM/R-MLM
False alarms per trial
Standard deviation of power est. (dB)
Standard deviation (beamwidths)
Array signal to noise ratio (dB)

Fig. A1.5

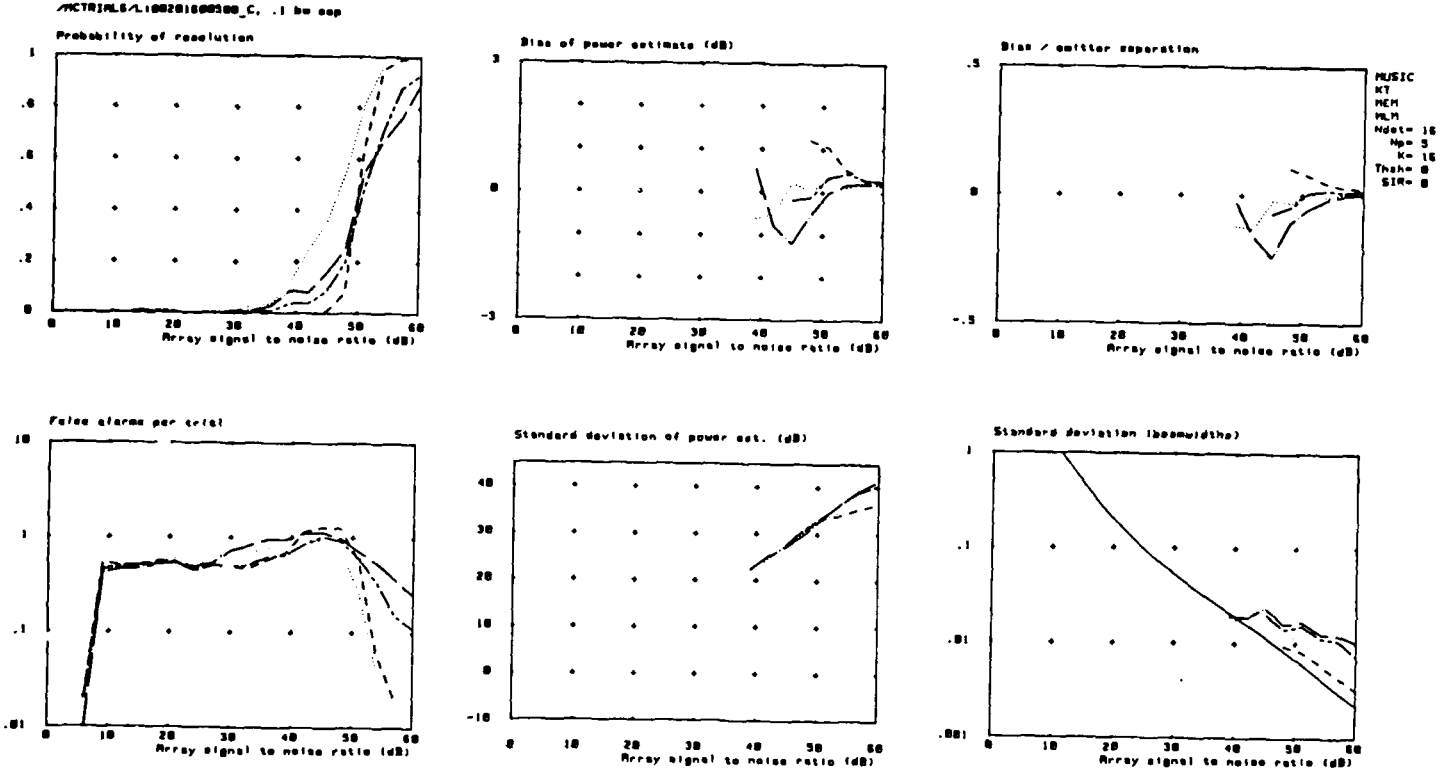
Probability of resolution
Array signal to noise ratio (dB)
Bias of power estimate (dB)
Array signal to noise ratio (dB)
Bias / emitter separation
Array signal to noise ratio (dB)
MUSIC
MLM
False alarms per trial
Array signal to noise ratio (dB)
Standard deviation of power est. (dB)
Array signal to noise ratio (dB)
Standard deviation (beamwidths)
Array signal to noise ratio (dB)

Fig. A1.6

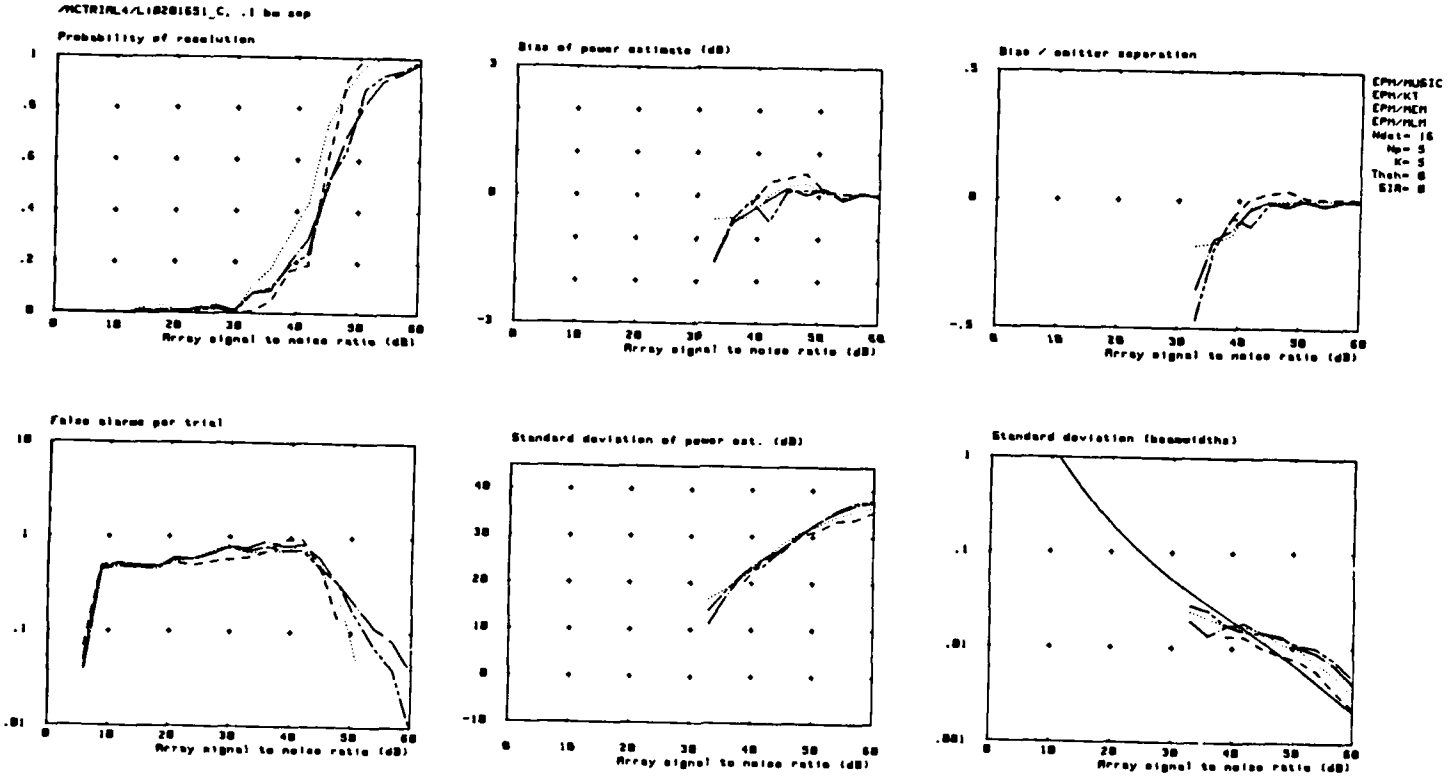
Probability of resolution
Array signal to noise ratio (dB)
Bias of power estimate (dB)
Array signal to noise ratio (dB)
Bias / emitter separation
EPM/MUSIC
EPM/KT
EPM/MEM
EPM/MLM
Array signal to noise ratio (dB)
False alarms per trial
Array signal to noise ratio (dB)
Standard deviation of power est. (dB)
Array signal to noise ratio (dB)
Standard deviation (beamwidths)
Array signal to noise ratio (dB)

Fig. A1.7

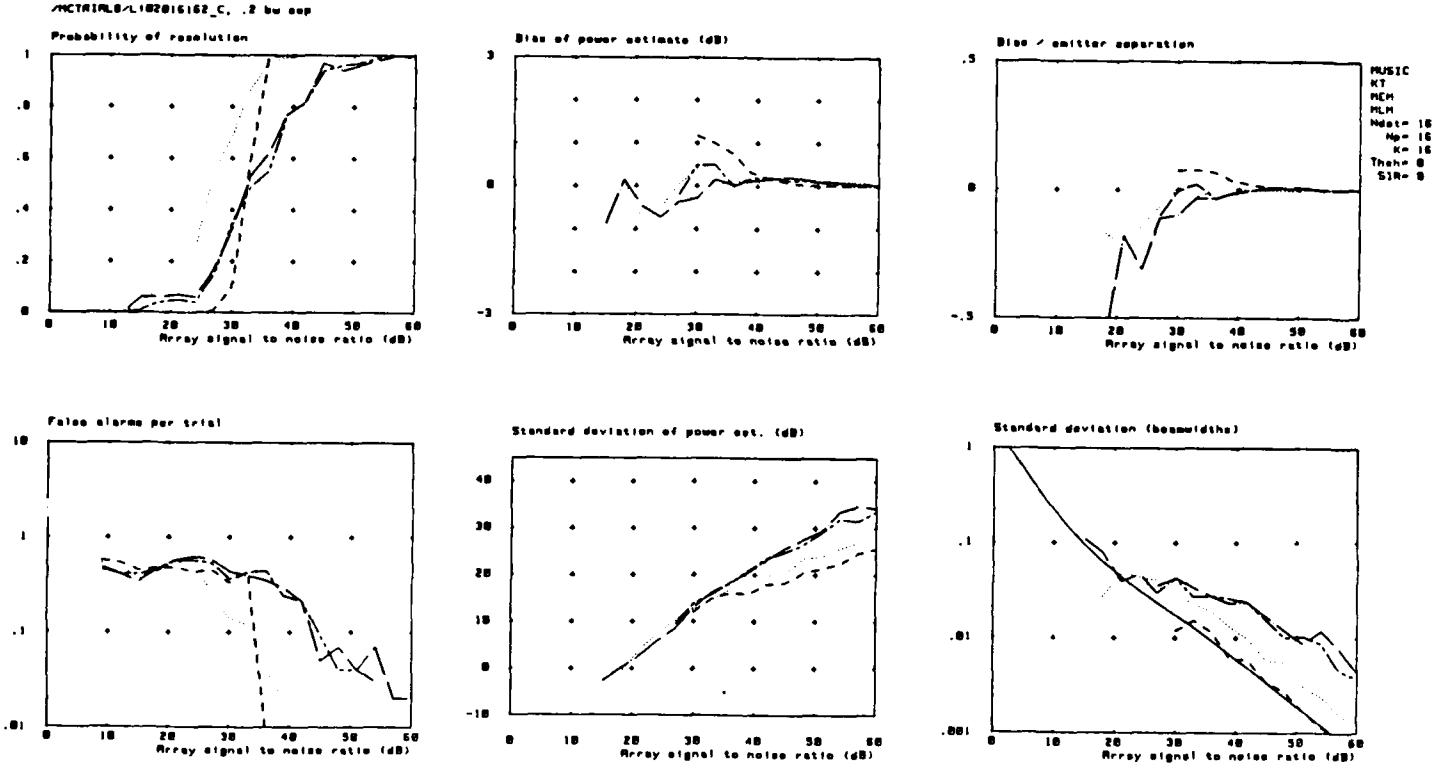
Probability of resolution
Bias of power estimate (dB)
Bias / emitter separation
MUSIC
KT
MEM
MLM
False alarms per trial
Standard deviation of power est. (dB)
Standard deviation (beamwidths)
Array signal to noise ratio (dB)

Fig. A1.8

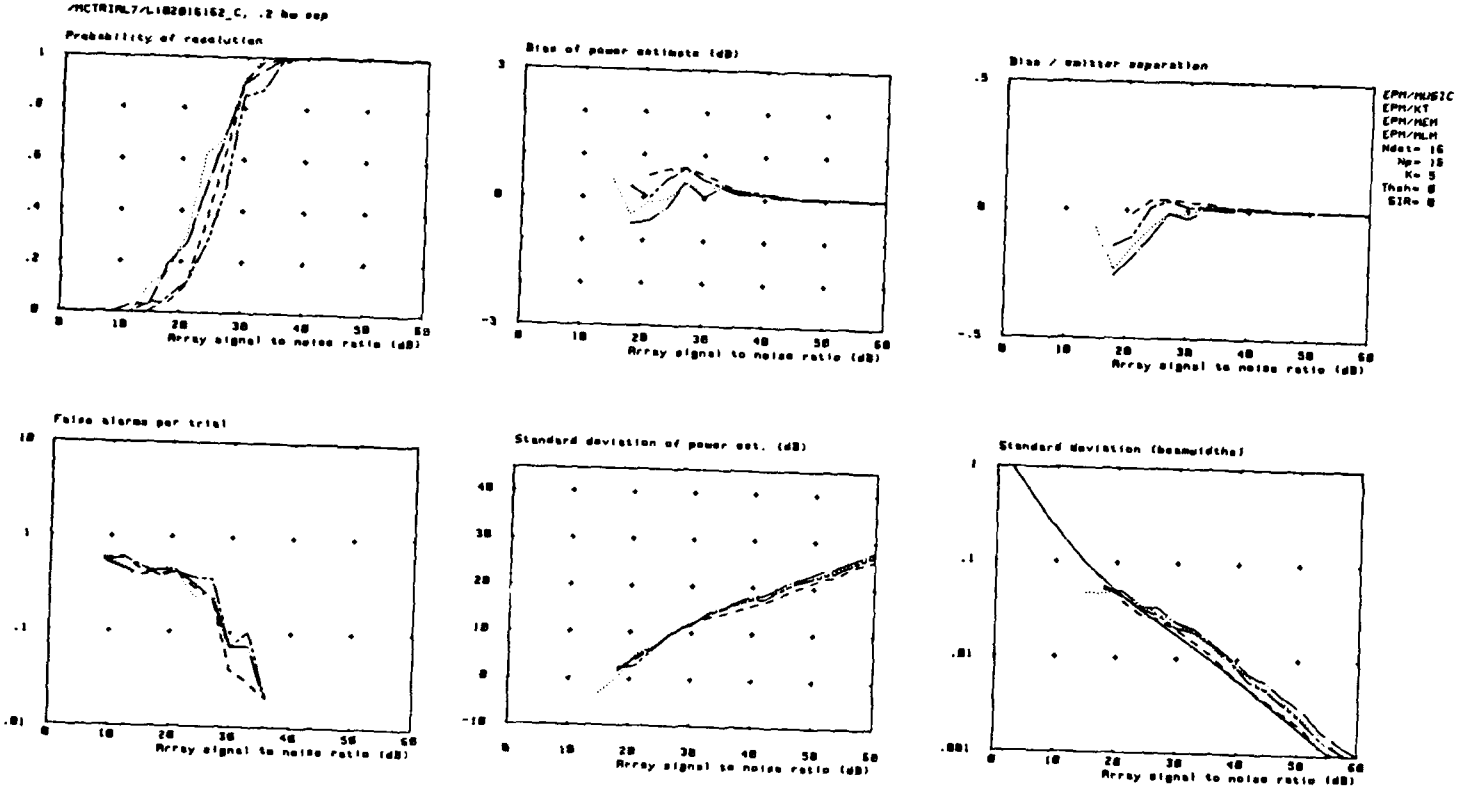
Probability of resolution
Bias of power estimate (dB)
Bias / emitter separation
EPM/MUSIC
EPM/KT
EPM/MEM
EPM/MLM
False alarms per trial
Standard deviation of power est. (dB)
Standard deviation (beamwidths)
Array signal to noise ratio (dB)

Fig. A1.9

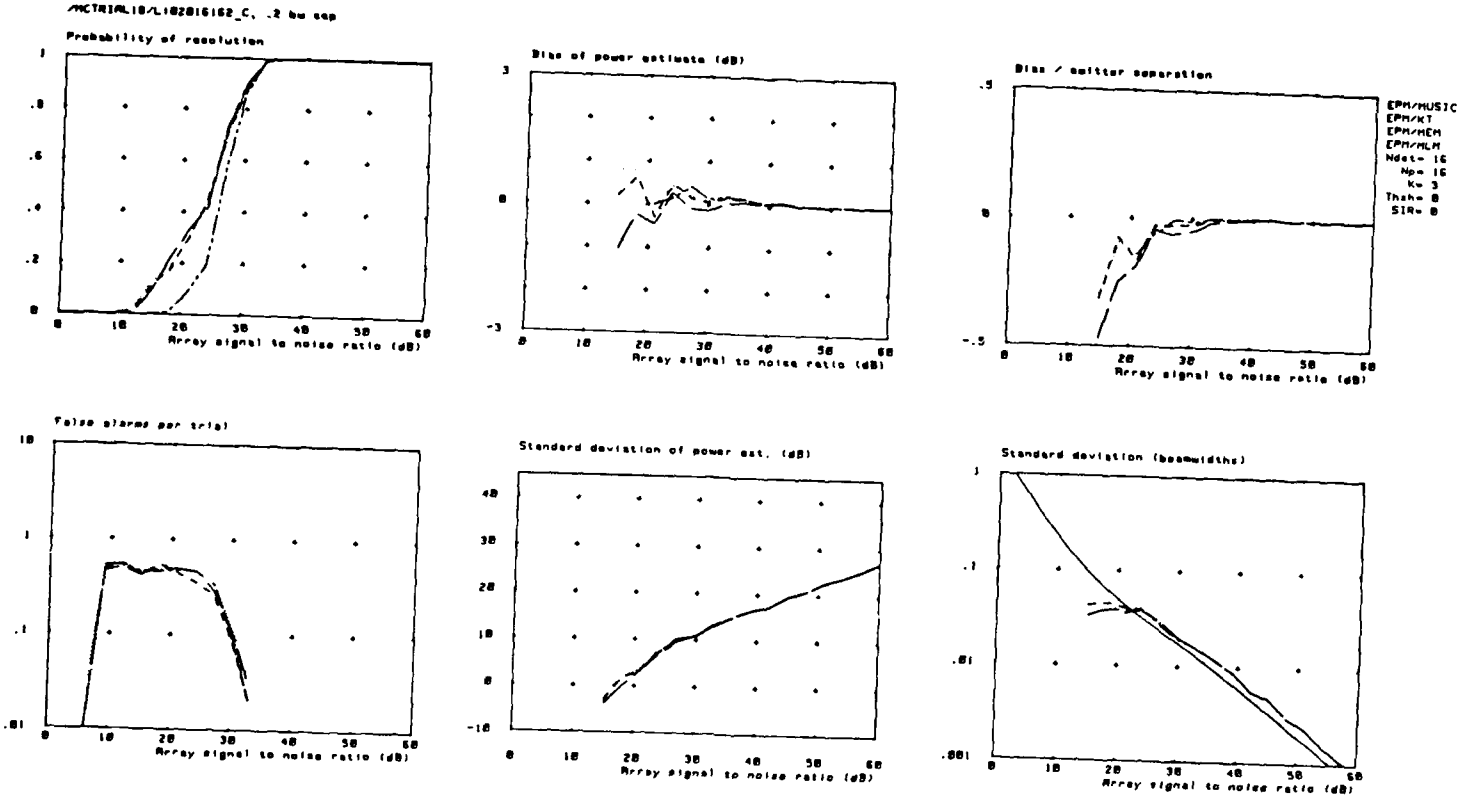
Probability of resolution
Bias of power estimate (dB)
Bias / emitter separation
EPM/MUSIC
EPM/RT
EPM/MEM
EPM/MLM
Ndet= 16
Npo= 16
Ks= 3
Thsh= 8
SIR= 8
False alarms per trial
Standard deviation of power est. (dB)
Standard deviation (beamwidths)
Array signal to noise ratio (dB)

Fig. A1.10

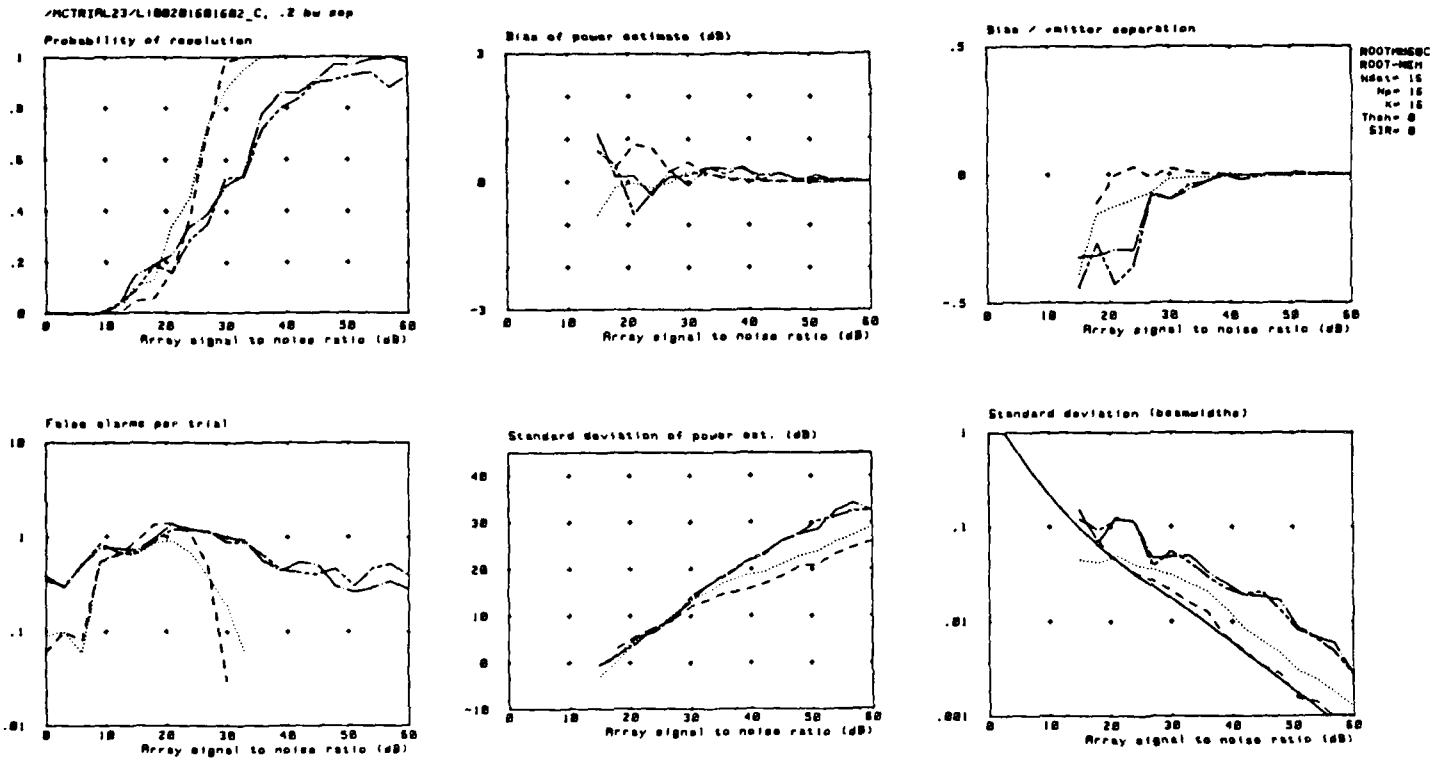
Probability of resolution
Array signal to noise ratio (dB)
Bias of power estimate (dB)
Array signal to noise ratio (dB)
Bias / emitter separation
Array signal to noise ratio (dB)
False alarms per trial
Array signal to noise ratio (dB)
Standard deviation of power est. (dB)
Array signal to noise ratio (dB)
Standard deviation (beamwidths)
Array signal to noise ratio (dB)

Fig. A1.11

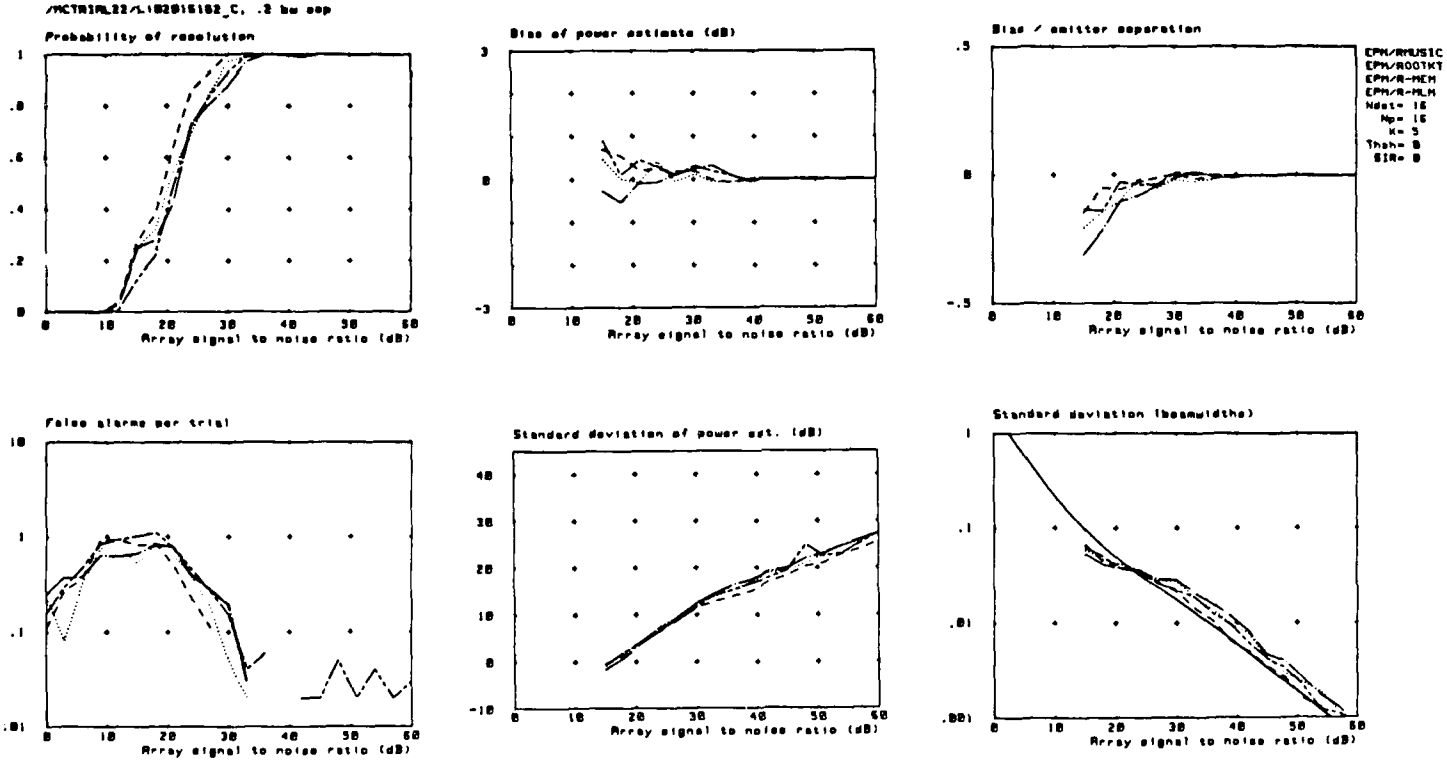
Probability of resolution
Array signal to noise ratio (dB)
Bias of power estimate (dB)
Array signal to noise ratio (dB)
Bias / emitter separation
EPM/MUSIC
EPM/ROOTKT
EPM/R-MEM
EPM/R-MLM
Array signal to noise ratio (dB)
False alarms per trial
Array signal to noise ratio (dB)
Standard deviation of power est. (dB)
Array signal to noise ratio (dB)
Standard deviation (beamwidths)
Array signal to noise ratio (dB)

Fig. A1.12

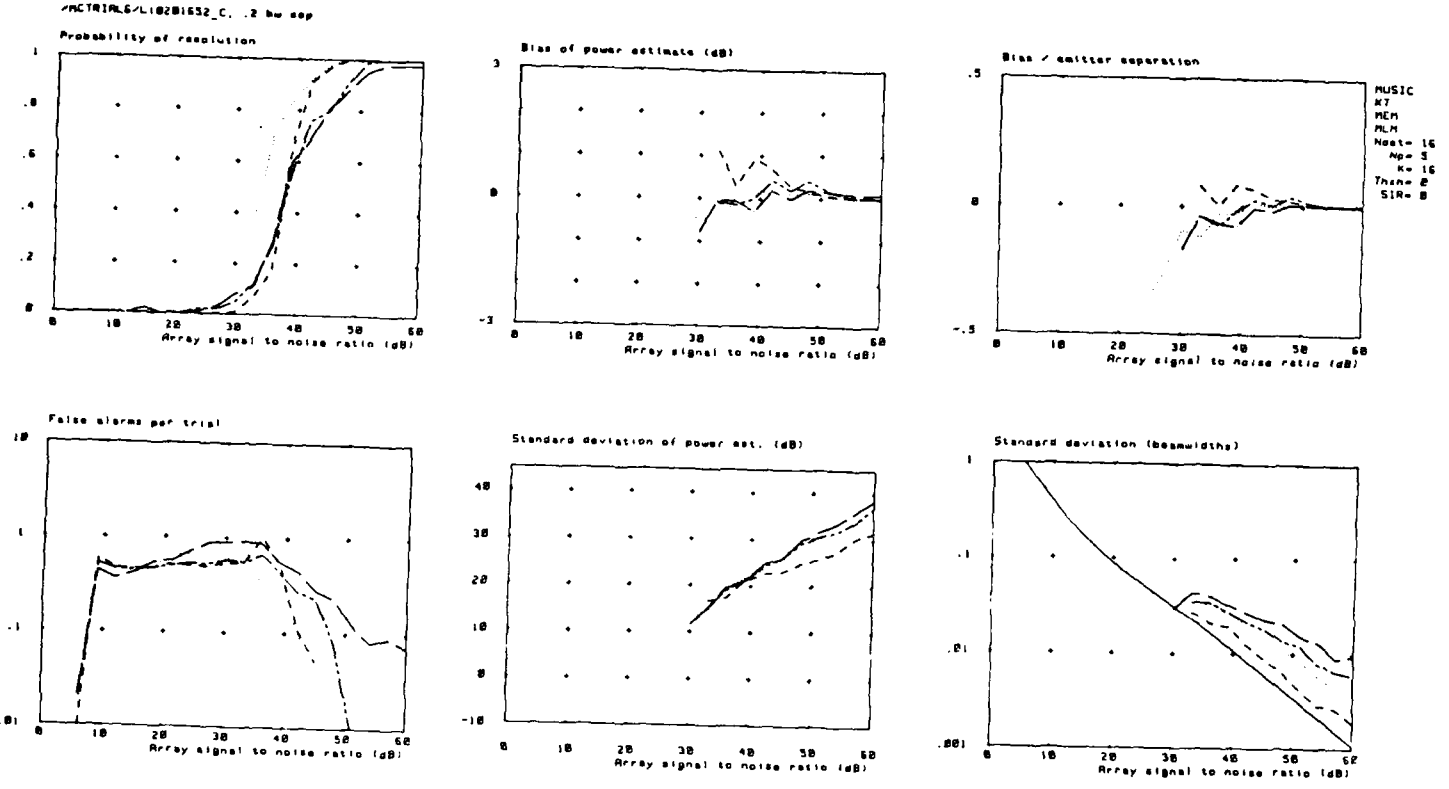
Probability of resolution
Array signal to noise ratio (dB)
Bias of power estimate (dB)
Array signal to noise ratio (dB)
Bias / emitter separation
Array signal to noise ratio (dB)
MUSIC
K7
MEM
MLM
False alarms per trial
Array signal to noise ratio (dB)
Standard deviation of power est. (dB)
Array signal to noise ratio (dB)
Standard deviation (beamwidths)
Array signal to noise ratio (dB)

Fig. A1.13

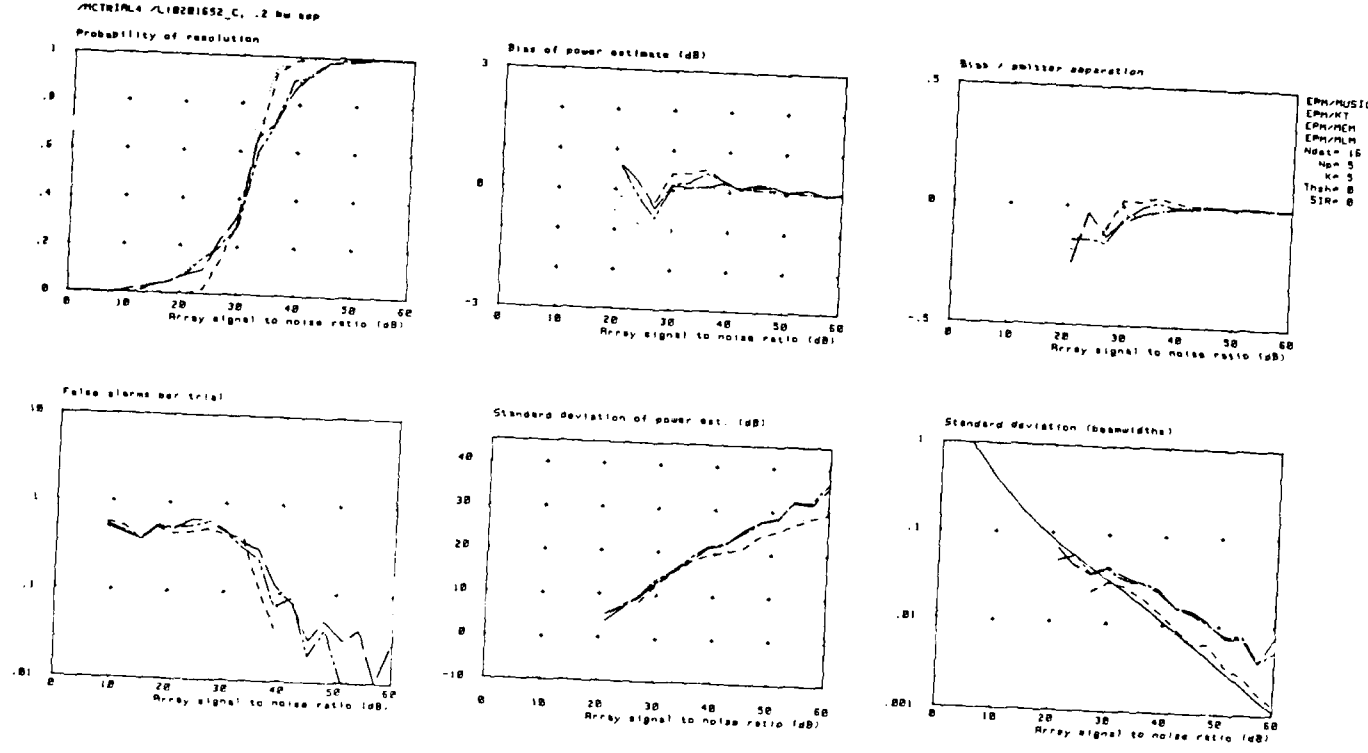
Probability of resolution
Bias of power estimate (dB)
Bias / emitter separation
EPM/MUSIC
EPM/KT
EPM/MEM
EPM/ALM
False alarms per trial
Standard deviation of power est. (dB)
Standard deviation (beamwidths)
Array signal to noise ratio (dB)

Fig. A1.14

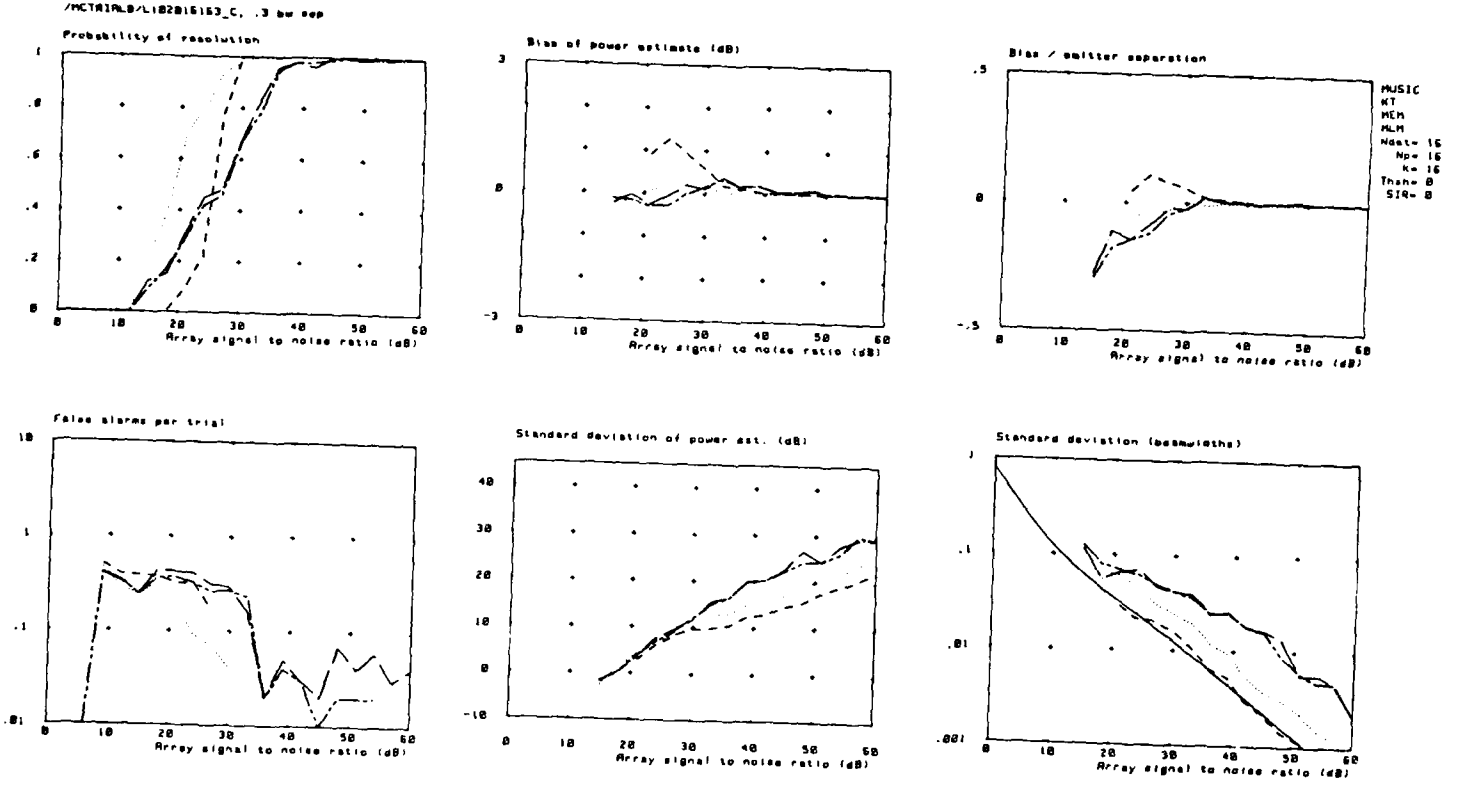
/MCTRIRLB/L1B2B1S1S3_C, .3 bw sep
Probability of resolution
Array signal to noise ratio (dB)
Bias of power estimate (dB)
Array signal to noise ratio (dB)
Bias / emitter separation
MUSIC
KT
MEM
MLM
Ndat= 16
Np= 16
K= 16
Thsh= 0
SIR= 0
Array signal to noise ratio (dB)
False alarms per trial
Array signal to noise ratio (dB)
Standard deviation of power est. (dB)
Array signal to noise ratio (dB)
Standard deviation (beamwidths)
Array signal to noise ratio (dB)

Fig. A1.15

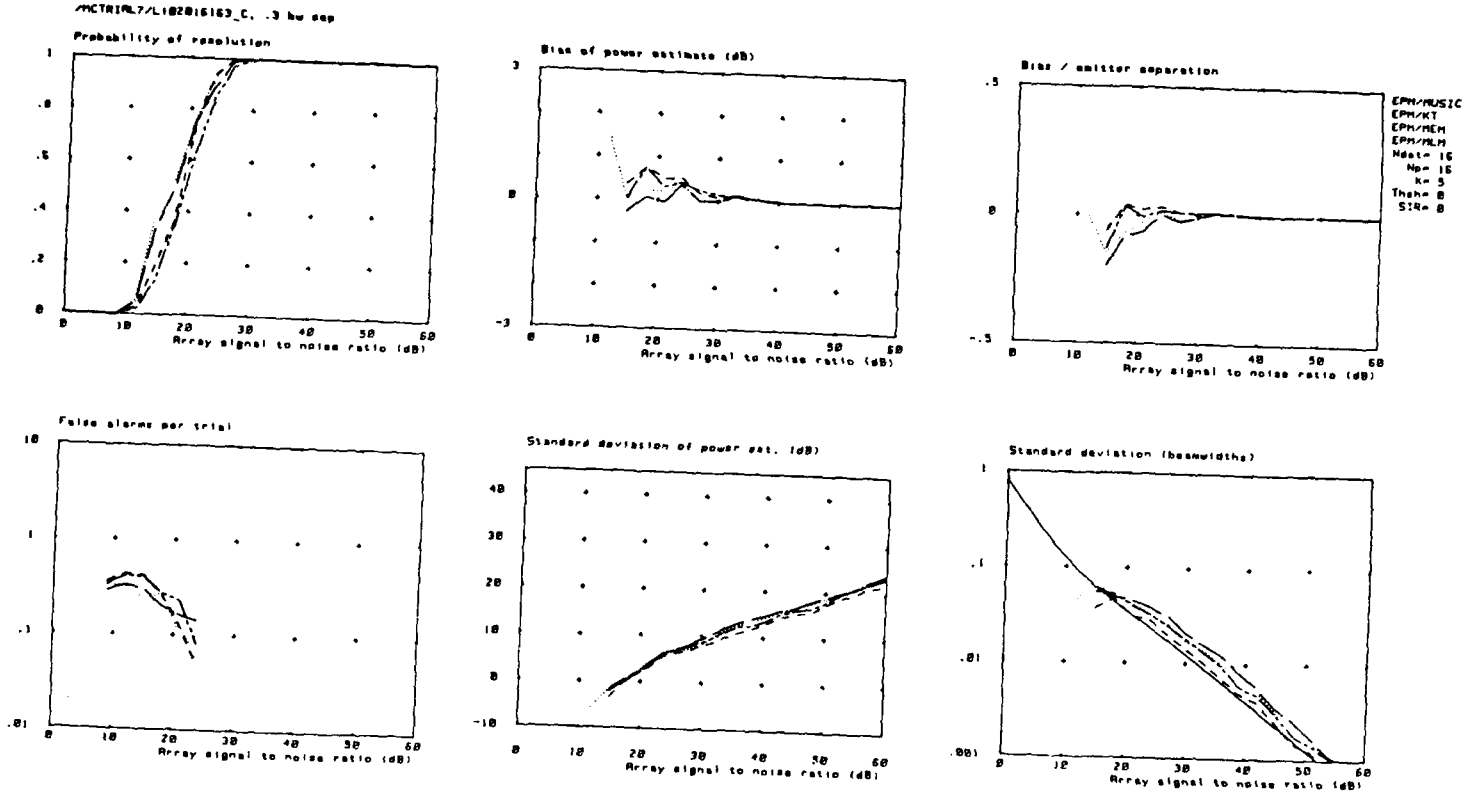
Probability of resolution
Array signal to noise ratio (dB)
Bias of power estimate (dB)
Array signal to noise ratio (dB)
Bias / emitter separation
EPM/MUSIC
EPM/KT
EPM/MEM
EPM/MLM
Array signal to noise ratio (dB)
False alarms per trial
Array signal to noise ratio (dB)
Standard deviation of power est. (dB)
Array signal to noise ratio (dB)
Standard deviation (beamwidths)
Array signal to noise ratio (dB)

Fig. A1.16

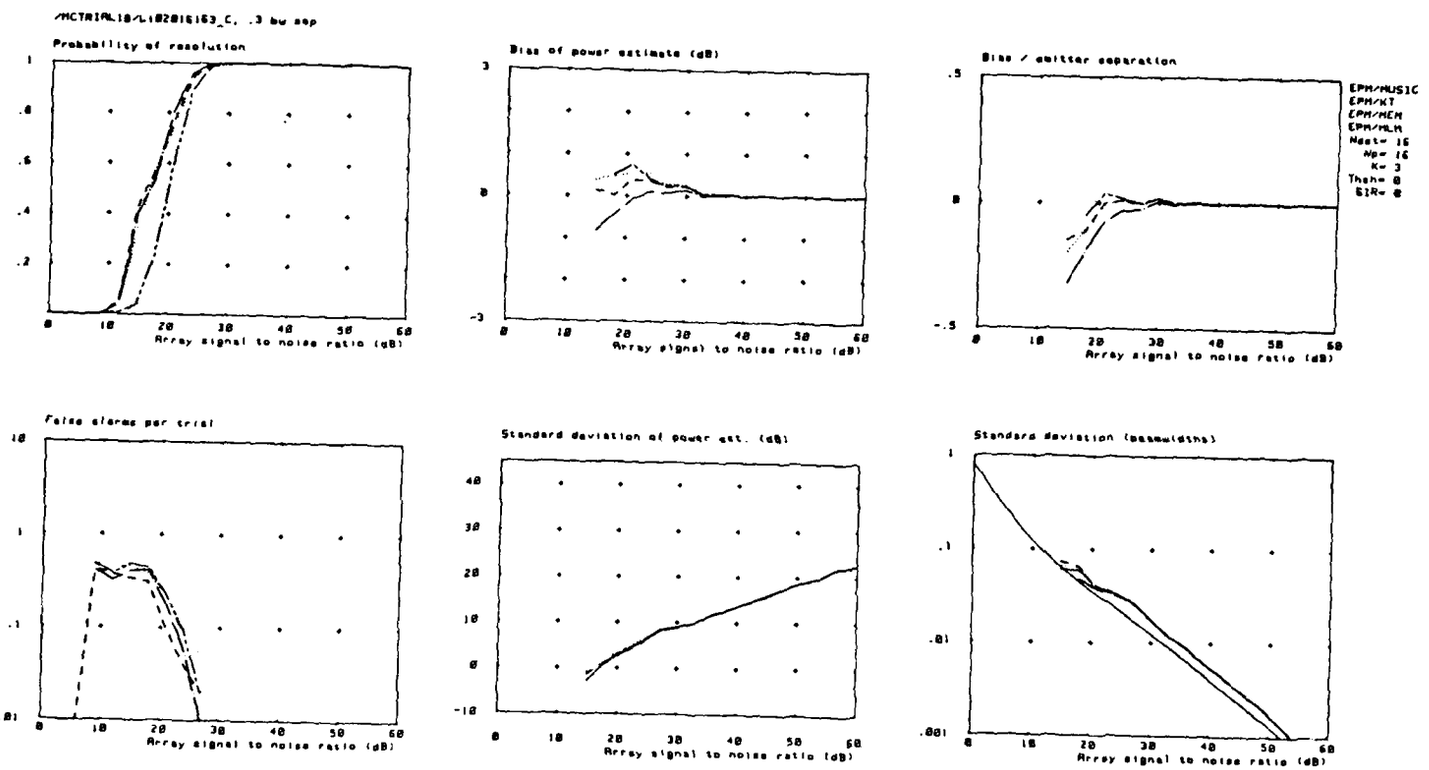
/MCTRIAL18/L18281613_C, .3 bw esp
Probability of resolution
Array signal to noise ratio (dB)
Bias of power estimate (dB)
Array signal to noise ratio (dB)
Bias / emitter separation
EPM/MUSIC
EPM/KT
EPM/MEM
EPM/MLM
Nest= 16
Np= 16
K= 3
Thsh= 0
SIR= 0
Array signal to noise ratio (dB)
False alarms per trial
Array signal to noise ratio (dB)
Standard deviation of power est. (dB)
Array signal to noise ratio (dB)
Standard deviation (beamwidths)
Array signal to noise ratio (dB)

Fig. A1.17

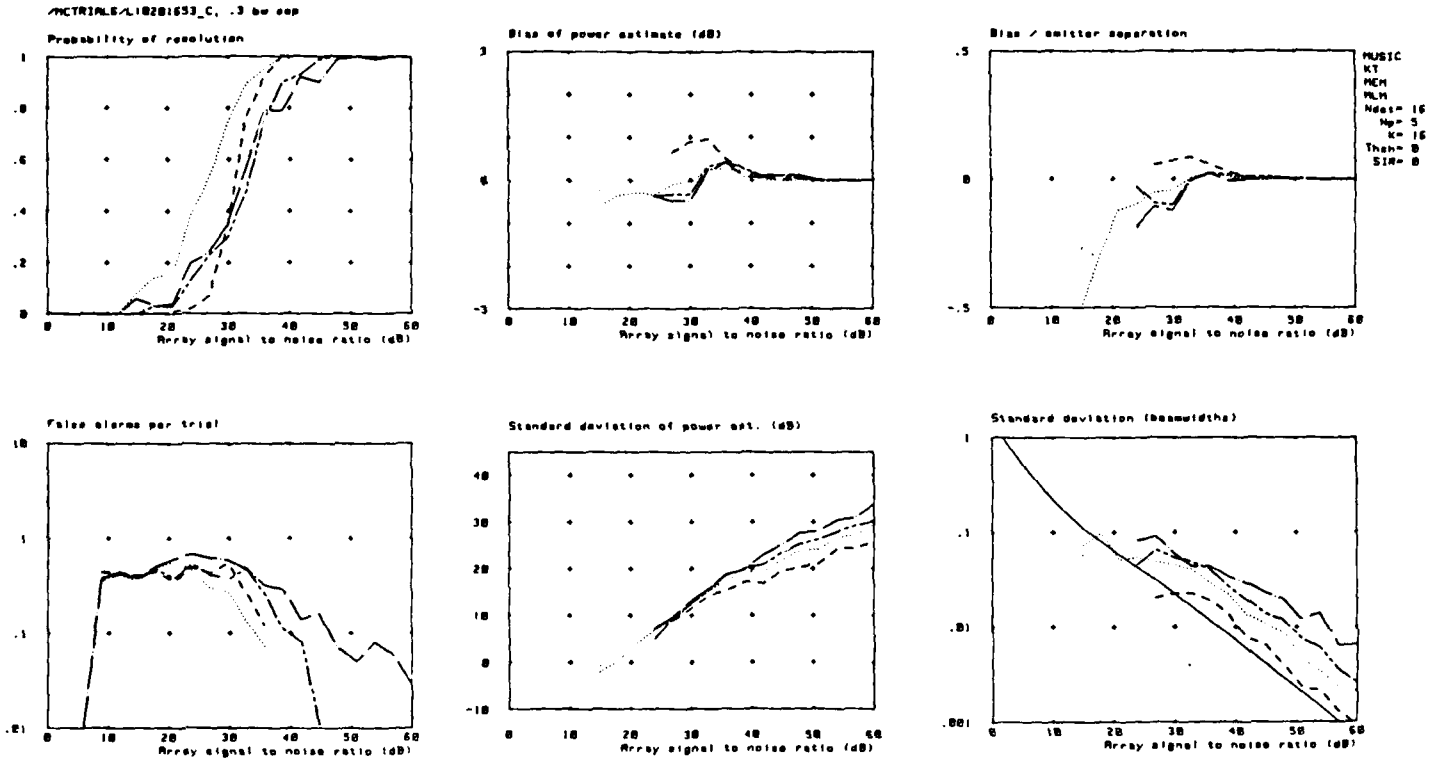
Probability of resolution
Bias of power estimate (dB)
Bias / emitter separation
MUSIC
KT
MEM
MLM
False alarms per trial
Standard deviation of power est. (dB)
Standard deviation (beamwidths)
Array signal to noise ratio (dB)

Fig. A1.18

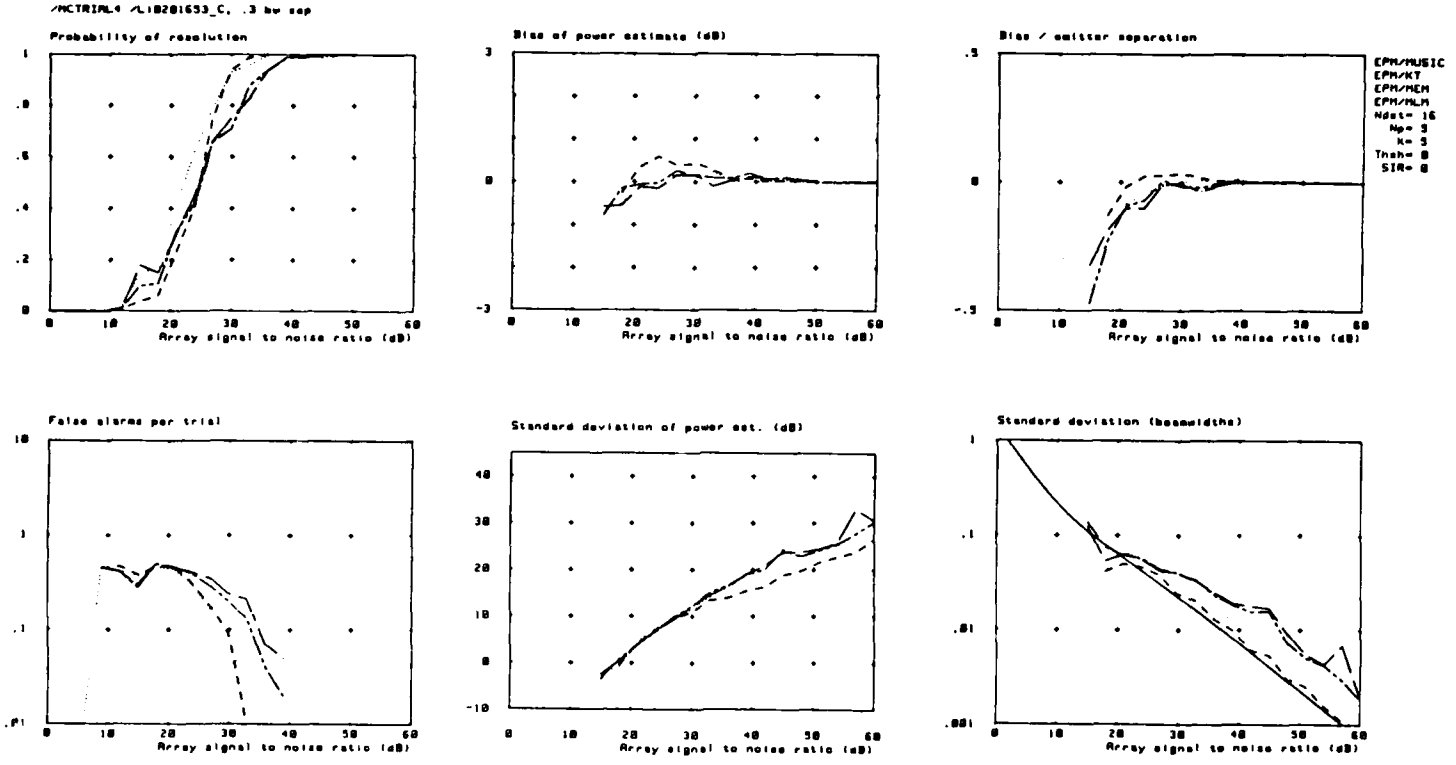
/MCTRIAL4 /L1B201653_C, .3 bw sep
Probability of resolution
Array signal to noise ratio (dB)
Bias of power estimate (dB)
Array signal to noise ratio (dB)
Bias / emitter separation
Array signal to noise ratio (dB)
EPM/MUSIC
EPM/KT
EPM/MEM
EPM/MLM
Ndat= 16
Np= 3
K= 3
Thsh= 0
SIR= 0
False alarms per trial
Array signal to noise ratio (dB)
Standard deviation of power est. (dB)
Array signal to noise ratio (dB)
Standard deviation (beamwidths)
Array signal to noise ratio (dB)

Fig. A1.19

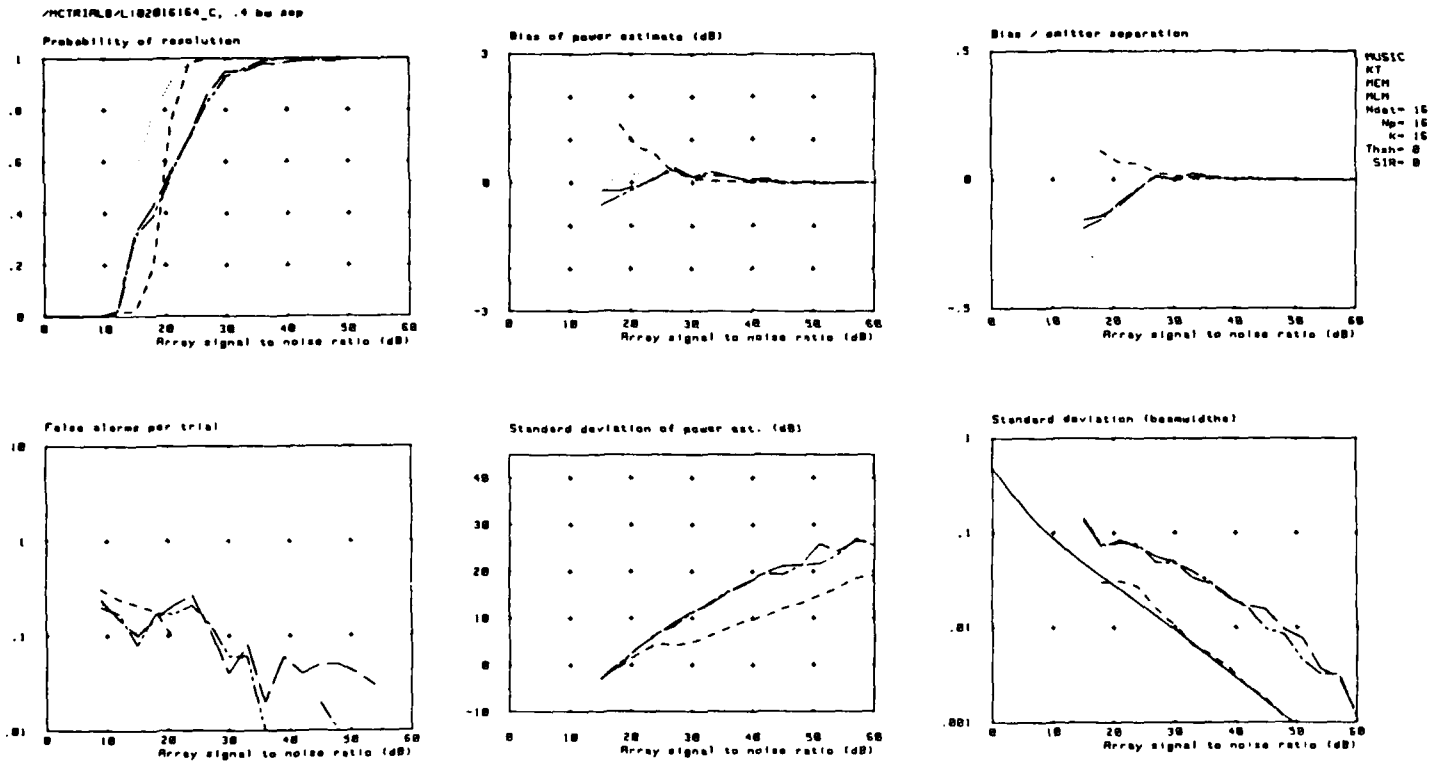
Probability of resolution
Array signal to noise ratio (dB)
Bias of power estimate (dB)
Array signal to noise ratio (dB)
Bias / emitter separation
MUSIC
RT
MEM
MLM
Array signal to noise ratio (dB)
False alarms per trial
Array signal to noise ratio (dB)
Standard deviation of power est. (dB)
Array signal to noise ratio (dB)
Standard deviation (beamwidths)
Array signal to noise ratio (dB)

Fig. A1.20

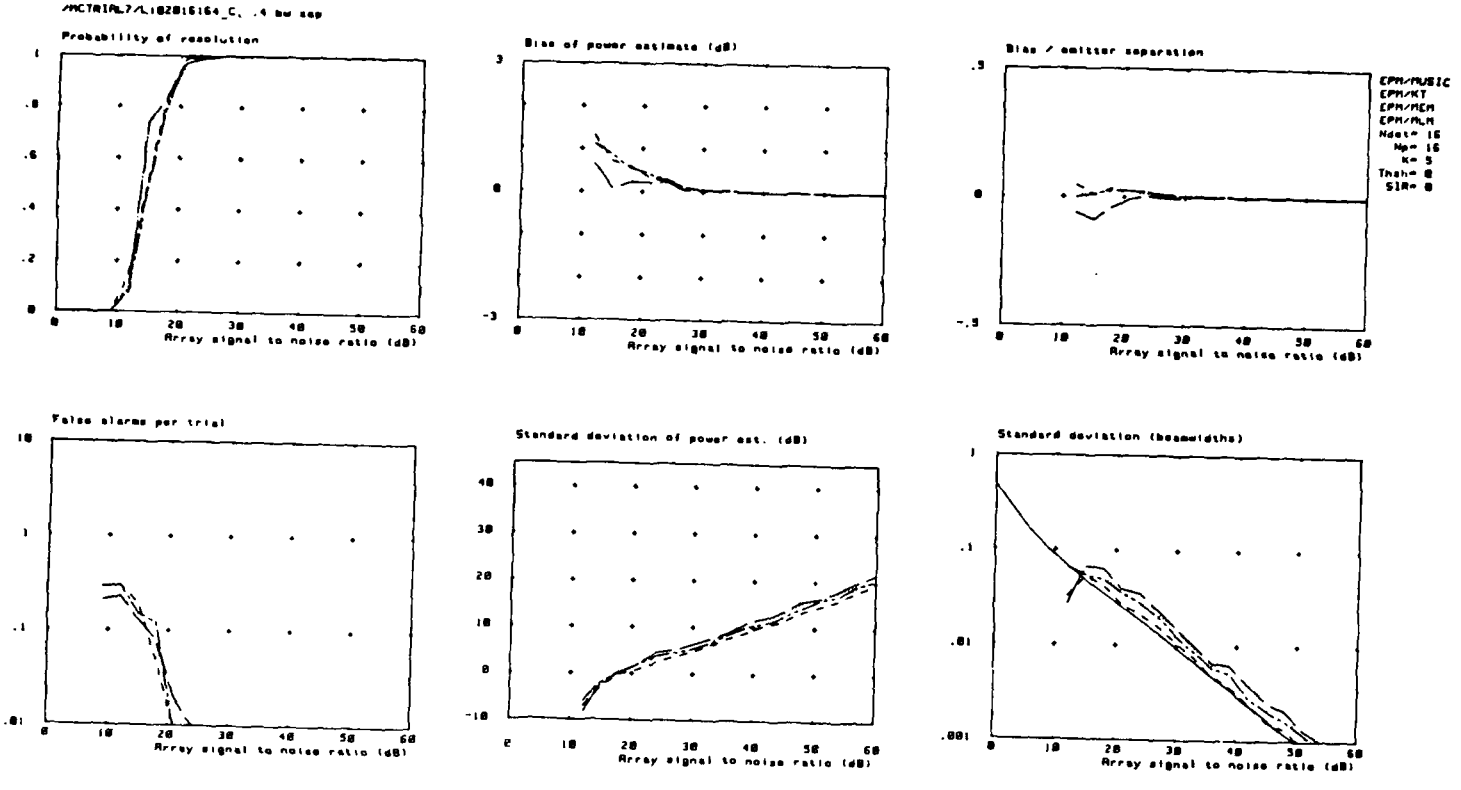
Probability of resolution
Bias of power estimate (dB)
Bias / emitter separation
EPM/MUSIC
EPM/KT
EPM/MEM
EPM/MLM
False alarms per trial
Standard deviation of power est. (dB)
Standard deviation (beamwidths)
Array signal to noise ratio (dB)

Fig. A1.21

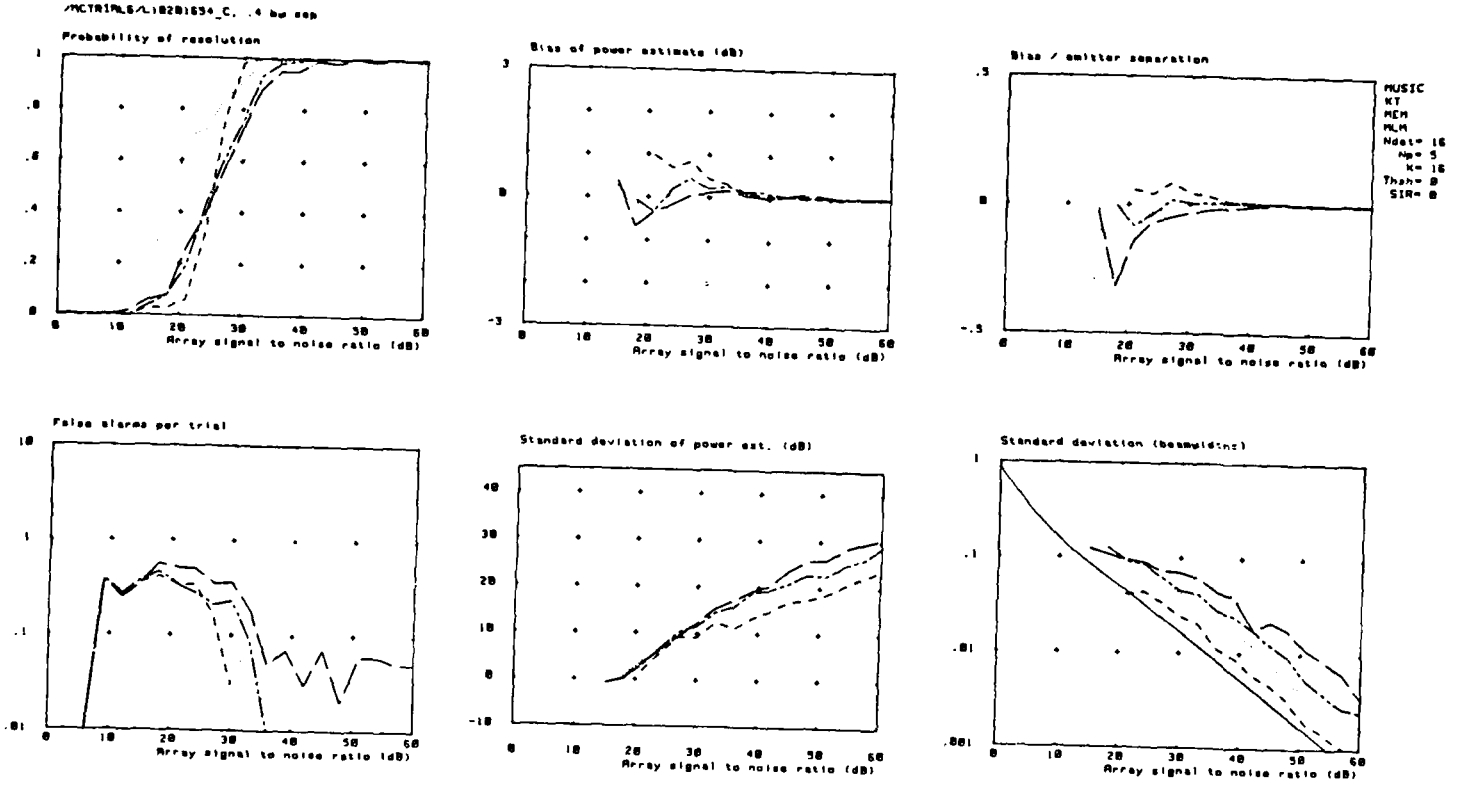
Probability of resolution
Array signal to noise ratio (dB)
Bias of power estimate (dB)
Array signal to noise ratio (dB)
Bias / emitter separation
Array signal to noise ratio (dB)
MUSIC
KT
MEM
MLM
False alarms per trial
Array signal to noise ratio (dB)
Standard deviation of power est. (dB)
Array signal to noise ratio (dB)
Standard deviation (beamforming)
Array signal to noise ratio (dB)

Fig. A1.22

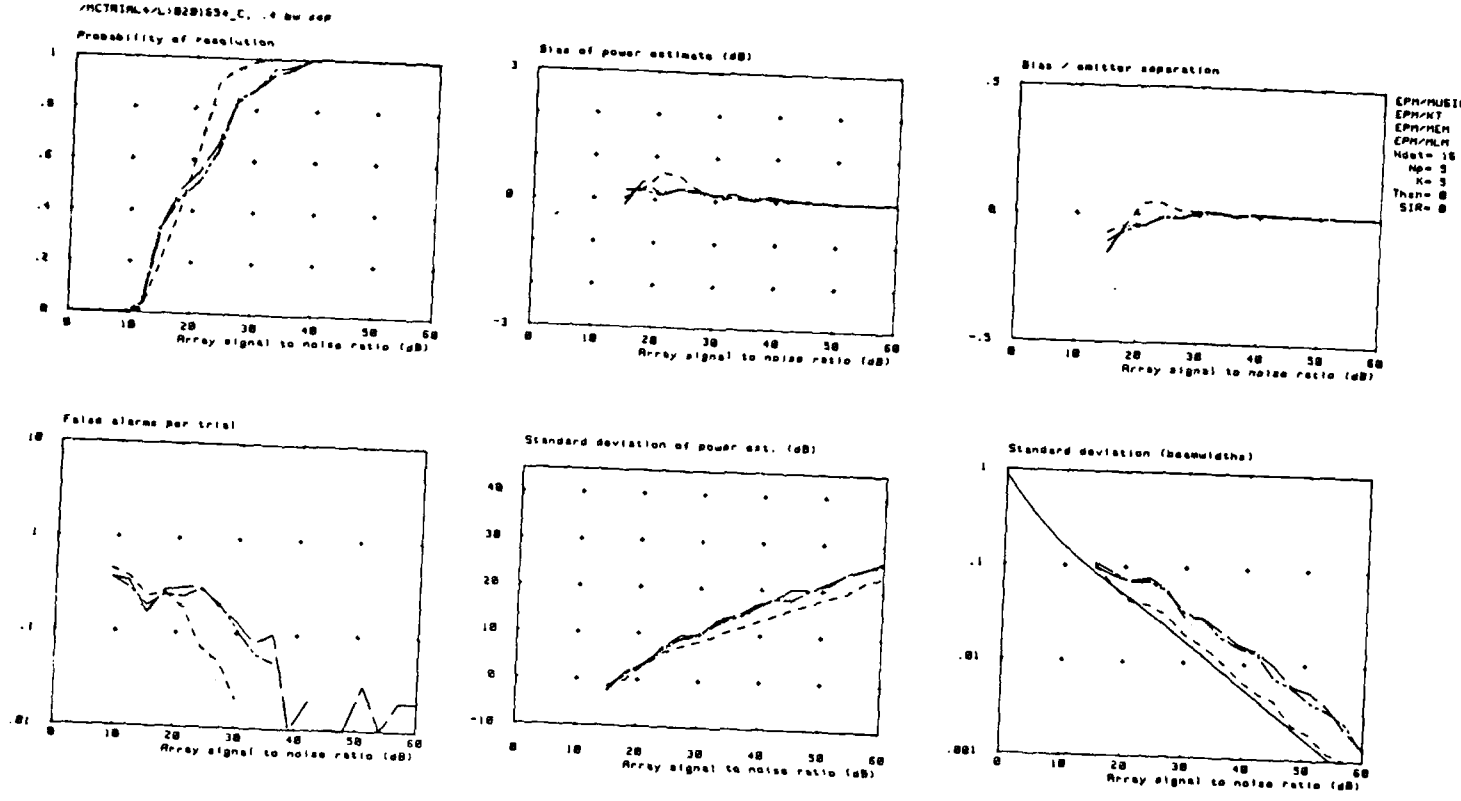
Probability of resolution
Bias of power estimate (dB)
Bias / emitter separation
EPM/MUSIC
EPM/RT
EPM/MEM
EPM/MLM
False alarms per trial
Standard deviation of power est. (dB)
Standard deviation (beamwidths)
Array signal to noise ratio (dB)

Fig. A1.23

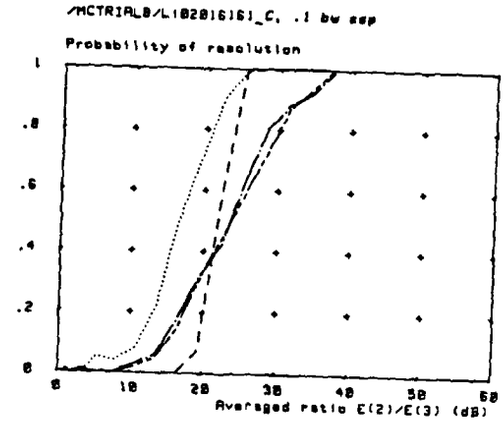

Fig. A1.24

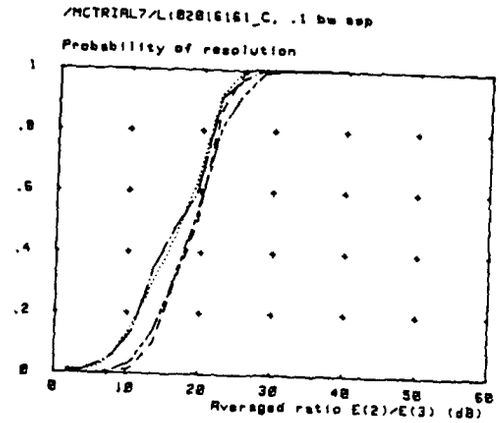

Fig. A1.25

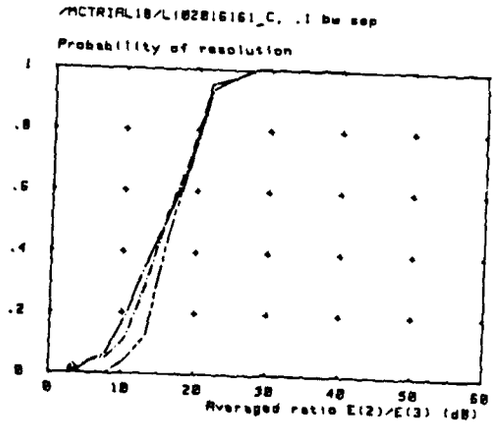

Fig. A1.26

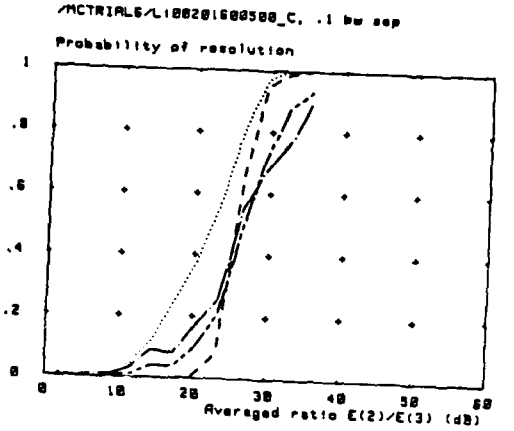

Fig. A1.27

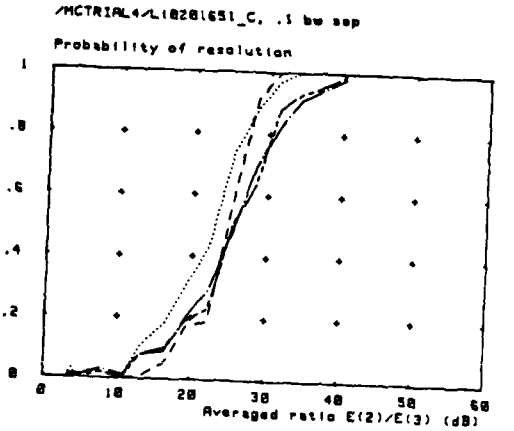

Fig. A1.28

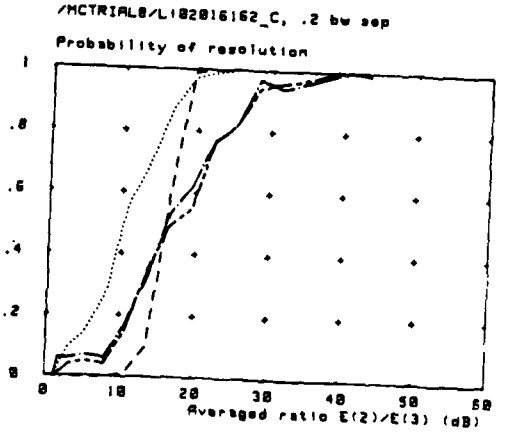

Fig. A1.29

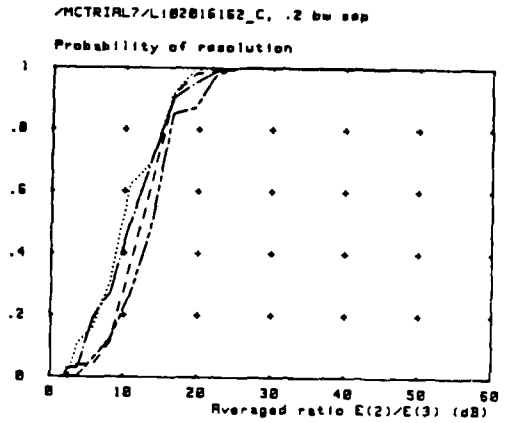

Fig. A1.30

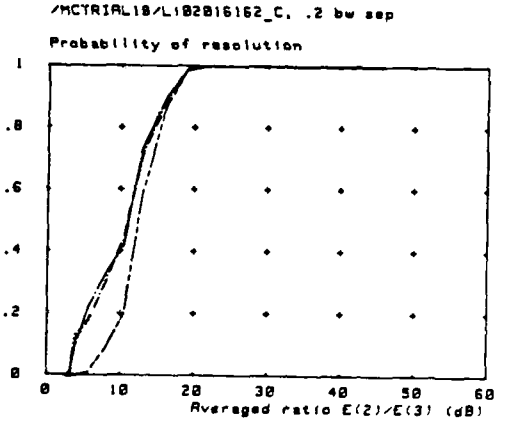

Fig. A1.31

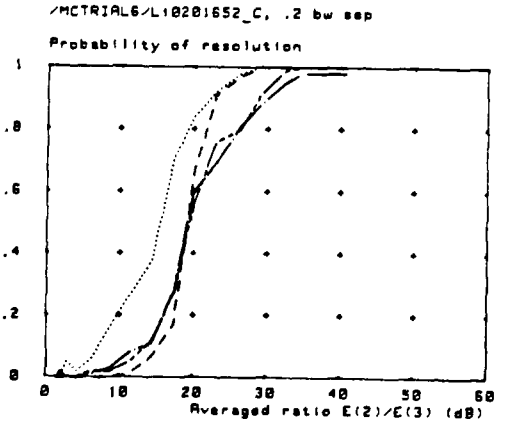

Fig. A1.32

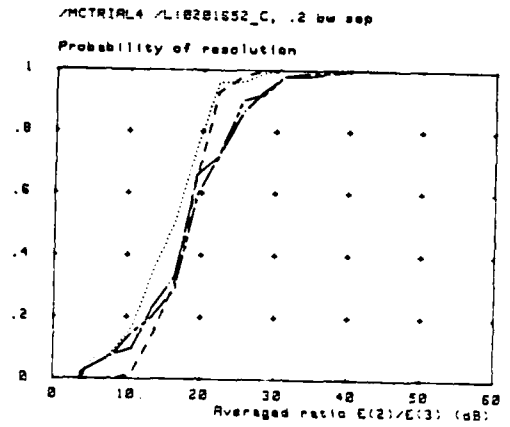

Fig. A1.33

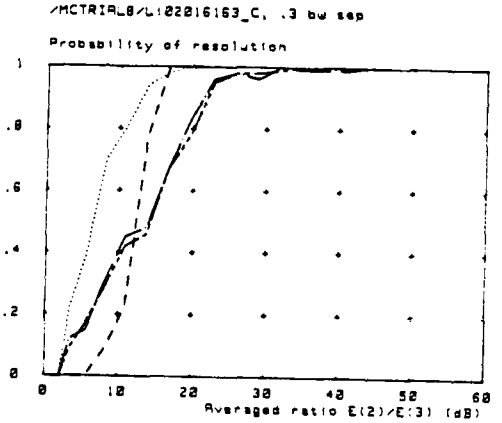

Fig. A1.34

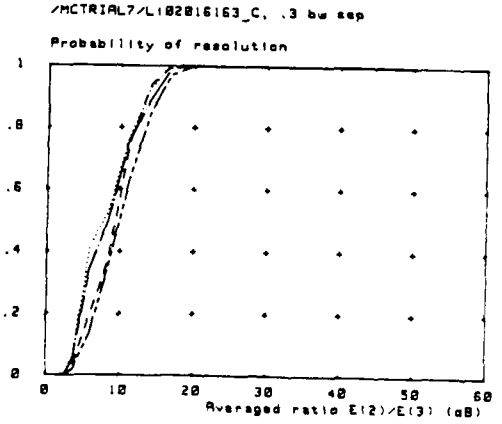

Fig. A1.35

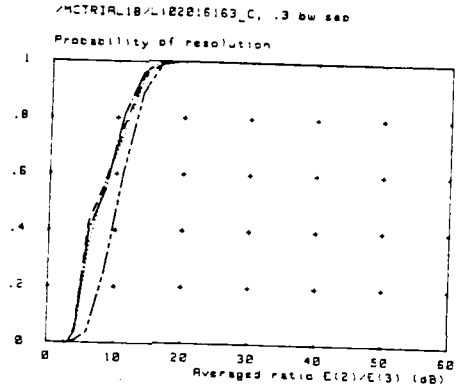

Fig. A1.36

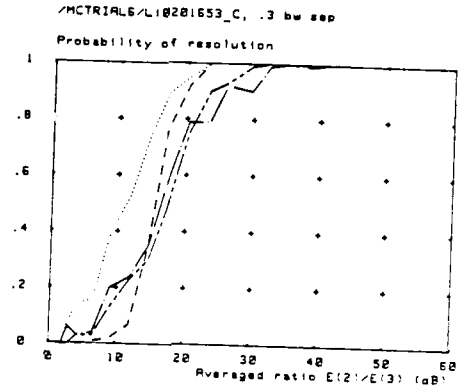

Fig. A1.37

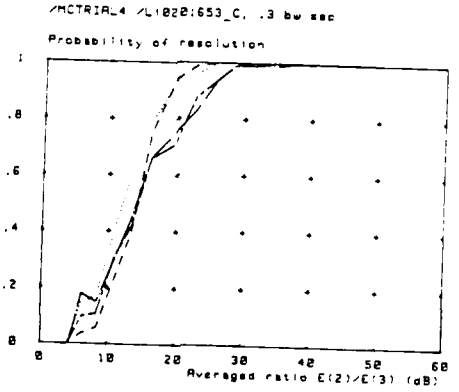

Fig. A1.38

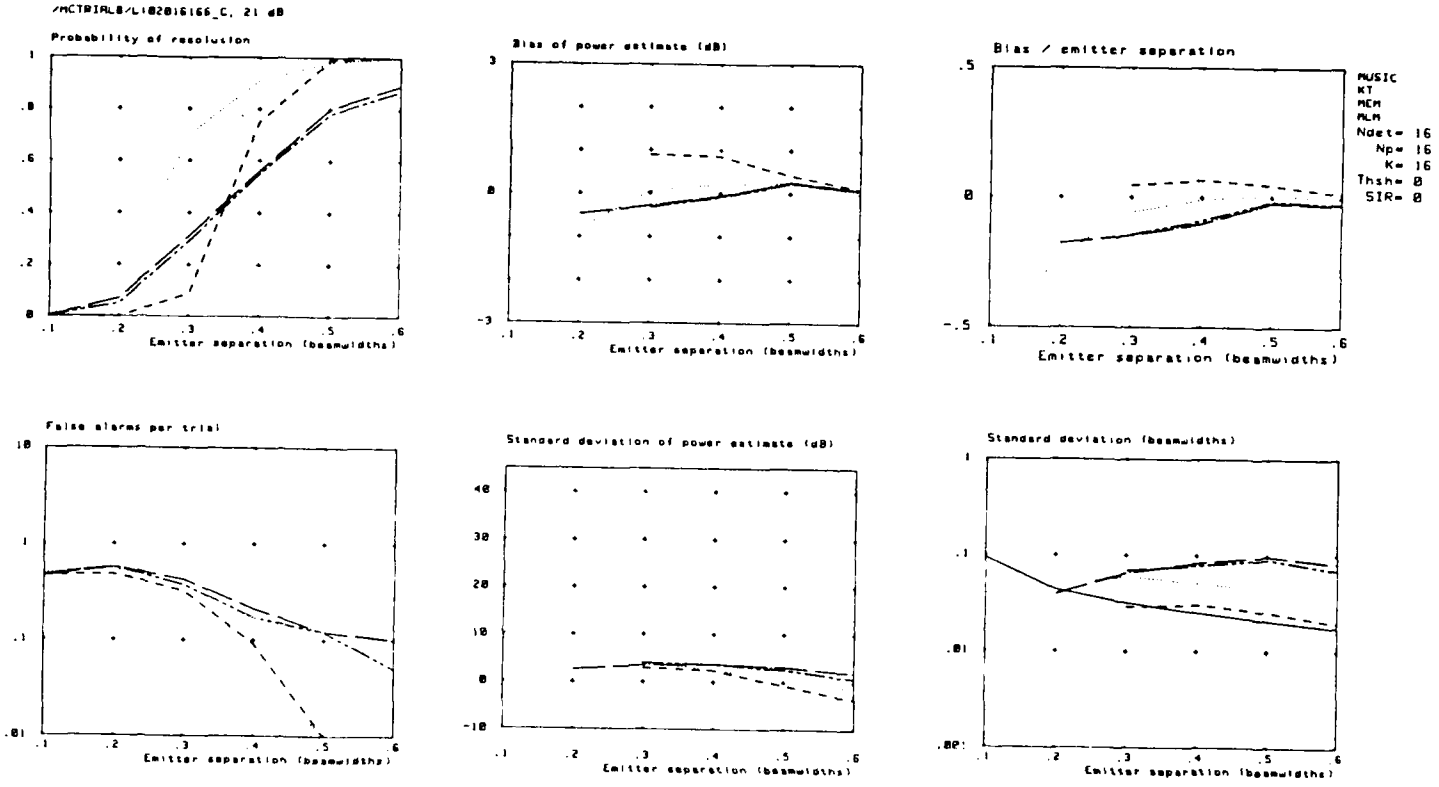
/MCTPIRL8/L18Z816166_C, 21 dB
Probability of resolution
Emitter separation (beamwidths)
Bias of power estimate (dB)
Emitter separation (beamwidths)
Bias / emitter separation
MUSIC
KT
MEM
MLM
Ndet= 16
Np= 16
K= 16
Thsh= 0
SIR= 0
Emitter separation (beamwidths)
False alarms per trial
Emitter separation (beamwidths)
Standard deviation of power estimate (dB)
Emitter separation (beamwidths)
Standard deviation (beamwidths)
Emitter separation (beamwidths)

Fig. A1.39

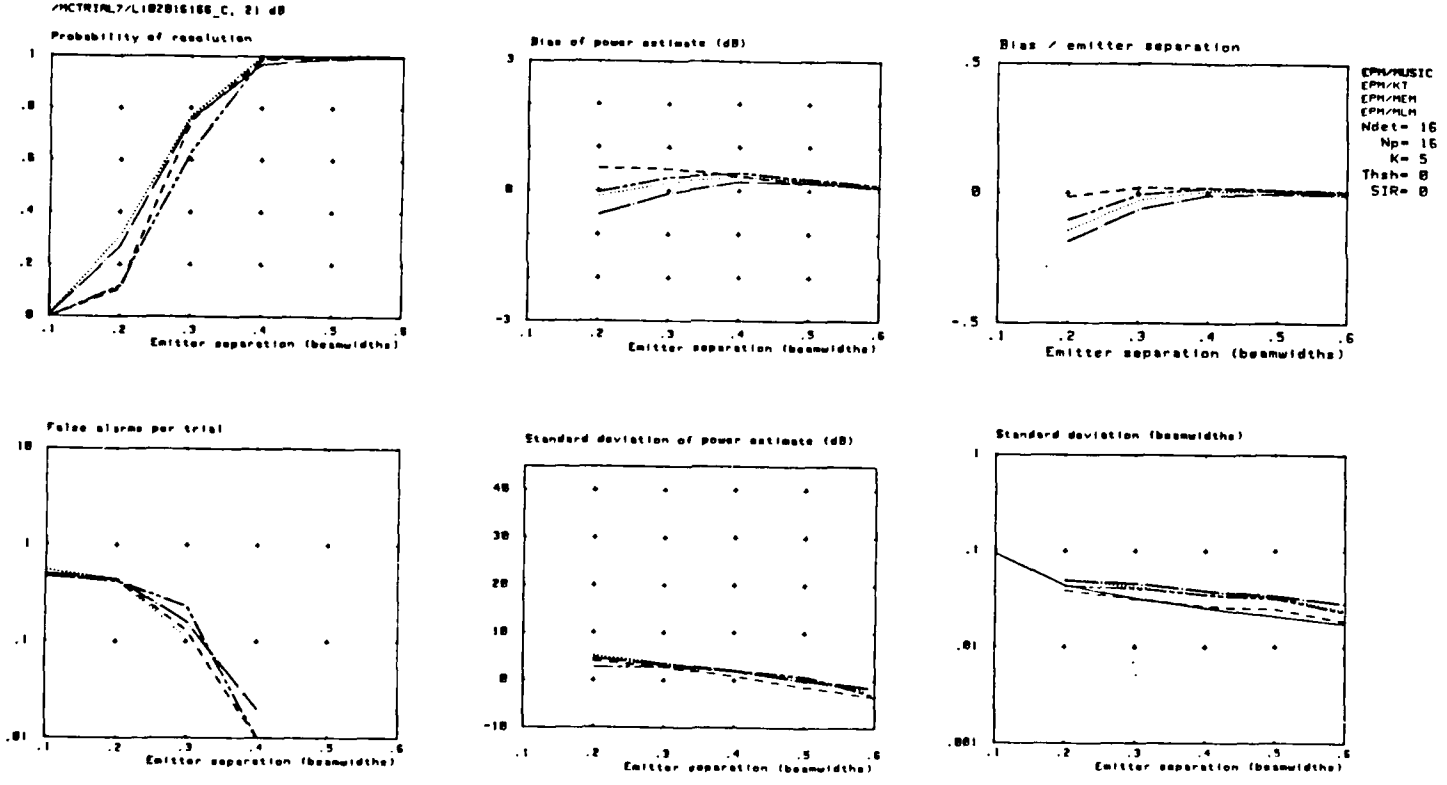
/MCTRIAL7/L1@2816166_C, 21 dB
Probability of resolution
Emitter separation (beamwidths)
Bias of power estimate (dB)
Emitter separation (beamwidths)
Bias / emitter separation
EPM/MUSIC
EPM/KT
EPM/MEM
EPM/MLM
Ndet= 16
Np= 16
K= 5
Thsh= 0
SIR= 0
Emitter separation (beamwidths)
False alarms per trial
Emitter separation (beamwidths)
Standard deviation of power estimate (dB)
Emitter separation (beamwidths)
Standard deviation (beamwidths)
Emitter separation (beamwidths)

Fig. A1.40

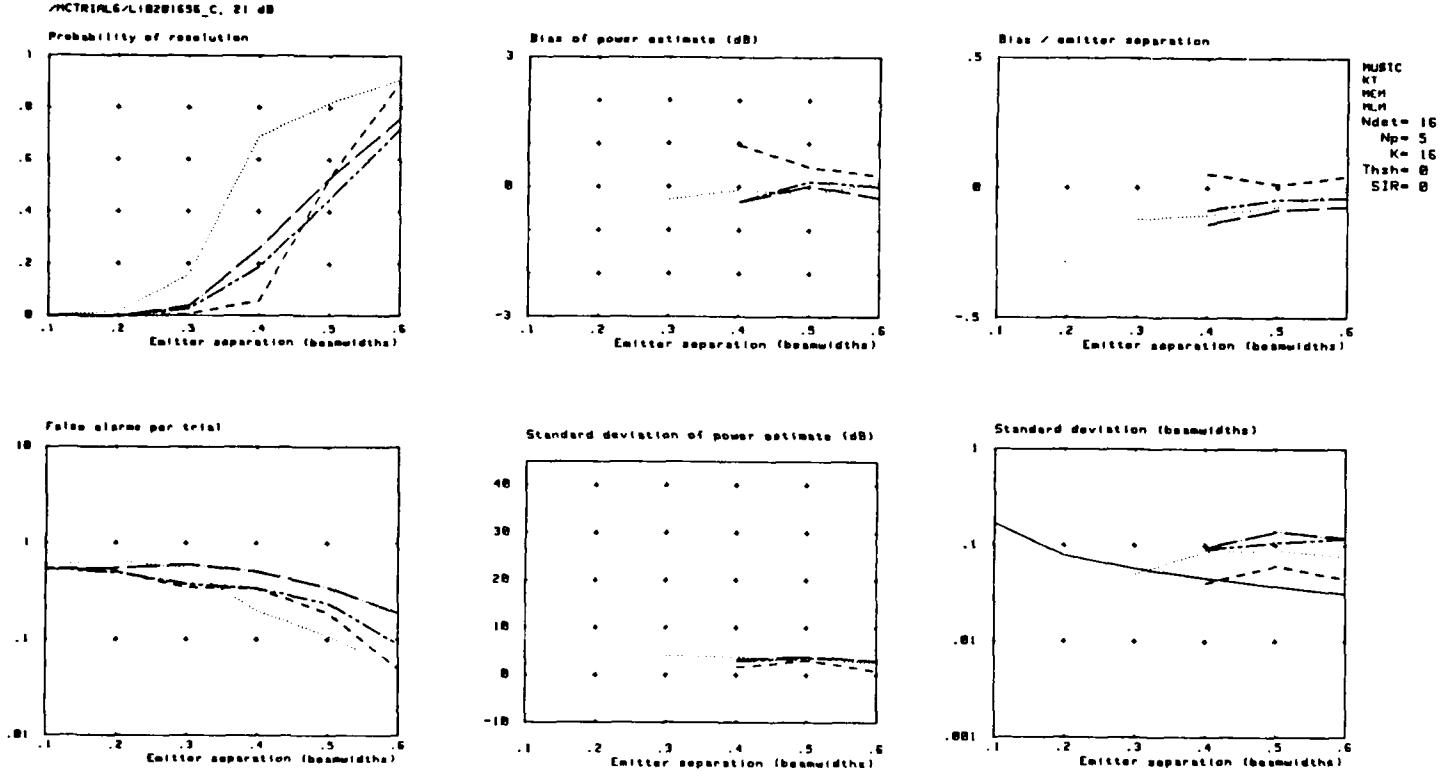
/MCTRIALS/L18281656_C, 21 dB
Probability of resolution
Emitter separation (beamwidths)
Bias of power estimate (dB)
Emitter separation (beamwidths)
Bias / emitter separation
Emitter separation (beamwidths)
MUSIC
KT
MCM
MLM
Ndet= 16
Np= 5
K= 16
Thsh= 0
SIR= 0
False alarms per trial
Emitter separation (beamwidths)
Standard deviation of power estimate (dB)
Emitter separation (beamwidths)
Standard deviation (beamwidths)
Emitter separation (beamwidths)

Fig. A1.41

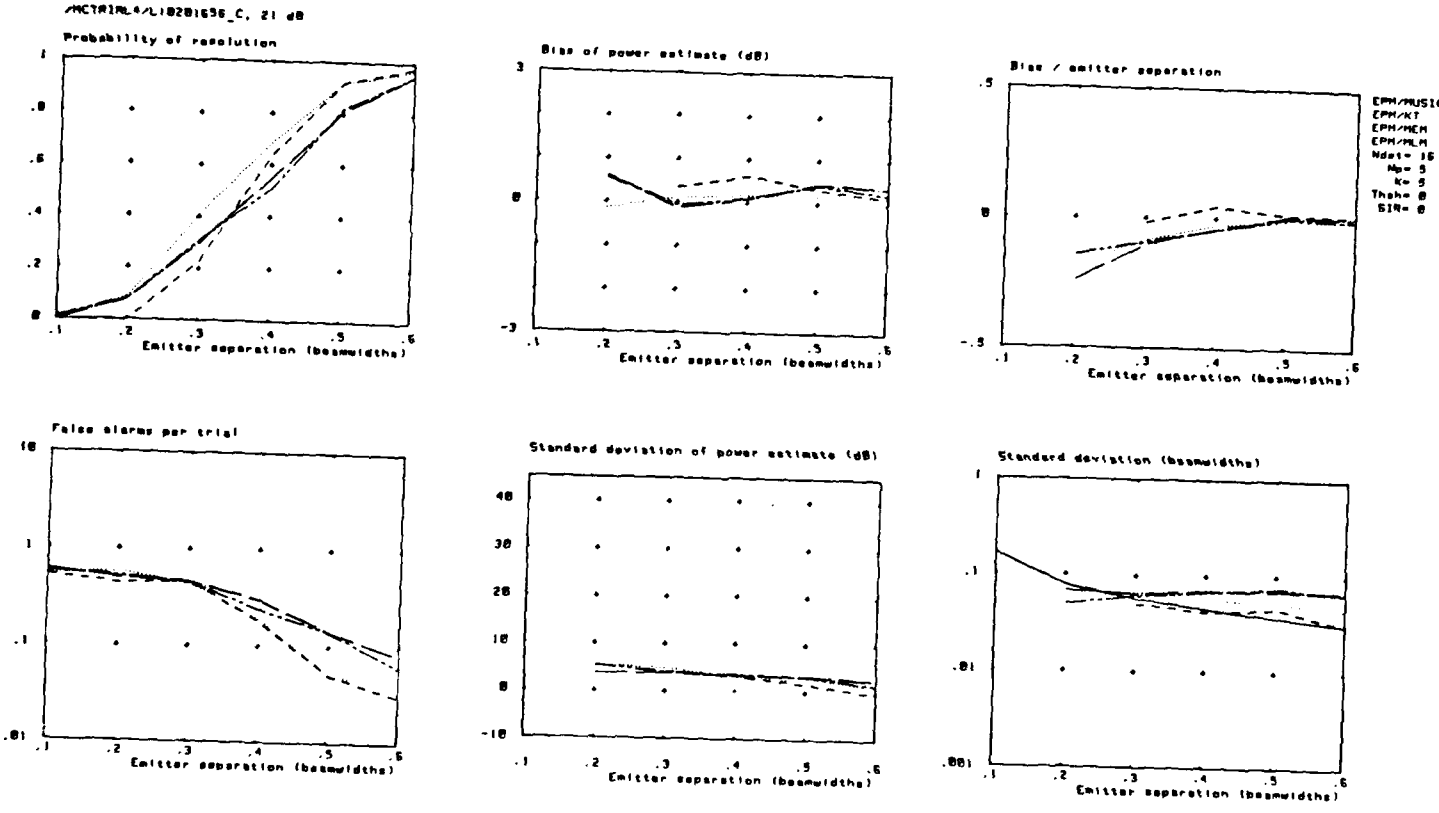
/MCTR1RL4/LI82B1656_C, 21 dB
Probability of resolution
Emitter separation (beamwidths)
Bias of power estimate (dB)
Emitter separation (beamwidths)
Bias / emitter separation
EPM/MUSIC
EPM/KT
EPM/MEM
EPM/MLM
Ndat= 16
Np= 5
Ks= 5
Thsh= 0
SIR= 0
Emitter separation (beamwidths)
False alarms per trial
Emitter separation (beamwidths)
Standard deviation of power estimate (dB)
Emitter separation (beamwidths)
Standard deviation (beamwidths)
Emitter separation (beamwidths)

Fig. A1.42

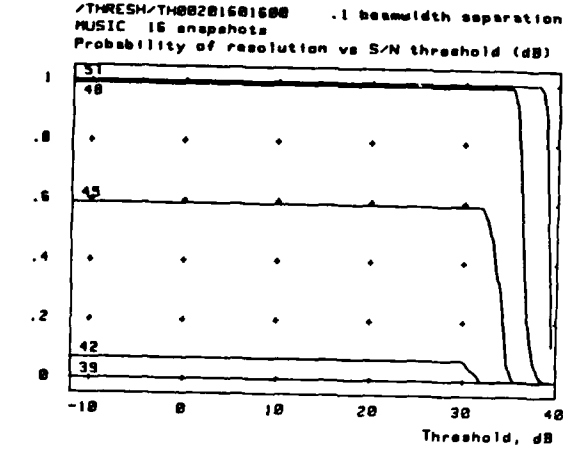

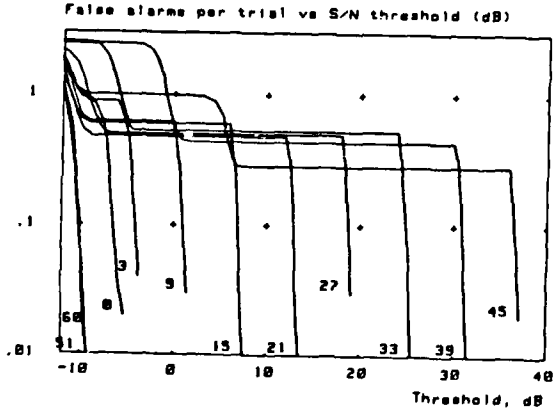

Fig. A1.43

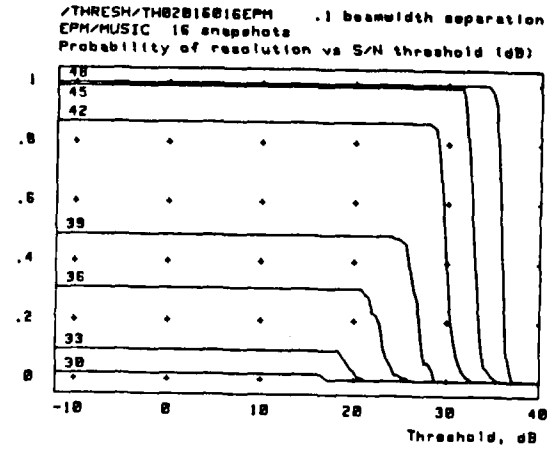

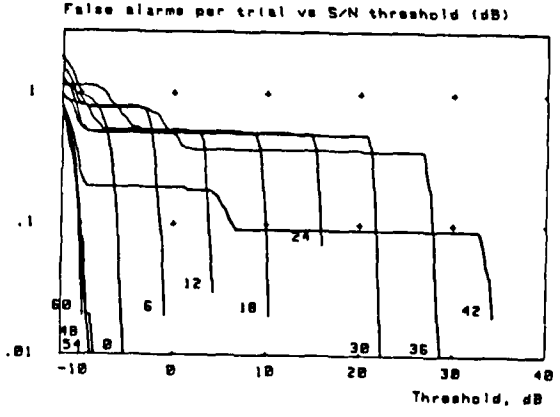

Fig. A1.44

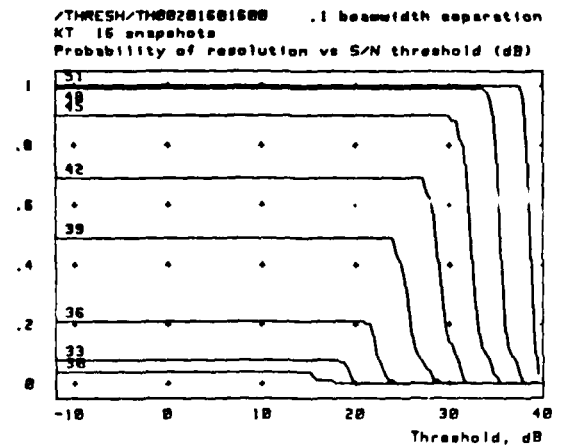

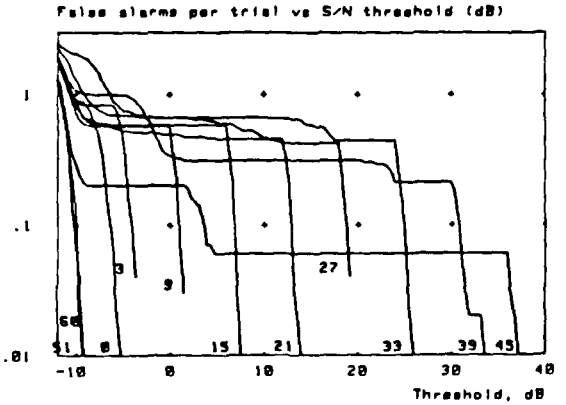

Fig. A1.45

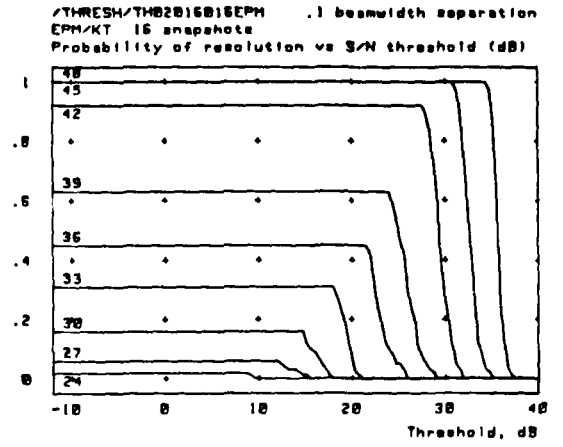

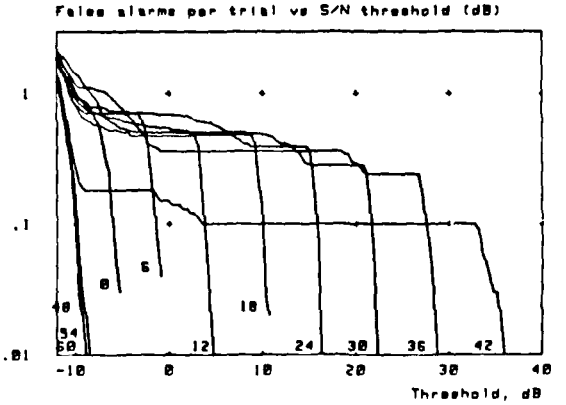

Fig. A1.46

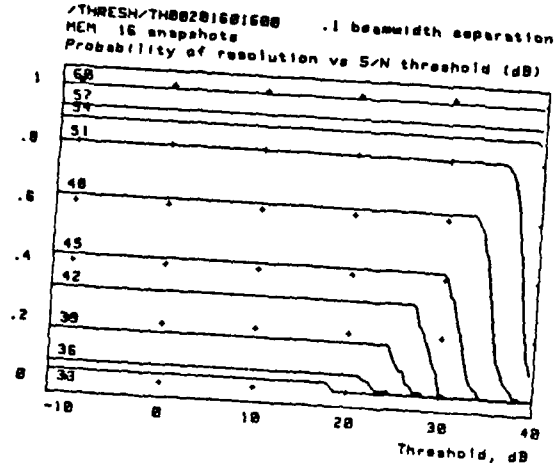

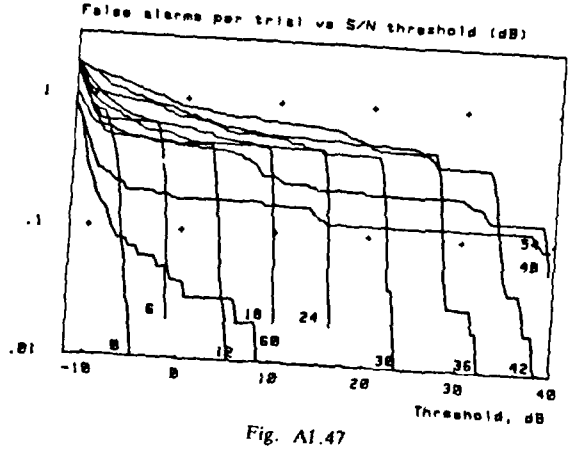

Fig. A1.47

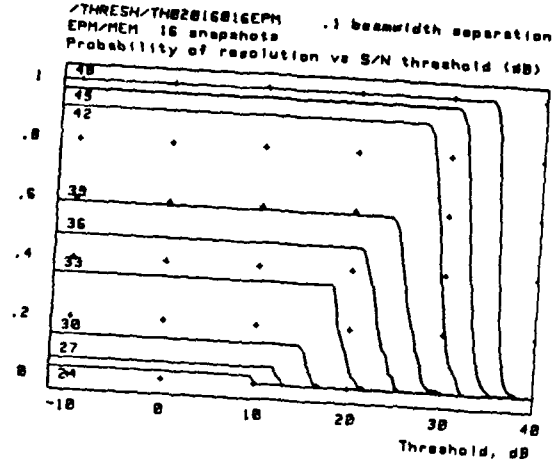

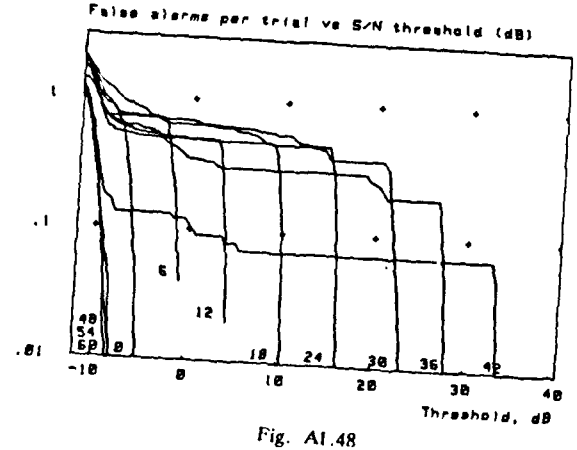

Fig. A1.48

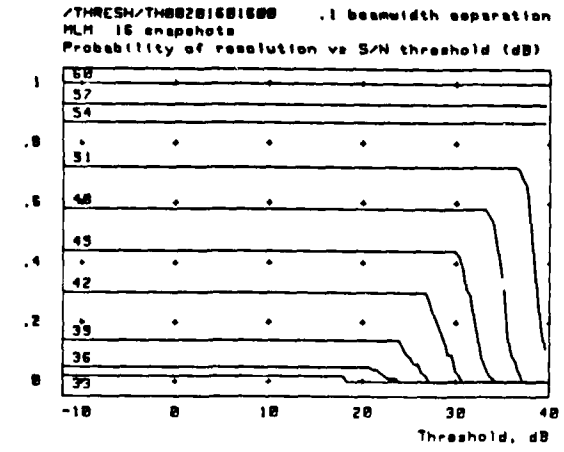

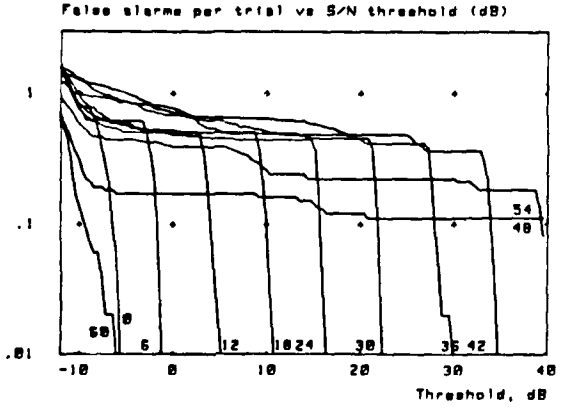

Fig. A1.49

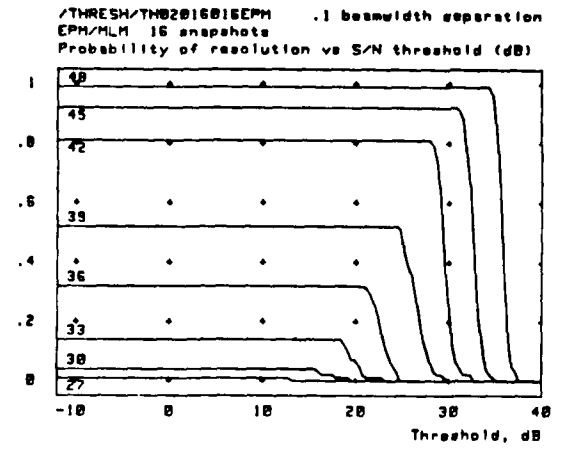

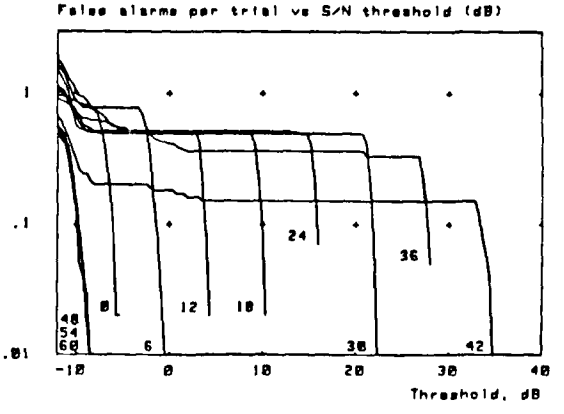

Fig. A1.50

APPENDIX 2. MONTE CARLO RESULTS: TWO TARGETS FAR FROM BROADSIDE

Contained in this appendix are a number of results relating to the problem described in section 5.2.3. Data from a uniformly weighted 16 element 0.5 wavelength spaced linear array, receiving signals from two far-field random phase point sources, has been simulated and analysed by a variety of high discrimination algorithms and their EPM pre-processed counterparts. Results, in terms of probability of resolution, false alarm rate, and bias and variance of the resolved angle and power estimates, are plotted in a variety of ways as follows:

Section A2.1: all as a function of ASNR, for a number of angular separations.
Section A2.2: probability of resolution as a function of the average ratio of second to third eigenvalue of the data covariance matrix.

Each set of plots corresponds to results from a particular group of algorithms, as follows:

A:	MUSIC -----	B:	EPM(k=5)/MUSIC
	KT ·····		EPM(k=5)/KT
	MEM -·-·-·-		EPM(k=5)/MEM
	MLM —-—-—		EPM(k=5)/MLM
C:	ROOT-MUSIC	D:	EPM(k=5)/ROOT-MUSIC
	ROOT-KT		EPM(k=5)/ROOT-KT
	ROOT-MEM		EPM(k=5)/ROOT-MEM
	ROOT-MLM		EPM(k=5)/ROOT-MLM

A2.1. RESULTS AS A FUNCTION OF ASNR

The results as a function of ASNR are plotted as follows:

Figure	Methods	Number of snapshots	Location of signals (beamwidths from boresight)
A2.1	A	16	7.8, 7.9
A2.2	B		
A2.3	C		
A2.4	D		
A2.5	A	16	7.7, 7.9
A2.6	B		
A2.7	C		
A2.8	D		
A2.9	A	16	7.6, 7.9
A2.10	B		
A2.11	C		
A2.12	D		

A2.2. RESULTS AS A FUNCTION OF EIGENVALUE RATIO

The remarks in section A1.2 are pertinent to the following plots of probability of resolution:

Figure	Methods	Number of snapshots	Location of signals (beamwidths from boresight)
A2.13 A2.14	A B	16	7.8, 7.9
A2.15 A2.16	A B	16	7.7, 7.9
A2.17 A2.18	A B	16	7.6, 7.9

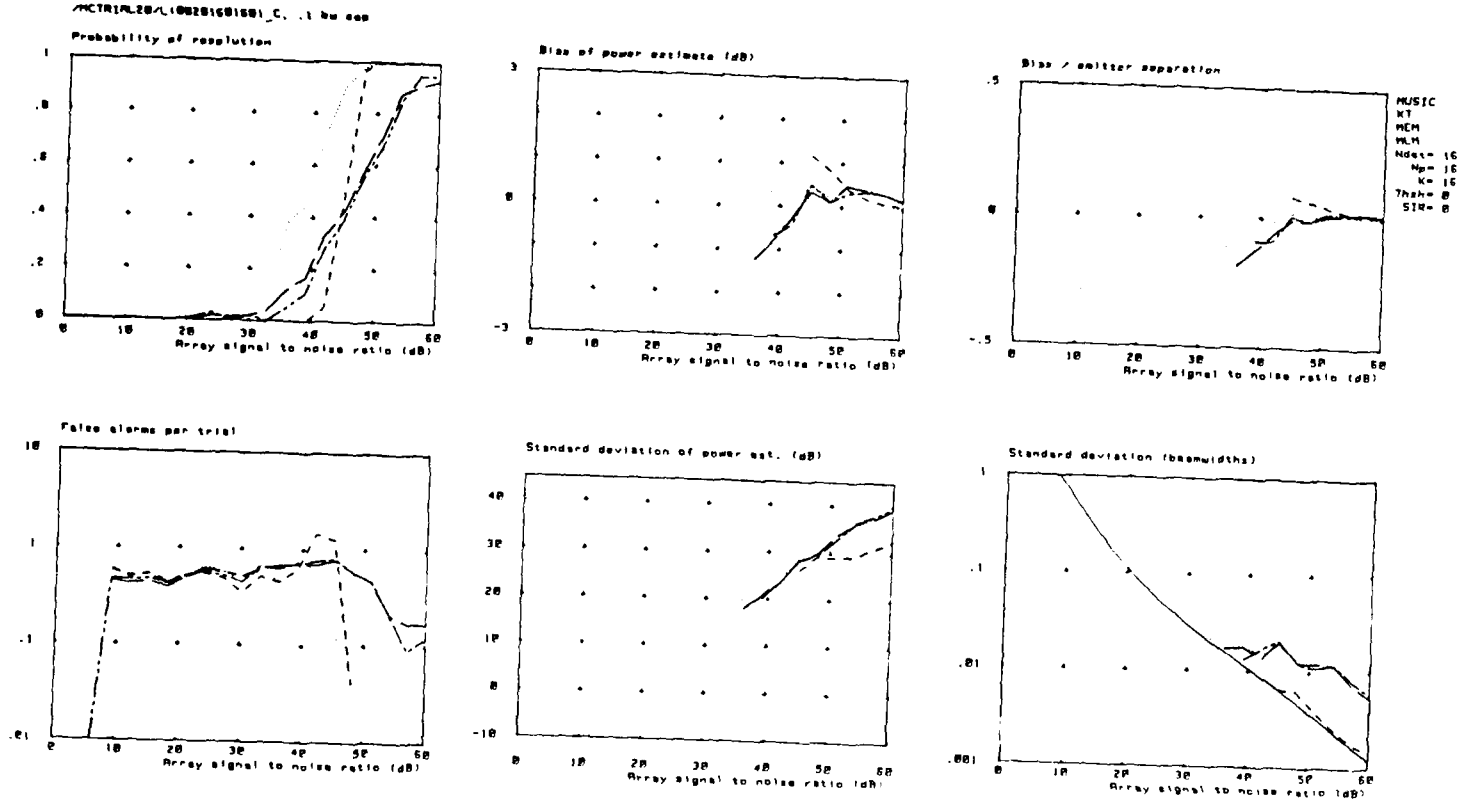
Probability of resolution
Array signal to noise ratio (dB)
Bias of power estimate (dB)
Array signal to noise ratio (dB)
Bias / emitter separation
Array signal to noise ratio (dB)
MUSIC
XT
MEM
MLM
False alarms per trial
Array signal to noise ratio (dB)
Standard deviation of power est. (dB)
Array signal to noise ratio (dB)
Standard deviation (beamwidths)
Array signal to noise ratio (dB)

Fig. A2.1

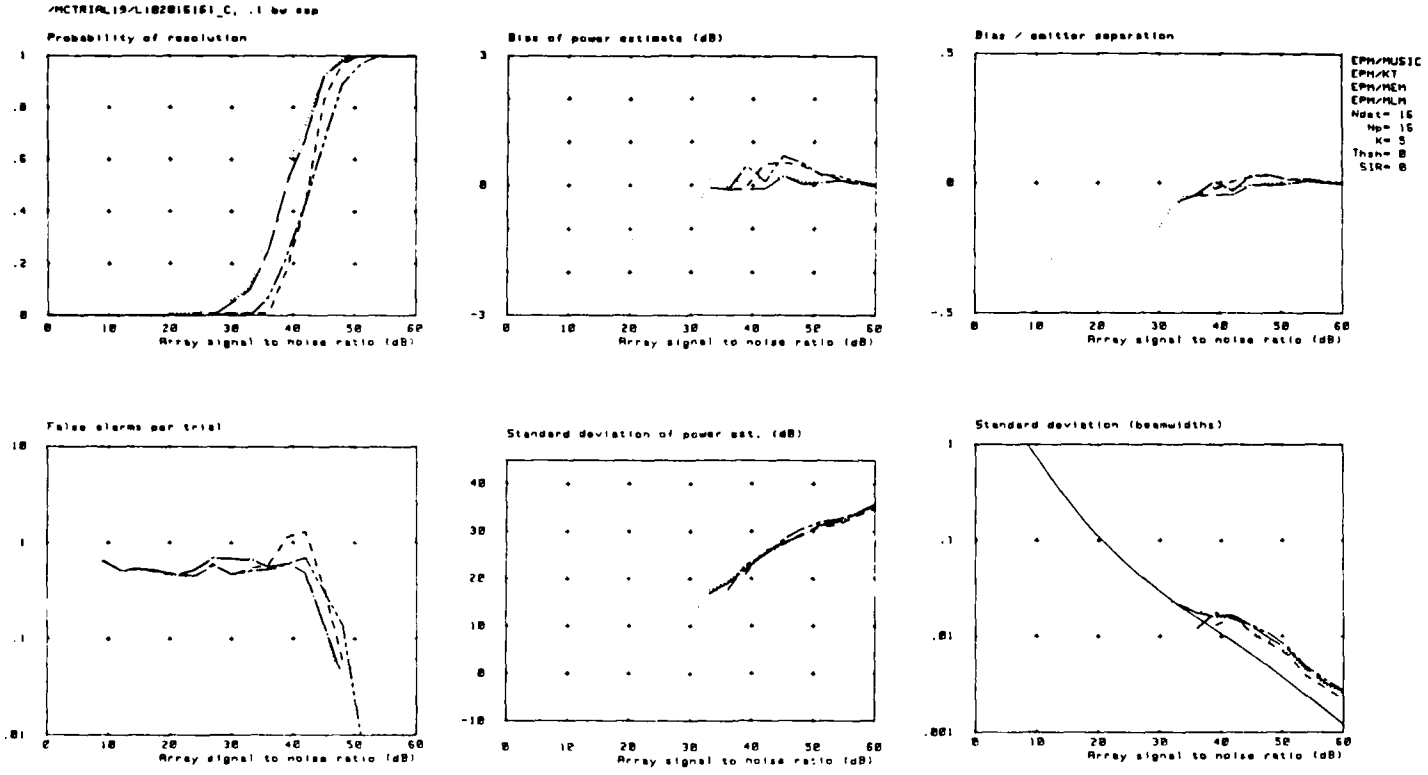
Probability of resolution
Array signal to noise ratio (dB)
Bias of power estimate (dB)
Array signal to noise ratio (dB)
Bias / emitter separation
EPM/MUSIC
EPM/KT
EPM/MEM
EPM/MLM
Ndat= 16
Np= 16
K= 5
Thsh= 8
SIR= 8
Array signal to noise ratio (dB)
False alarms per trial
Array signal to noise ratio (dB)
Standard deviation of power est. (dB)
Array signal to noise ratio (dB)
Standard deviation (beamwidths)
Array signal to noise ratio (dB)

Fig. A2.2

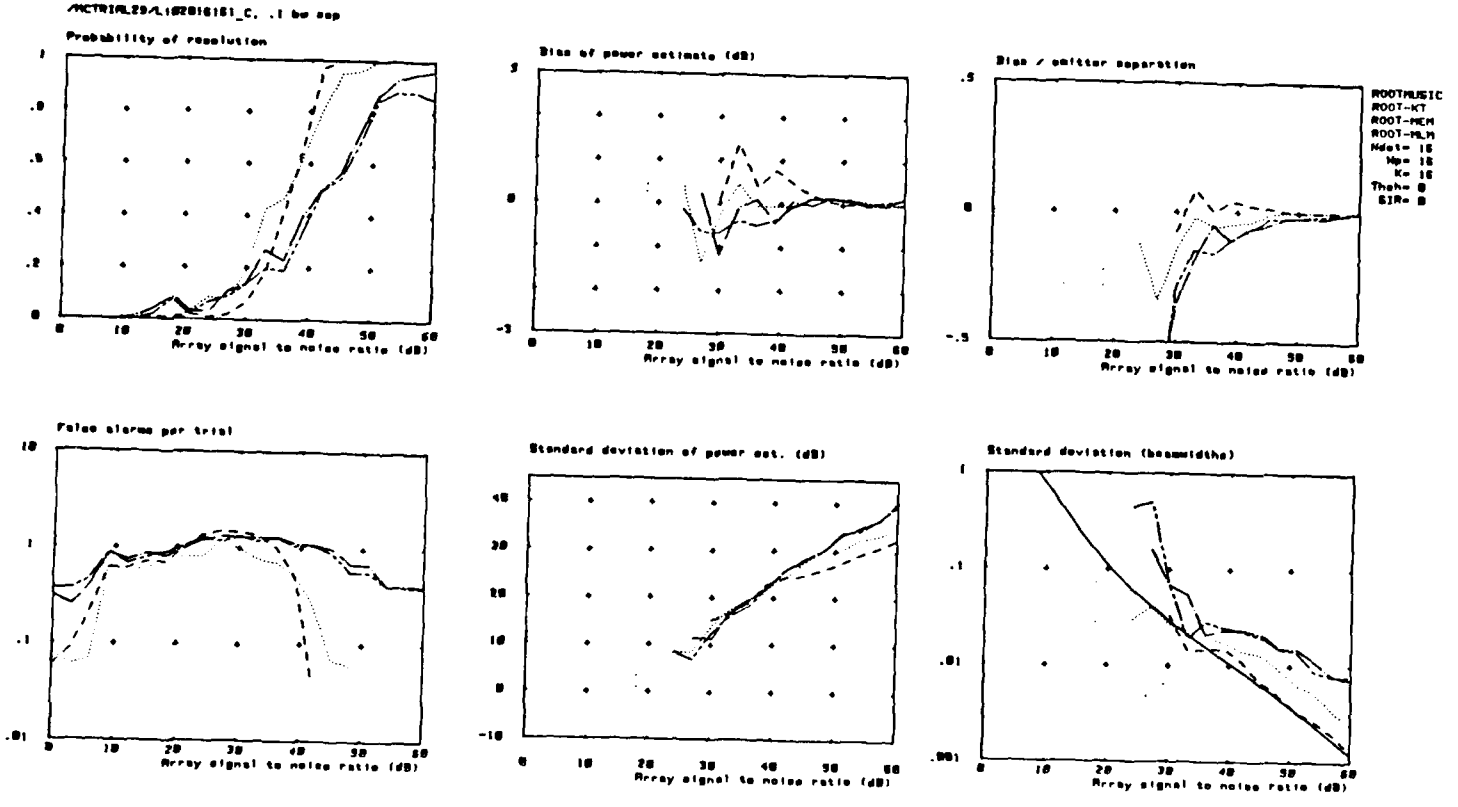
Probability of resolution
Bias of power estimate (dB)
Bias / emitter separation
ROOTMUSIC
ROOT-WT
ROOT-MEM
ROOT-MLM
False alarms per trial
Standard deviation of power est. (dB)
Standard deviation (beamwidths)
Array signal to noise ratio (dB)

Fig. A2.3

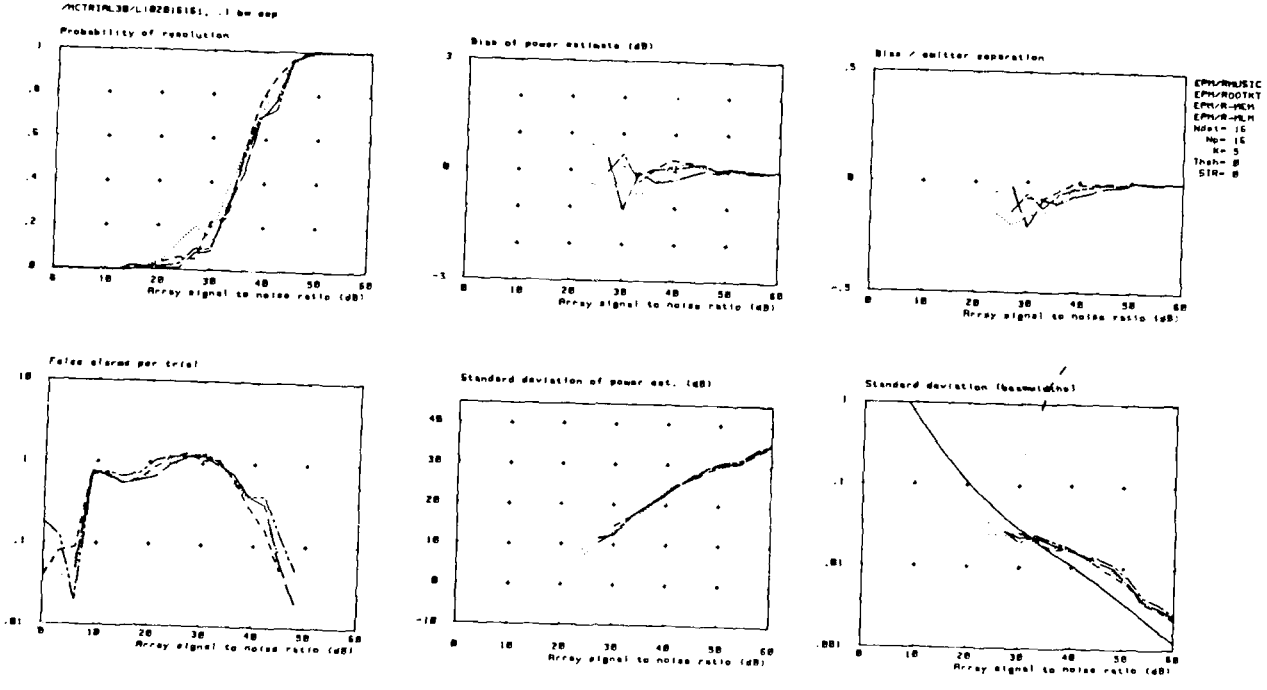
Probability of resolution
Array signal to noise ratio (dB)
Bias of power estimate (dB)
Array signal to noise ratio (dB)
Bias / scatter separation
Array signal to noise ratio (dB)
False alarms per trial
Array signal to noise ratio (dB)
Standard deviation of power est. (dB)
Array signal to noise ratio (dB)
Array signal to noise ratio (dB)

Fig. A2.4

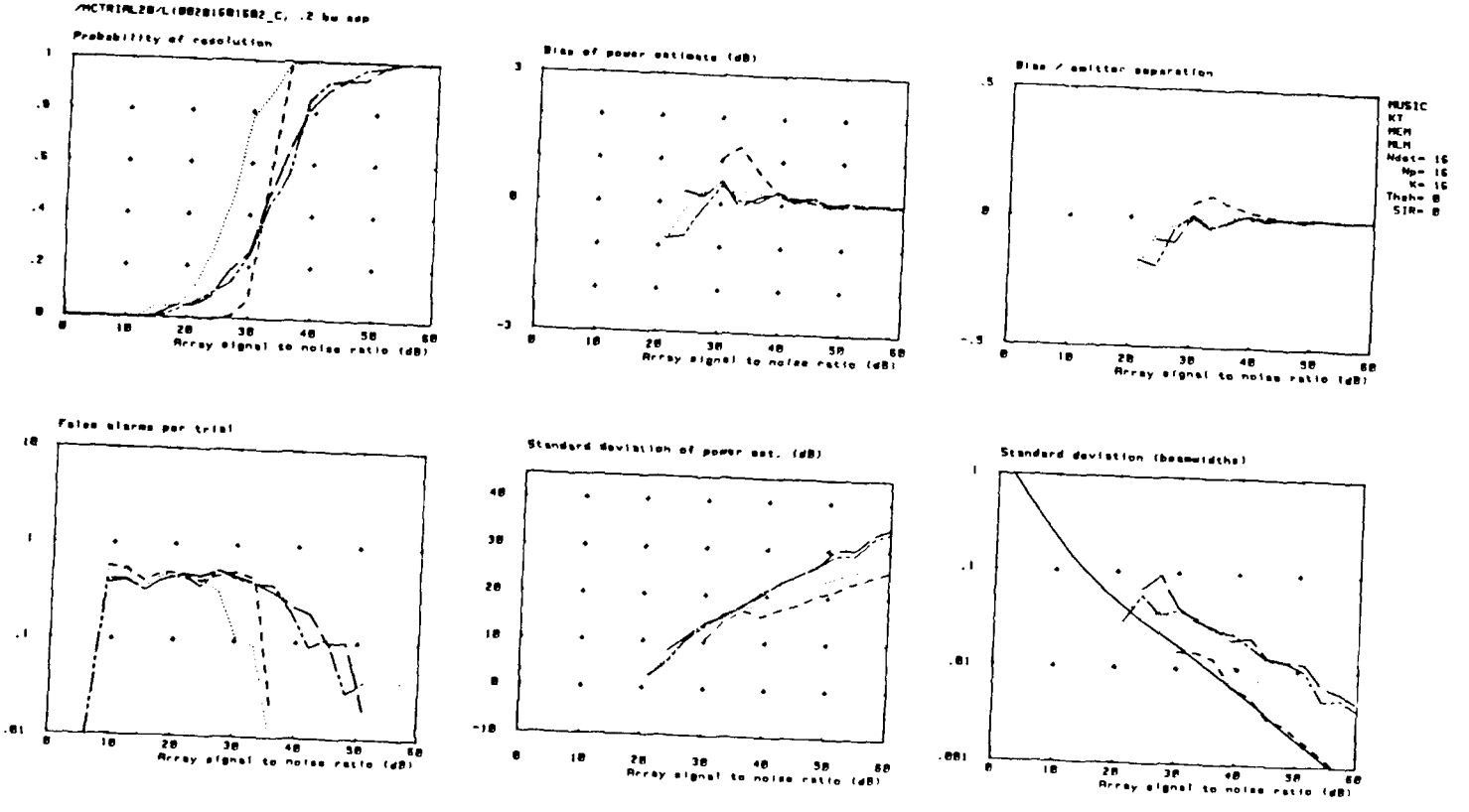
Probability of resolution
Array signal to noise ratio (dB)
Bias of power estimate (dB)
Array signal to noise ratio (dB)
Bias / emitter separation
Array signal to noise ratio (dB)
MUSIC
KT
MEM
MLM
Ndet= 16
Np= 16
K= 16
Thsh= 0
SIR= 0
False alarms per trial
Array signal to noise ratio (dB)
Standard deviation of power est. (dB)
Array signal to noise ratio (dB)
Standard deviation (beamwidths)
Array signal to noise ratio (dB)

Fig. A2.5

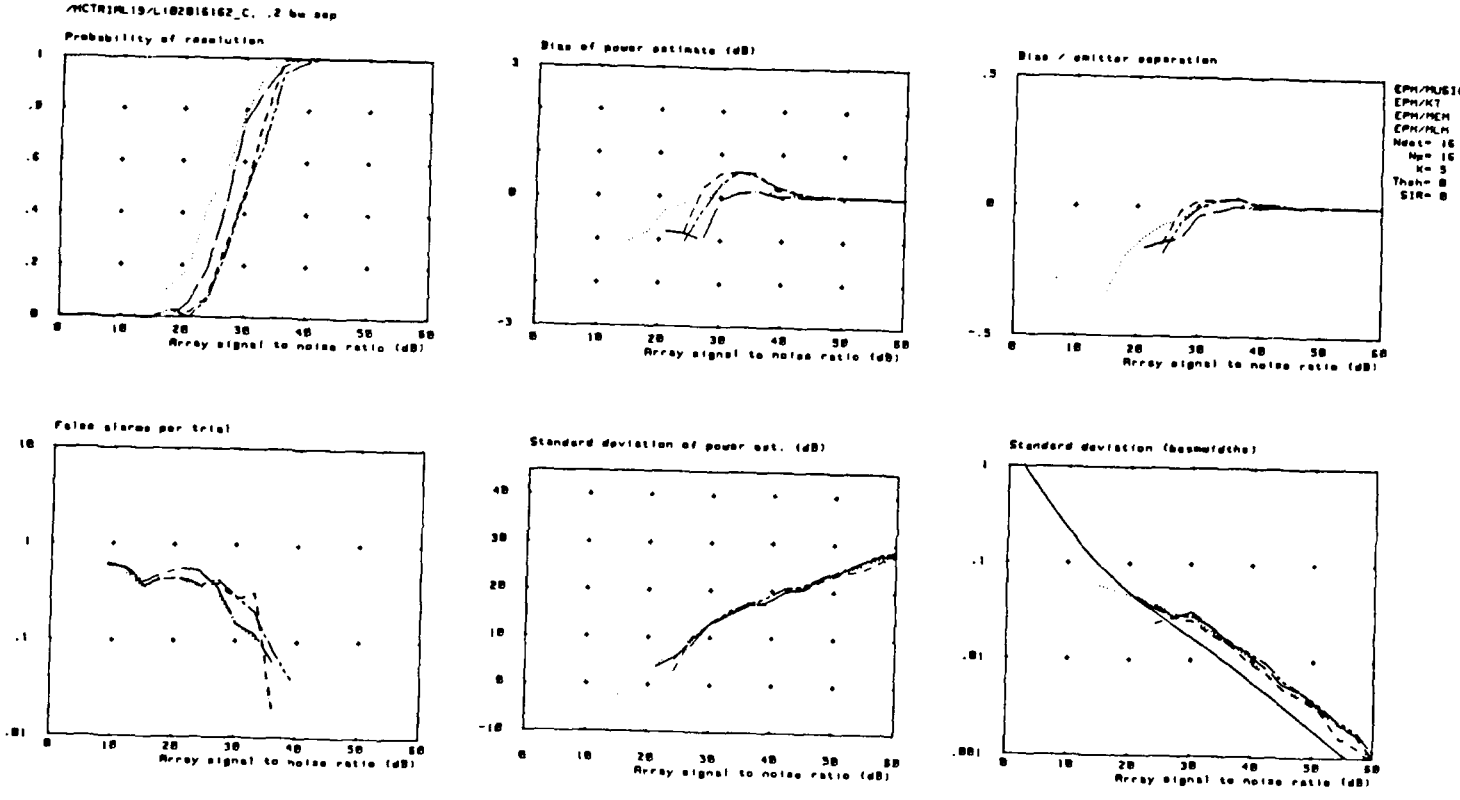
Probability of resolution
Bias of power estimate (dB)
Bias / emitter separation
EPM/MUSIC
EPM/KT
EPM/MEM
EPM/MLM
False alarms per trial
Standard deviation of power est. (dB)
Standard deviation (beamwidths)
Array signal to noise ratio (dB)

Fig. A2.6

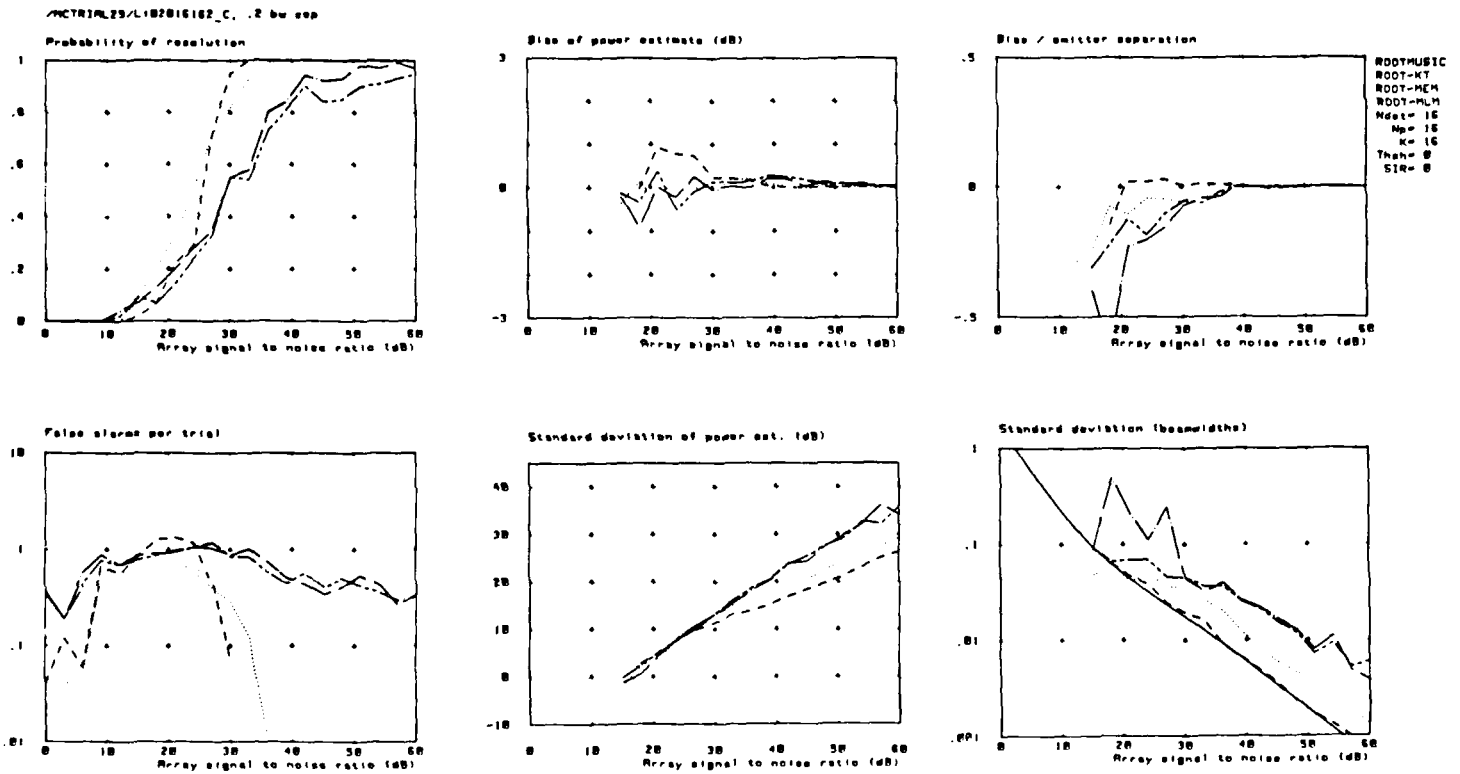
Probability of resolution
Bias of power estimate (dB)
Bias / emitter separation
ROOTMUSIC
ROOT-KT
ROOT-MEM
ROOT-MLM
False alarms per trial
Standard deviation of power est. (dB)
Standard deviation (beamwidths)
Array signal to noise ratio (dB)

Fig. A2.7

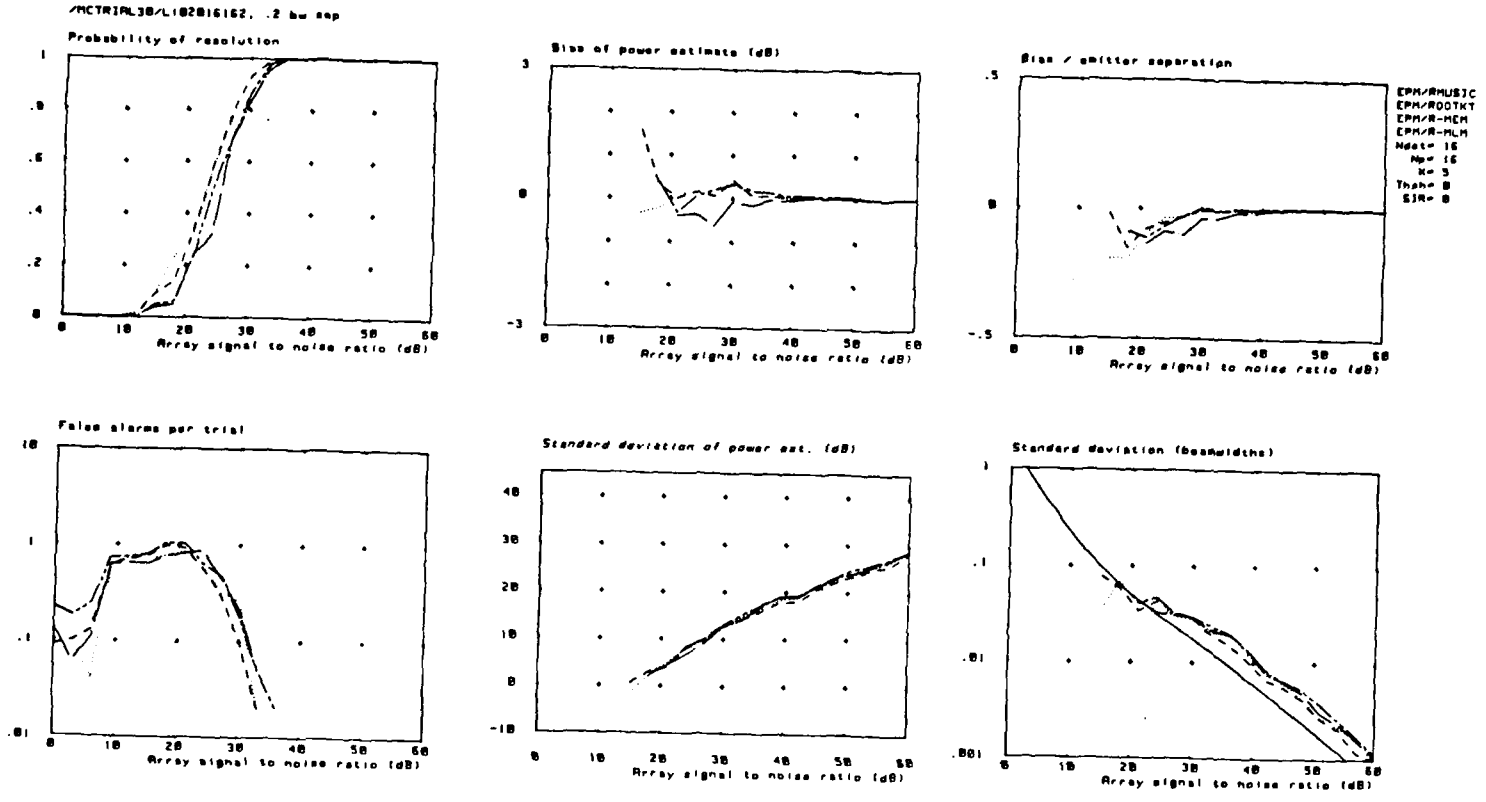
/MCTRIAL30/L102816152, .2 bw sep
Probability of resolution
Array signal to noise ratio (dB)
Bias of power estimate (dB)
Array signal to noise ratio (dB)
Bias / emitter separation
EPM/RMUSIC
EPM/ROOTKT
EPM/R-MEM
EPM/R-MLM
Ndata= 16
Ns= 16
K= 3
Thsh= 0
SIR= 0
Array signal to noise ratio (dB)
False alarms per trial
Array signal to noise ratio (dB)
Standard deviation of power est. (dB)
Array signal to noise ratio (dB)
Standard deviation (beamwidths)
Array signal to noise ratio (dB)

Fig. A2.8

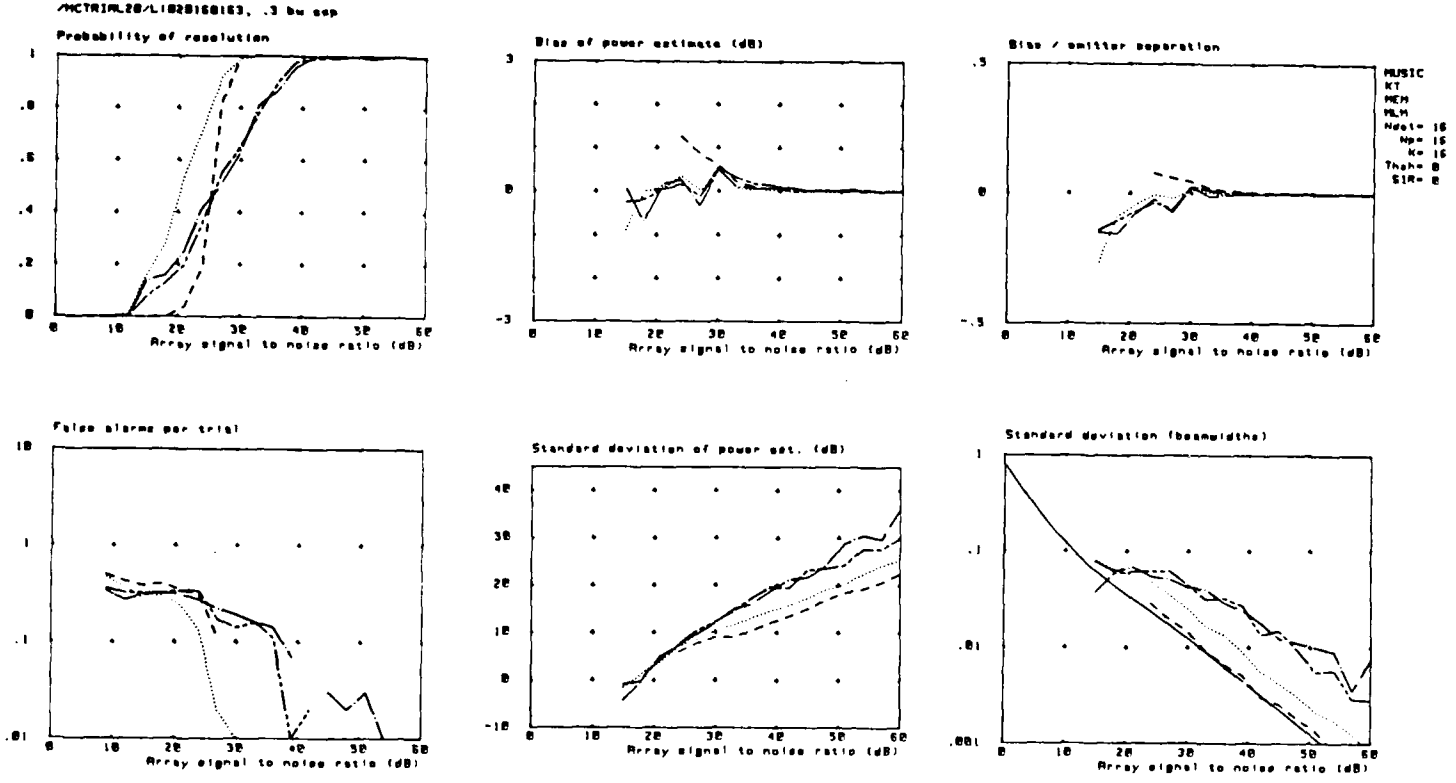
/MCTRIAL20/L1020160163, .3 bw esp
Probability of resolution
Array signal to noise ratio (dB)
Bias of power estimate (dB)
Array signal to noise ratio (dB)
Bias / emitter separation
Array signal to noise ratio (dB)
MUSIC
KT
MEM
MLM
Ndet= 16
Np= 16
K= 16
Thsh= 0
SIR= 0
False alarms per trial
Array signal to noise ratio (dB)
Standard deviation of power est. (dB)
Array signal to noise ratio (dB)
Standard deviation (beamwidths)
Array signal to noise ratio (dB)

Fig. A2.9

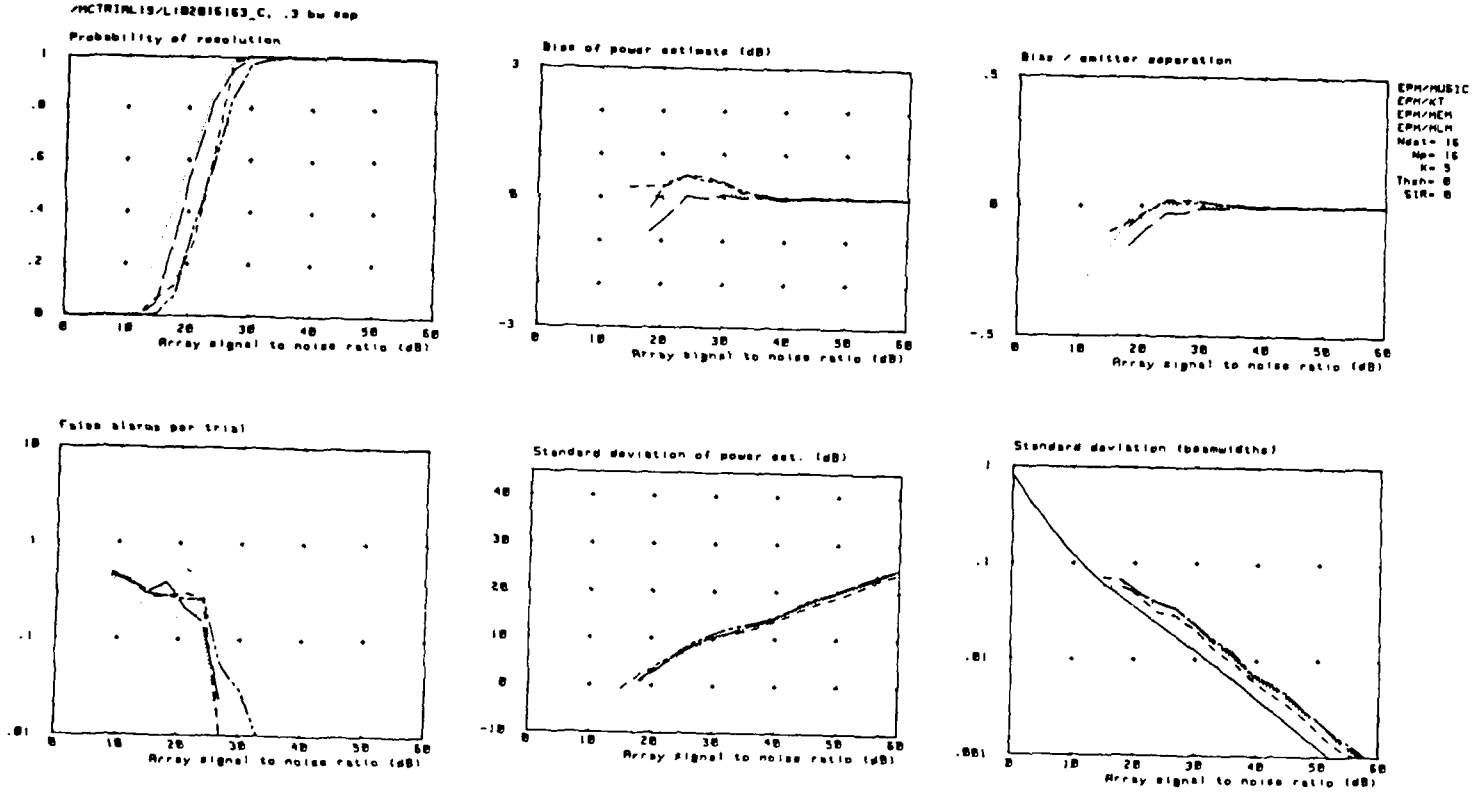
/MCTRIALS3/L1B2B1S163_C, .3 bw sep
Probability of resolution
Array signal to noise ratio (dB)
Bias of power estimate (dB)
Array signal to noise ratio (dB)
Bias / emitter separation
Array signal to noise ratio (dB)
EPM/MUSIC
EPM/KT
EPM/MEM
EPM/MLM
Ndat= 16
Np= 16
K= 3
Thsh= 0
SIR= 0
False alarms per trial
Array signal to noise ratio (dB)
Standard deviation of power est. (dB)
Array signal to noise ratio (dB)
Standard deviation (beamwidths)
Array signal to noise ratio (dB)

Fig. A2.10

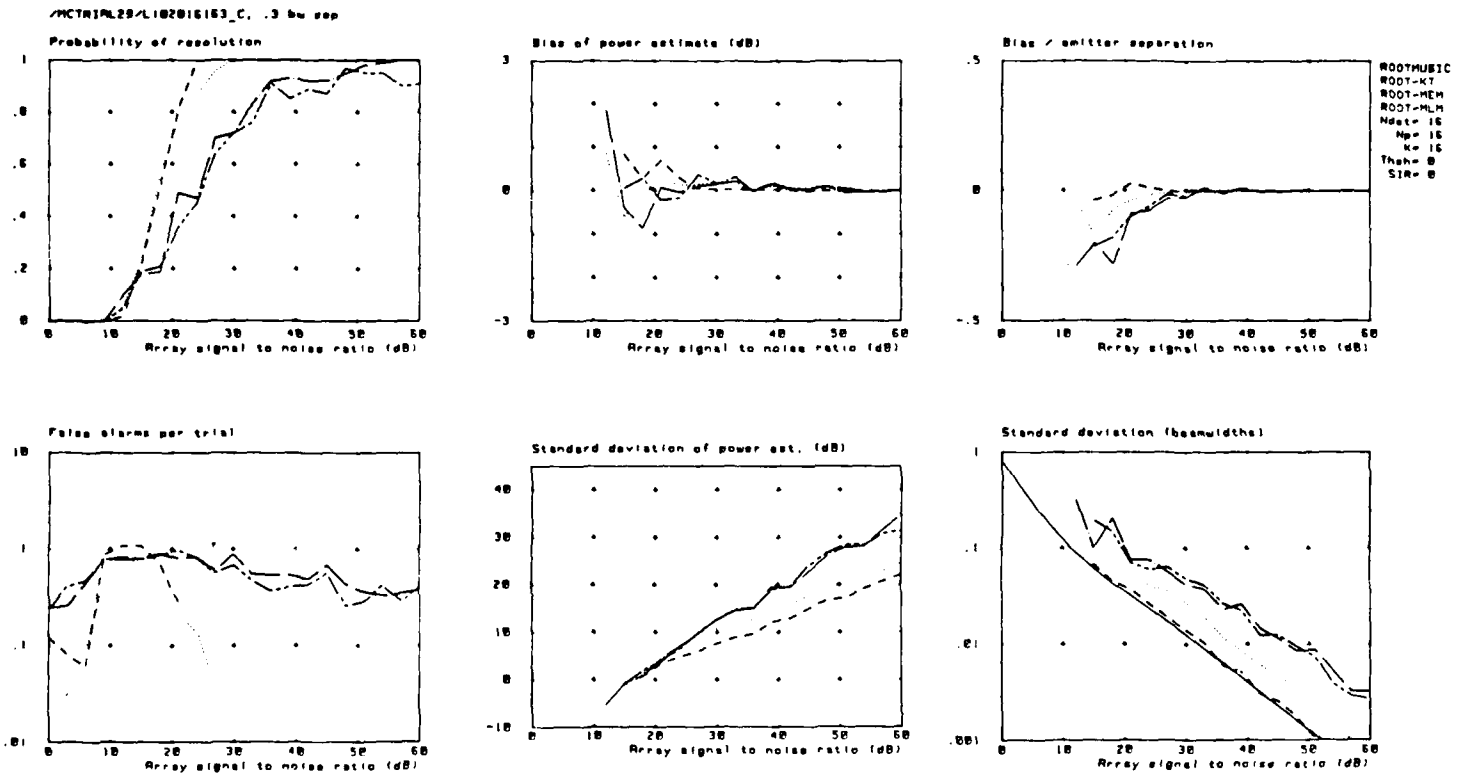
/MCTRIAL29/L18Z0161&3_C, .3 bw sep
Probability of resolution
Array signal to noise ratio (dB)
Bias of power estimate (dB)
Array signal to noise ratio (dB)
Bias / emitter separation
Array signal to noise ratio (dB)
ROOTMUSIC
ROOT-KT
ROOT-MEM
ROOT-MLM
Ndet= 16
Np= 16
K= 16
Thsh= 0
SIR= 0
False alarms per trial
Array signal to noise ratio (dB)
Standard deviation of power est. (dB)
Array signal to noise ratio (dB)
Standard deviation (beamwidths)
Array signal to noise ratio (dB)

Fig. A2.11

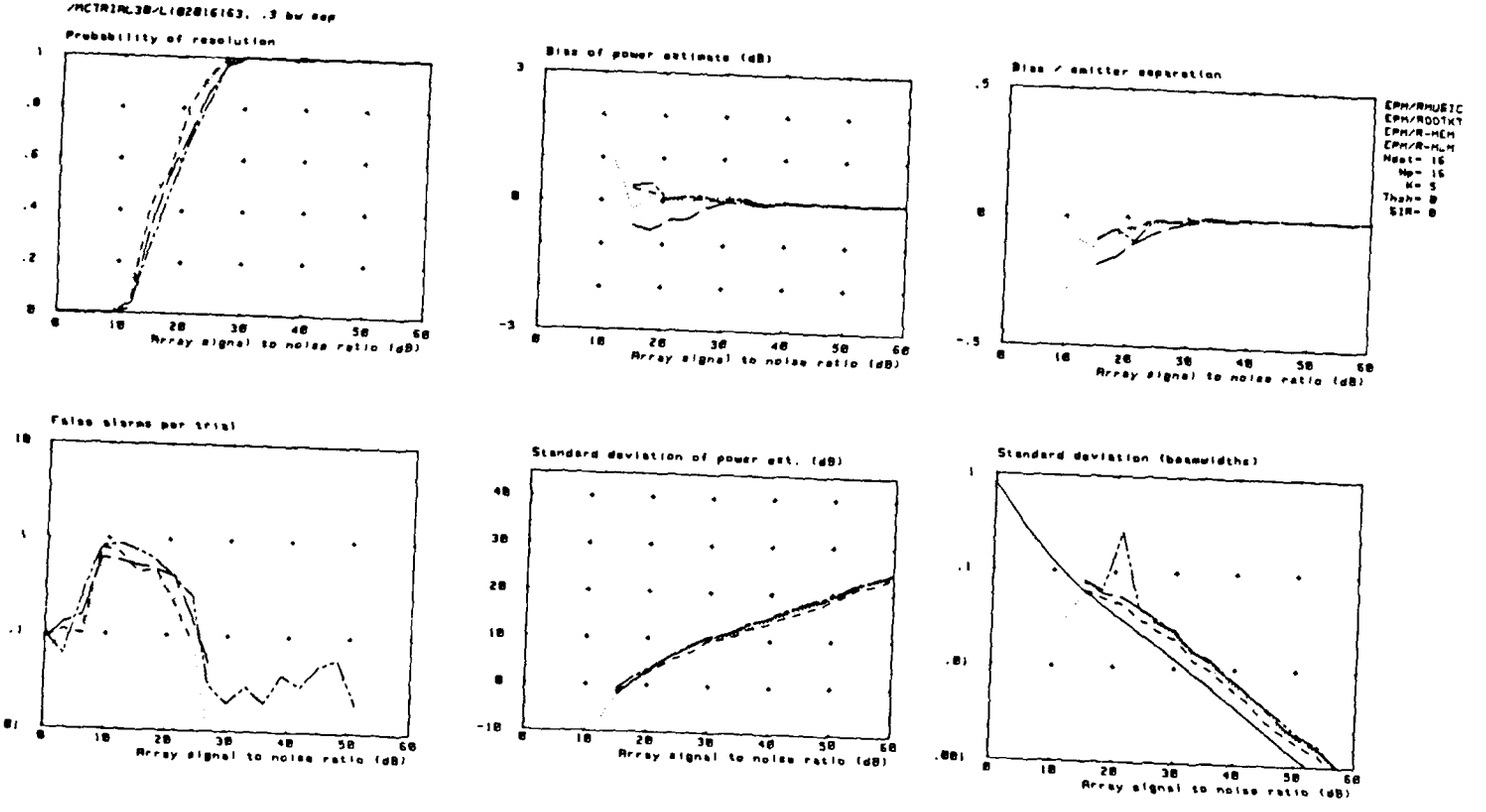
/MCTRIAL30/L102816163, .3 bw sep
Probability of resolution
Array signal to noise ratio (dB)
Bias of power estimate (dB)
Array signal to noise ratio (dB)
Bias / emitter separation
Array signal to noise ratio (dB)
EPM/RMUSIC
EPM/ROOTKY
EPM/R-MEM
EPM/R-MLM
Nsnap= 16
Np= 16
K= 5
Thsh= 0
SIR= 0
False alarms per trial
Array signal to noise ratio (dB)
Standard deviation of power est. (dB)
Array signal to noise ratio (dB)
Standard deviation (beamwidths)
Array signal to noise ratio (dB)

Fig. A2.12

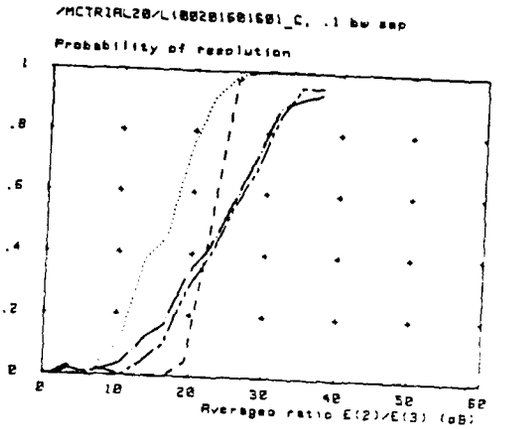

Fig. A2.13

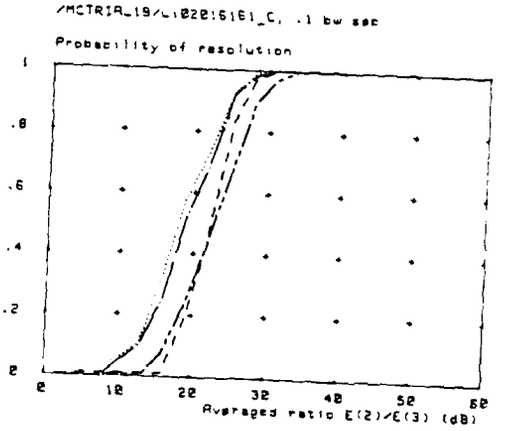

Fig. A2.14

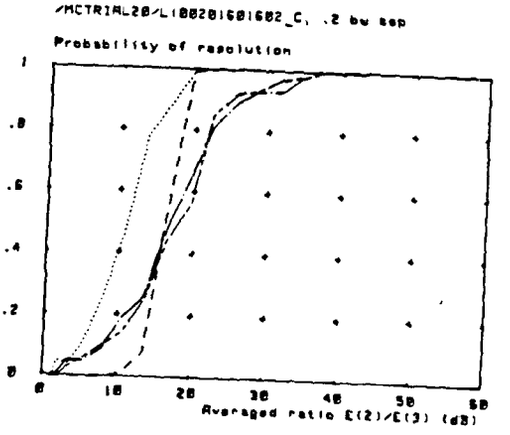

Fig. A2.15

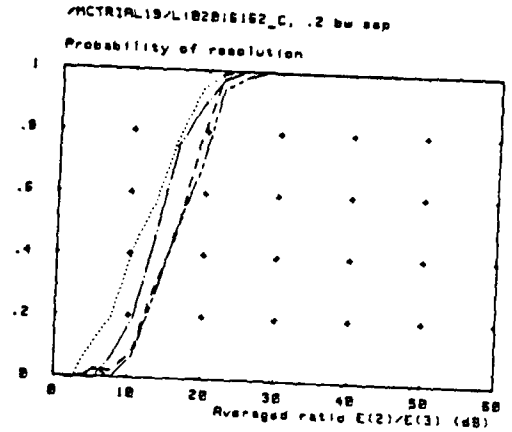

Fig. A2.16

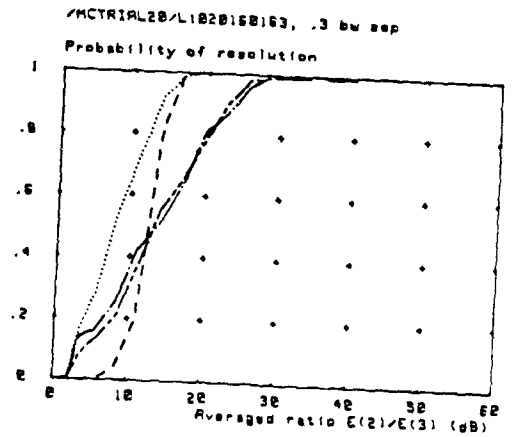

Fig. A2.17

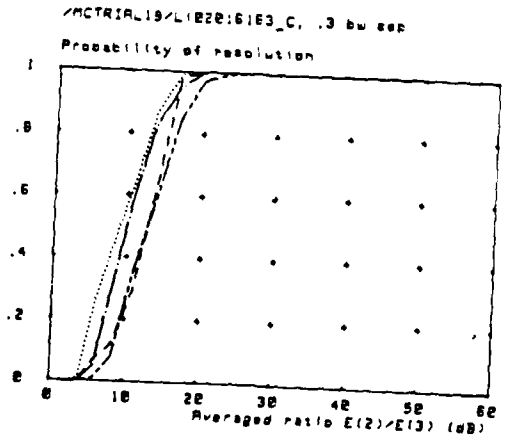

Fig. A2.18

APPENDIX 3. MONTE CARLO RESULTS: TWO UNEQUAL POWER SIGNALS

Contained in this appendix are a number of results relating to the problem described in section 5.2.4. Data from a uniformly weighted 16 element 0.5 wavelength spaced linear array, receiving signals from two far-field random phase point sources, has been simulated and analysed by a variety of high discrimination algorithms and their EPM pre-processed counterparts. Results, in terms of probability of resolution, false alarm rate, and bias and variance of the resolved angle and power estimates, are plotted as follows:

Section A3.1: all as a function of (ASNR) for a variety of angular separations.
Section A3.2: probability of resolution as a function of the average ratio of second to third eigenvalue fo the data covariance matrix.
Section A3.3: all as a function of angular separation for a given ASNR.

The ratio, P1/P2, where P1 is the power of the source at 0 beamwidths and P2 is the power of the other signal, is maintained at -20dB throughout. The ASNR scale in each of the graphs corresponds to the lower power signal.

Each set of plots corresponds to results from a particular group of algorithms, as follows:

A:	MUSIC -----	B:	EPM(k=5)/MUSIC
	KT ·····		EPM(k=5)/KT
	MEM -·-·-·-		EPM(k=5)/MEM
	MLM —-—-—		EPM(k=5)/MLM
C:	ROOT-MUSIC	D:	EPM(k=5)/ROOT-MUSIC
	ROOT-KT		EPM(k=5)/ROOT-KT
	ROOT-MEM		EPM(k=5)/ROOT-MEM
	ROOT-MLM		EPM(k=5)/ROOT-MLM

A3.1 RESULTS AS A FUNCTION OF ASNR

The results as a function of ASNR are plotted as follows:

Figure	Methods	Number of snapshots	Location of signals (beamwidths from boresight)
A3.1	A	16	0, 0.1
A3.2	B		
A3.3	C		
A3.4	D		
A3.5	A	16	0, 0.2
A3.6	B		
A3.7	C		
A3.8	D		
A3.9	A	16	0, 0.3
A3.10	B		
A3.11	C		
A3.12	D		

A3.2. RESULTS AS A FUNCTION OF EIGENVALUE RATIO

A selection of probability of resolution curves have been re-plotted as a function of E(2)/E(3), where E(2) and E(3) are respectively the average values of the second and third largest eigenvalues of the sample covariance estimates.

Figure	Methods	Number of snapshots	Location of signals (beamwidths from boresight)
A3.13 A3.14	A B	16	0, 0.1
A3.15 A3.16	A B	16	0, 0.2
A3.17 A3.18	A B	16	0, 0.3

A3.3. RESULTS AS A FUNCTION OF ANGULAR SEPARATION

A selection of results have been replotted as a function of angular separation for a given ASNR (corresponding to the signal located at broadside), as follows:

Figure	Methods	Number of snapshots	ASNR (dB)
A3.19 A3.20	A B	16	21

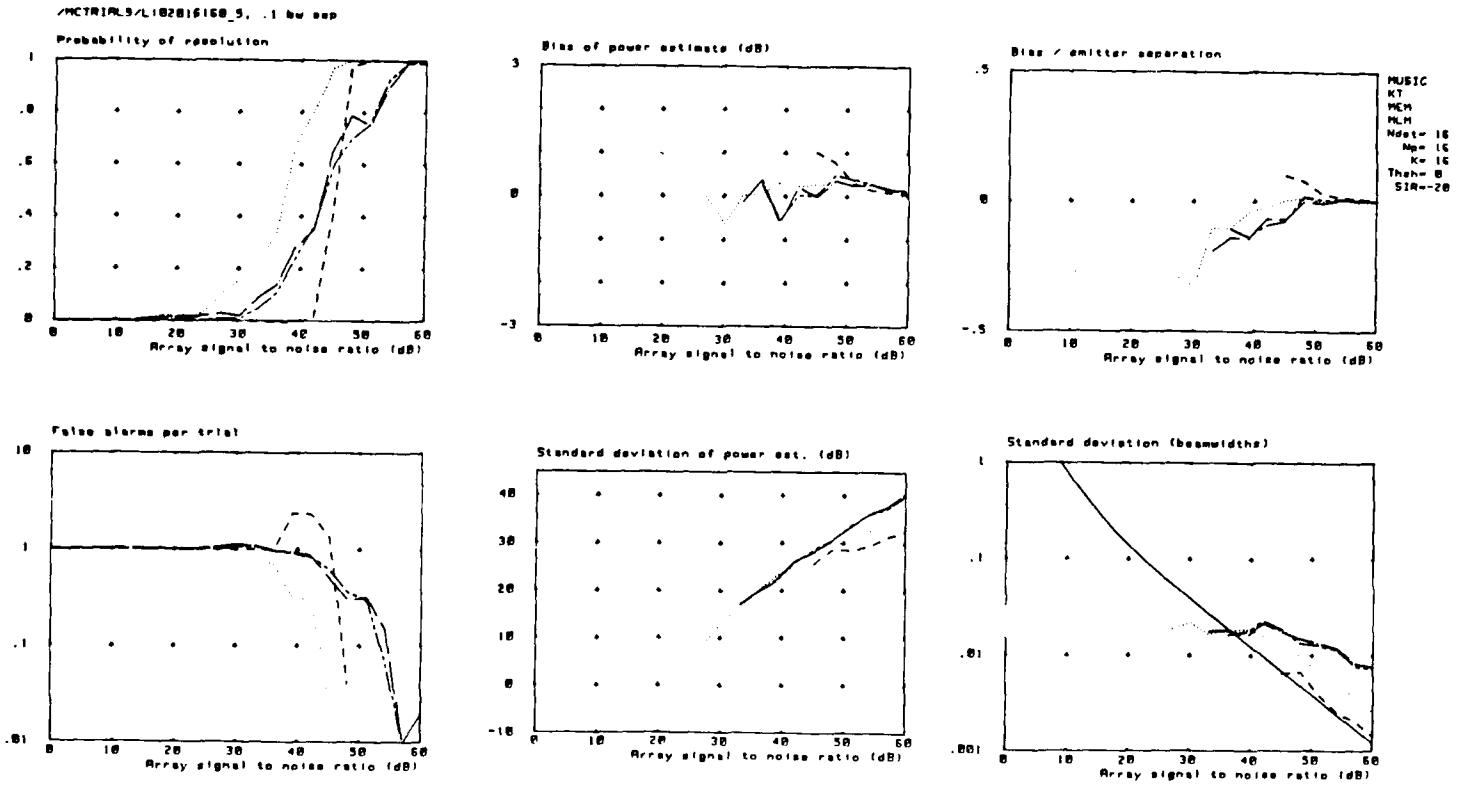
/MCTRIAL5/L102816168_5, .1 bw esp
Probability of resolution
Array signal to noise ratio (dB)
Bias of power estimate (dB)
Array signal to noise ratio (dB)
Bias / emitter separation
MUSIC
KT
MEM
MLM
Ndat= 16
Ns= 16
K= 16
Thsh= 0
SIR=-20
Array signal to noise ratio (dB)
False alarms per trial
Array signal to noise ratio (dB)
Standard deviation of power est. (dB)
Array signal to noise ratio (dB)
Standard deviation (beamwidths)
Array signal to noise ratio (dB)

Fig. A3.1

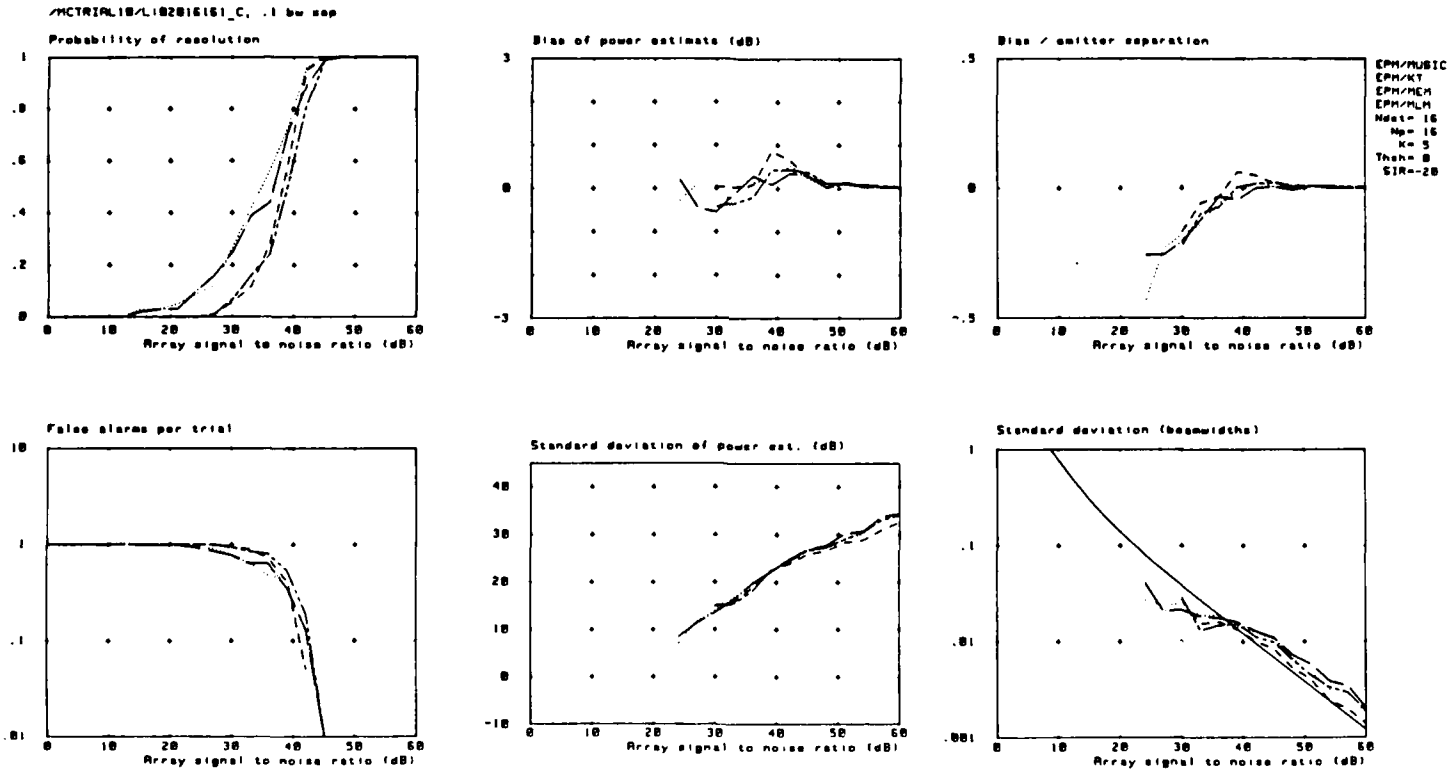
/MCTRIAL18/L18281616I_C, .1 bw sep
Probability of resolution
Bias of power estimate (dB)
Bias / emitter separation
EPM/MUSIC
EPM/KT
EPM/MEM
EPM/MLM
Ndat= 16
Np= 16
K= 5
Thsh= 8
SIR=-20
False alarms per trial
Standard deviation of power est. (dB)
Standard deviation (beamwidths)
Array signal to noise ratio (dB)

Fig. A3.2

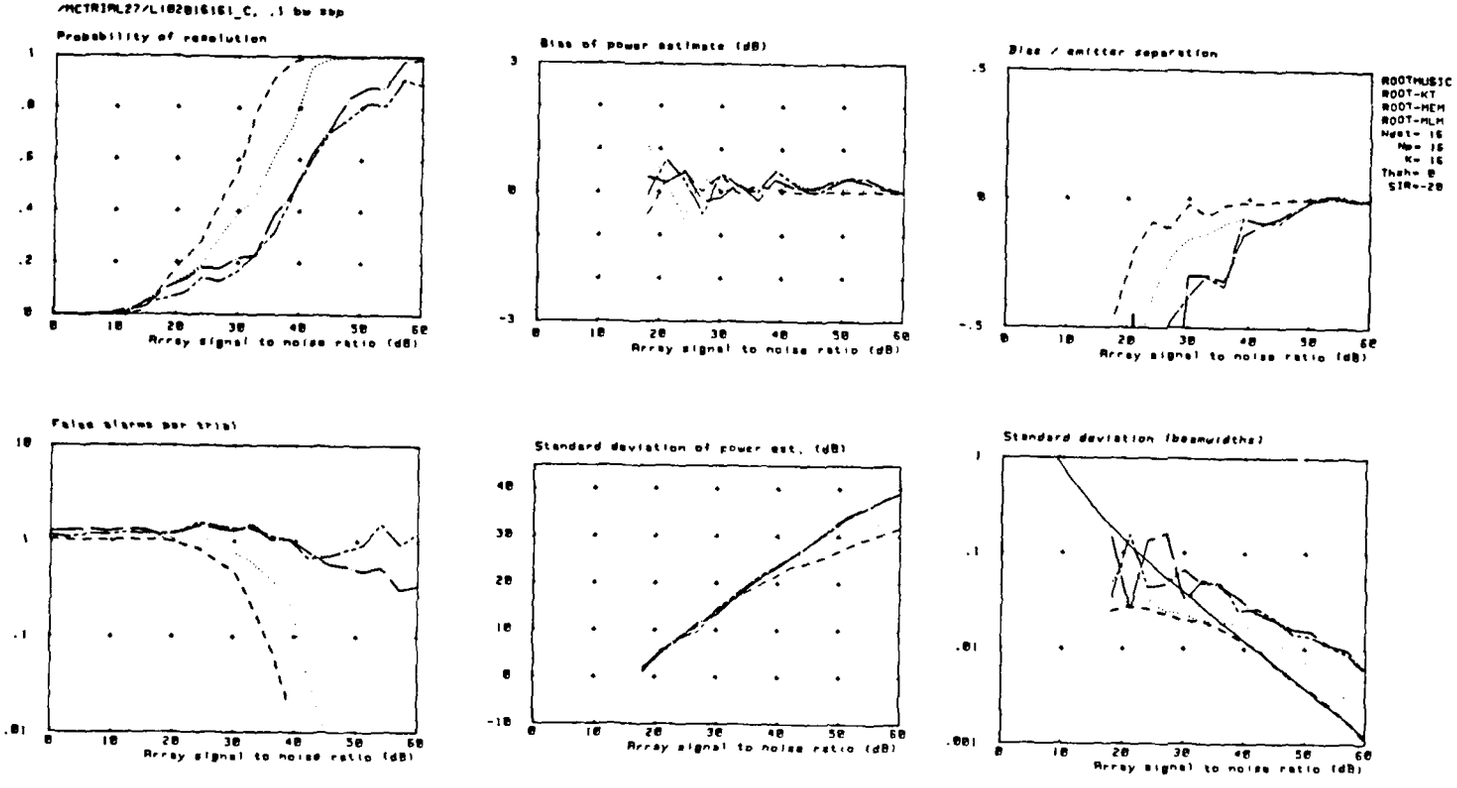
/MCTRIAL27/L102B1616I_C, .1 bw sep
Probability of resolution
Array signal to noise ratio (dB)
Bias of power estimate (dB)
Array signal to noise ratio (dB)
Bias / emitter separation
ROOTMUSIC
ROOT-KT
ROOT-MEM
ROOT-MLM
Nest= 16
Ns= 16
K= 16
Thsh= 0
SIR=-20
Array signal to noise ratio (dB)
False alarms per trial
Array signal to noise ratio (dB)
Standard deviation of power est. (dB)
Array signal to noise ratio (dB)
Standard deviation (beamwidths)
Array signal to noise ratio (dB)

Fig. A3.3

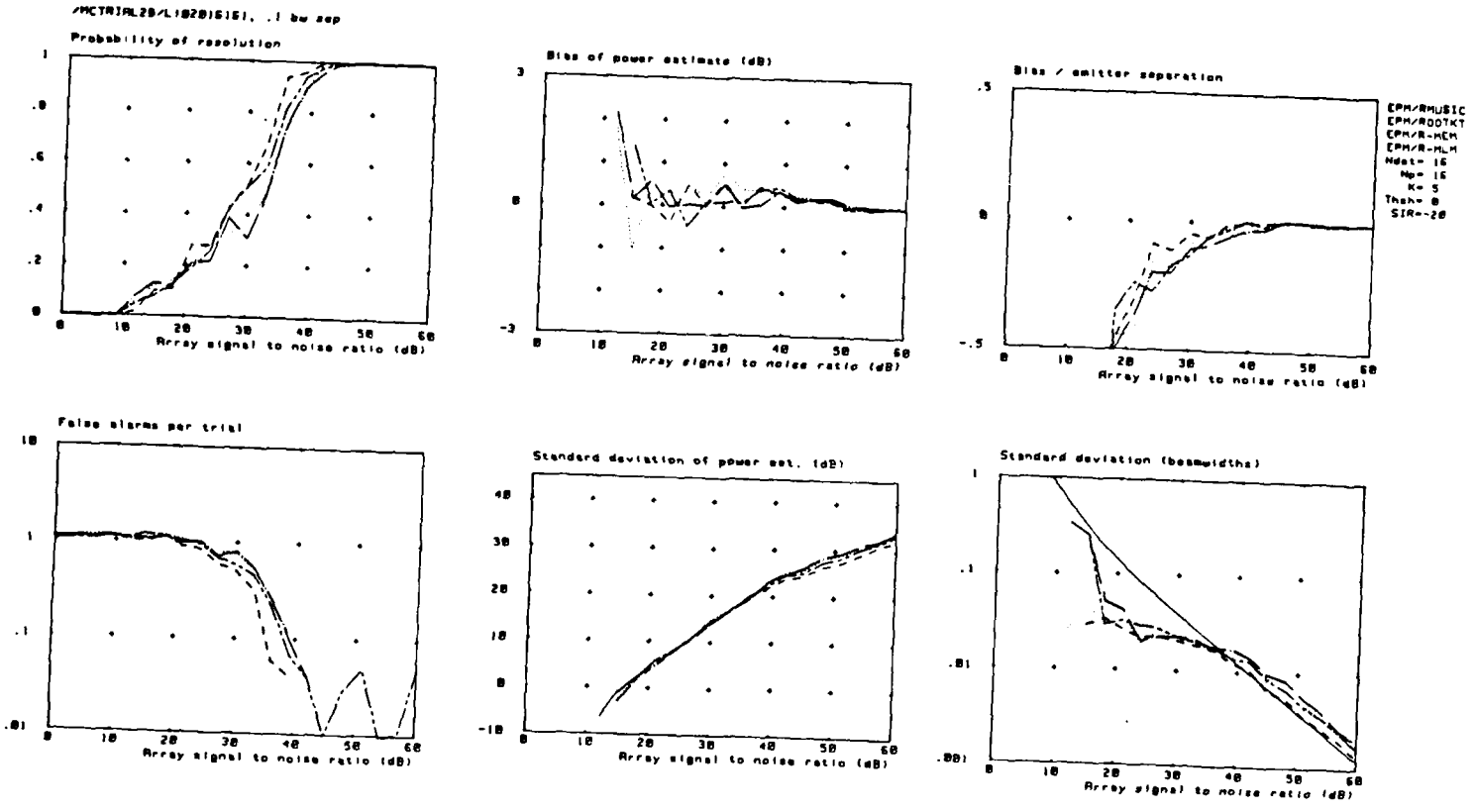
Probability of resolution
Array signal to noise ratio (dB)
Bias of power estimate (dB)
Array signal to noise ratio (dB)
Bias / emitter separation
EPM/RMUSIC
EPM/ROOTKT
EPM/R-MEM
EPM/R-MLM
Ndat= 16
Np= 16
K= 5
Thsh= 0
SIR=-20
Array signal to noise ratio (dB)
False alarms per trial
Array signal to noise ratio (dB)
Standard deviation of power est. (dB)
Array signal to noise ratio (dB)
Standard deviation (beamwidths)
Array signal to noise ratio (dB)

Fig. A3.4

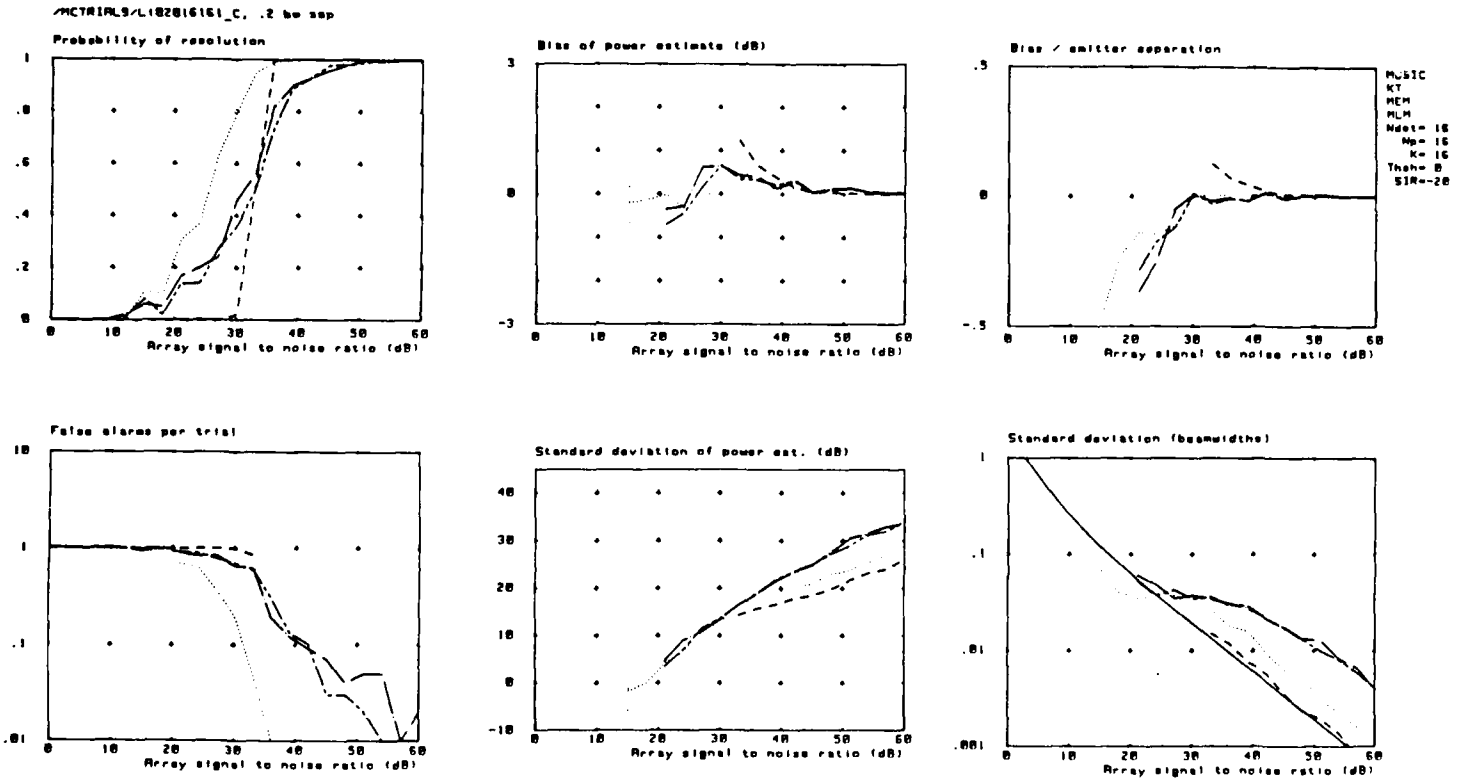
/MCTRIRLS/L1B2B16161_C, .2 bw sep
Probability of resolution
Array signal to noise ratio (dB)
Bias of power estimate (dB)
Array signal to noise ratio (dB)
Bias / emitter separation
Array signal to noise ratio (dB)
MUSIC
KT
MEM
MLM
Ndet= 16
Ns= 16
K= 16
Theta= 0
SIR=-20
False alarms per trial
Array signal to noise ratio (dB)
Standard deviation of power est. (dB)
Array signal to noise ratio (dB)
Standard deviation (beamwidths)
Array signal to noise ratio (dB)

Fig. A3.5

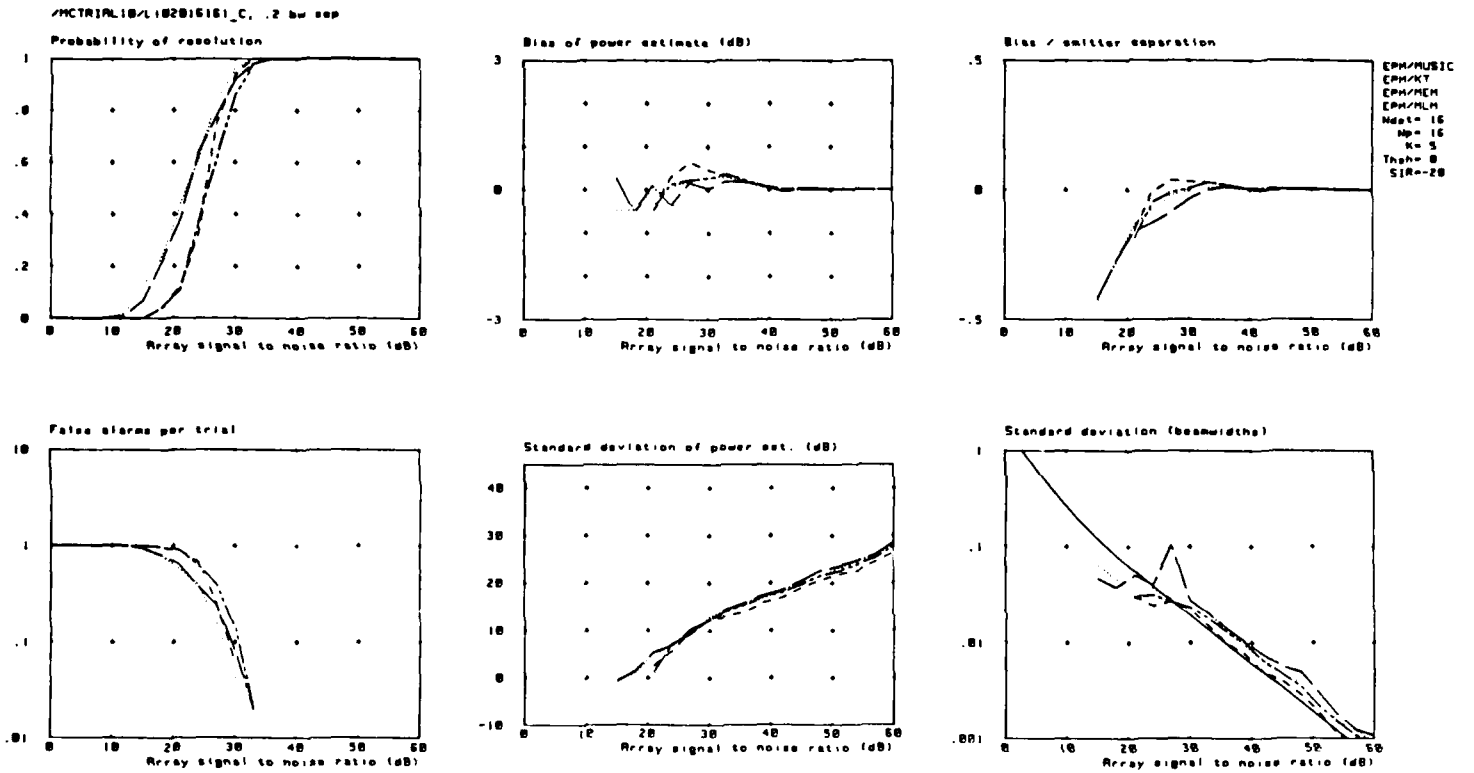
/MCTRIAL10/L10201616)_C, .2 bw sep
Probability of resolution
Array signal to noise ratio (dB)
Bias of power estimate (dB)
Array signal to noise ratio (dB)
Bias / emitter separation
EPM/MUSIC
EPM/RT
EPM/MEM
EPM/MLM
Nsnt= 16
Mp= 16
K= 5
Thsh= 0
SIR=-20
Array signal to noise ratio (dB)
False alarms per trial
Array signal to noise ratio (dB)
Standard deviation of power est. (dB)
Array signal to noise ratio (dB)
Standard deviation (beamwidths)
Array signal to noise ratio (dB)

Fig. A3.6

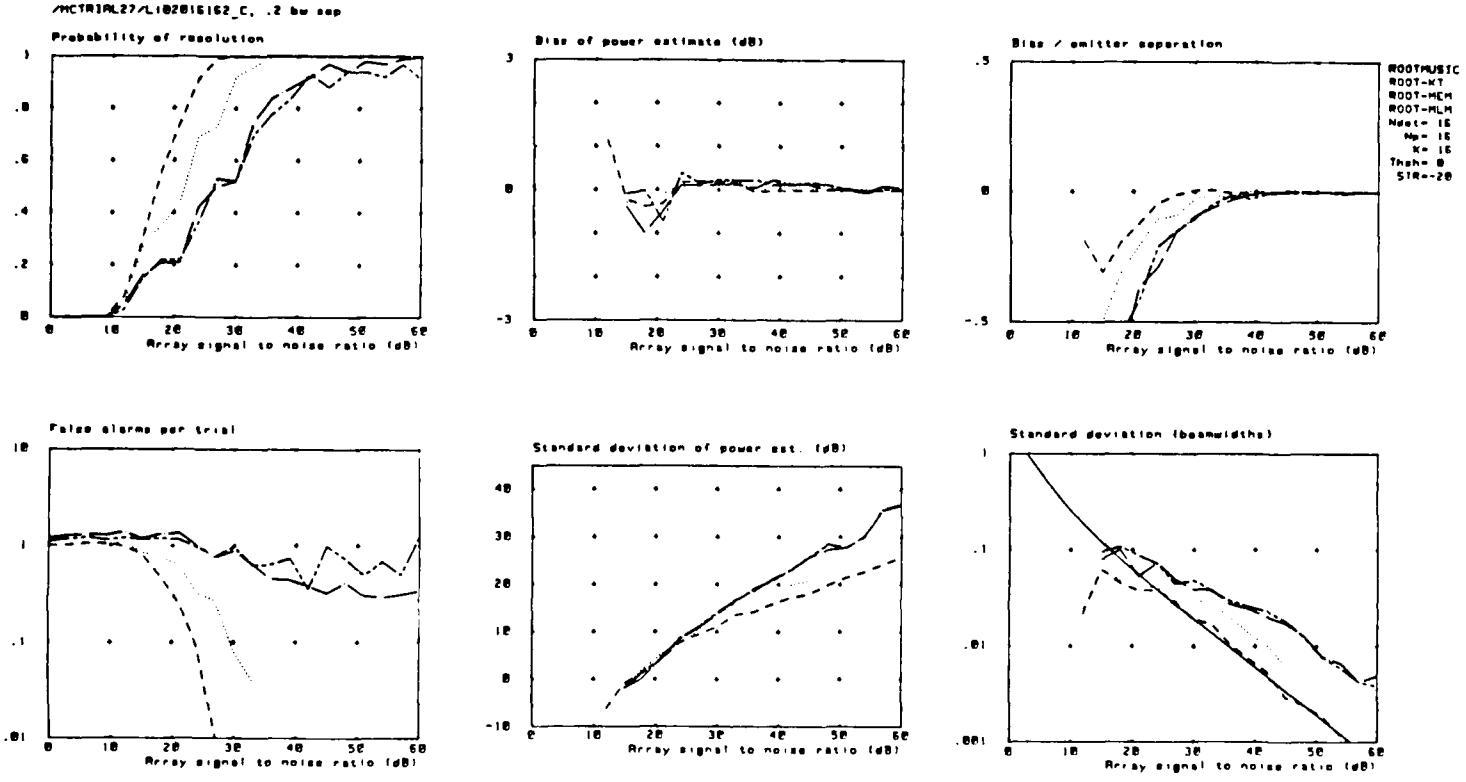
/HCTR1RL27/L1@2B1S1S2_C, .2 bw sep
Probability of resolution
Array signal to noise ratio (dB)
Bias of power estimate (dB)
Array signal to noise ratio (dB)
Bias / emitter separation
Array signal to noise ratio (dB)
ROOTMUSIC
ROOT-KT
ROOT-MEM
ROOT-MLM
False alarms per trial
Array signal to noise ratio (dB)
Standard deviation of power est. (dB)
Array signal to noise ratio (dB)
Standard deviation (beamwidths)
Array signal to noise ratio (dB)

Fig. A3.7

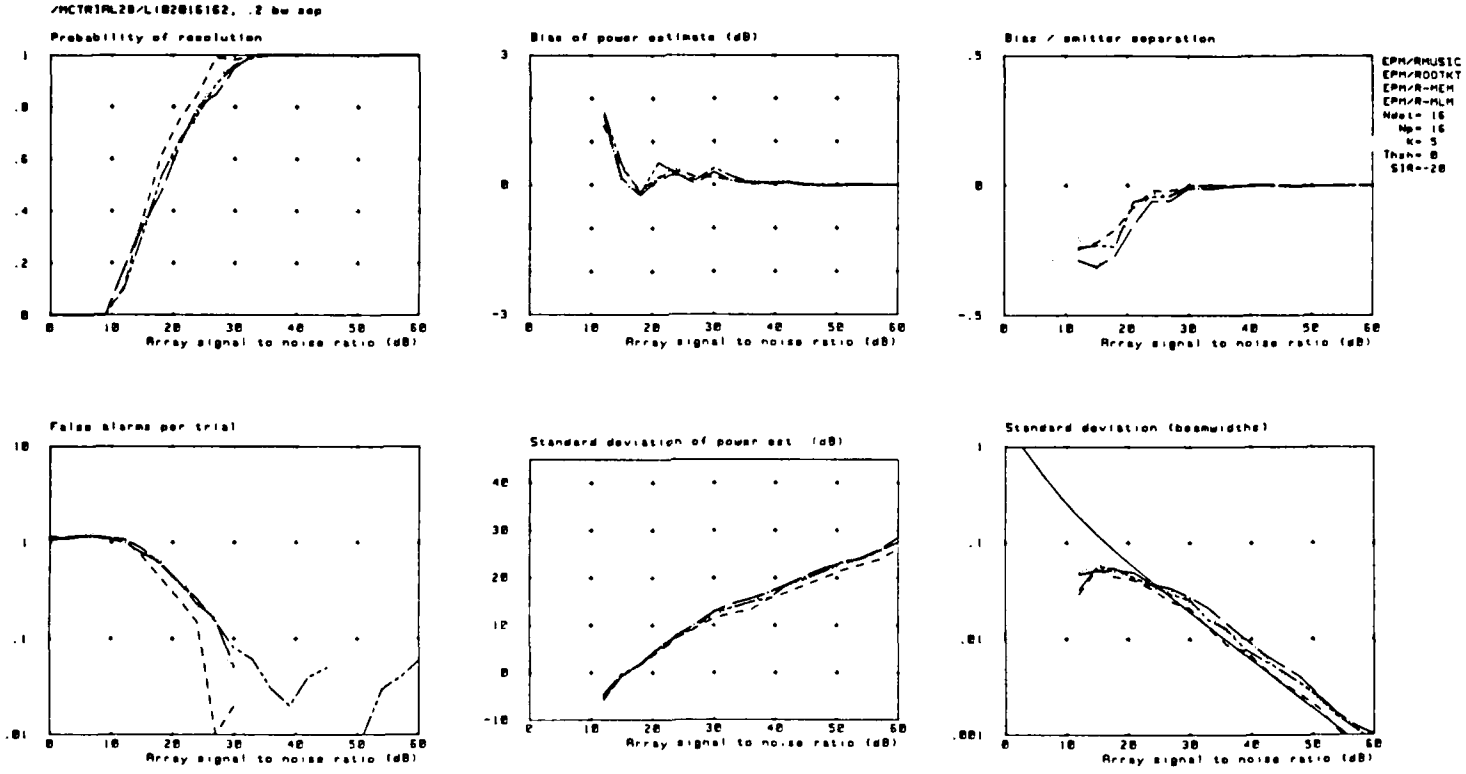
/MCTRIAL28/LIB2816162, .2 bw sep
Probability of resolution
Bias of power estimate (dB)
Bias / emitter separation
EPM/RMUSIC
EPM/ROOTKT
EPM/R-MEM
EPM/R-MLM
Ndel= 16
Np= 16
K= 5
Thsw= 0
SIG=-20
False alarms per trial
Standard deviation of power est (dB)
Standard deviation (beamwidths)
Array signal to noise ratio (dB)

Fig. A3.8

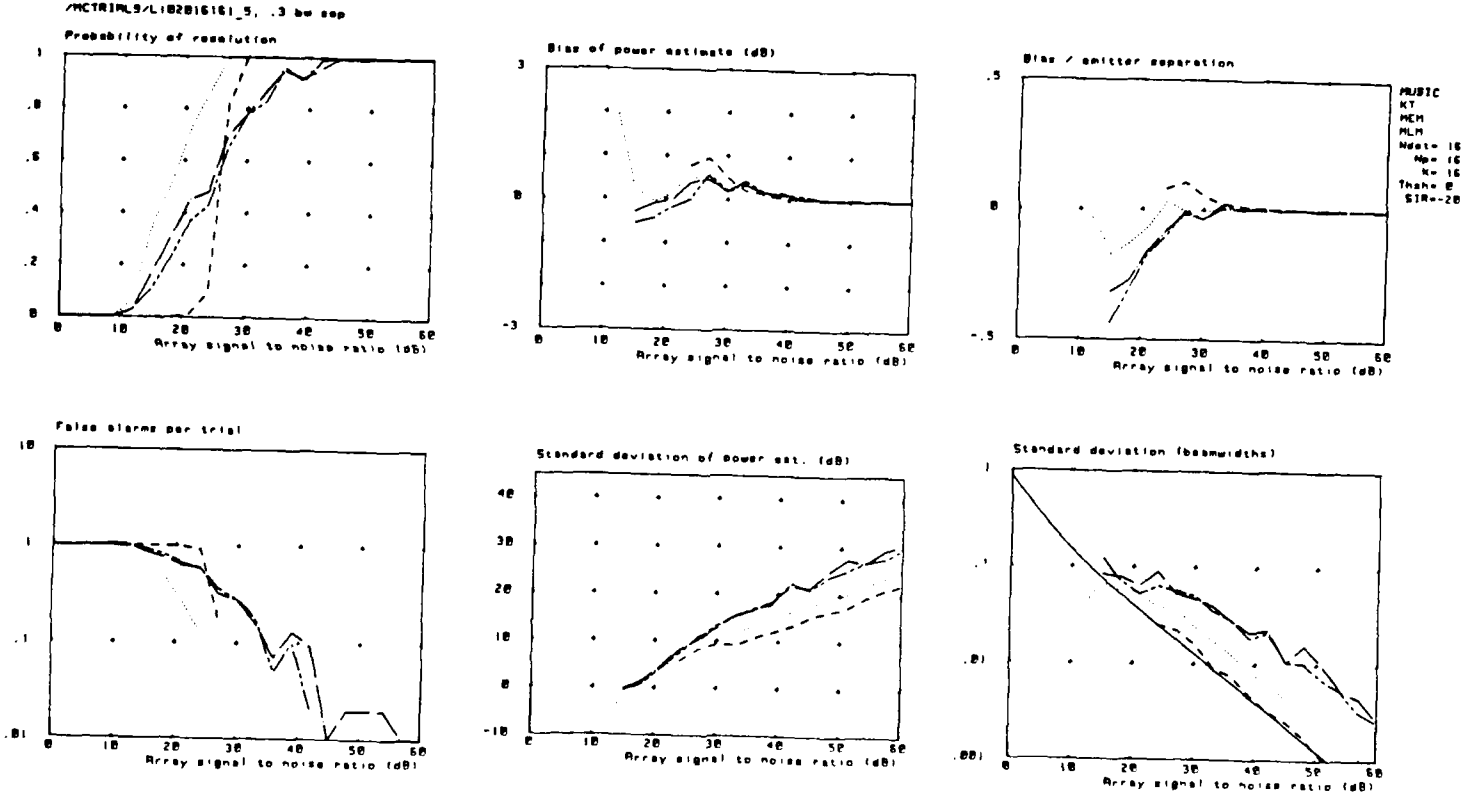
/MCTRIAL9/L1B2B1616I_5, .3 bw sep
Probability of resolution
Array signal to noise ratio (dB)
Bias of power estimate (dB)
Array signal to noise ratio (dB)
Bias / emitter separation
Array signal to noise ratio (dB)
MUSIC
KT
MEM
MLM
Ndat= 16
Np= 16
N= 16
Thsh= 0
SIR=-20
False alarms per trial
Array signal to noise ratio (dB)
Standard deviation of power est. (dB)
Array signal to noise ratio (dB)
Standard deviation (beamwidths)
Array signal to noise ratio (dB)

Fig. A3.9

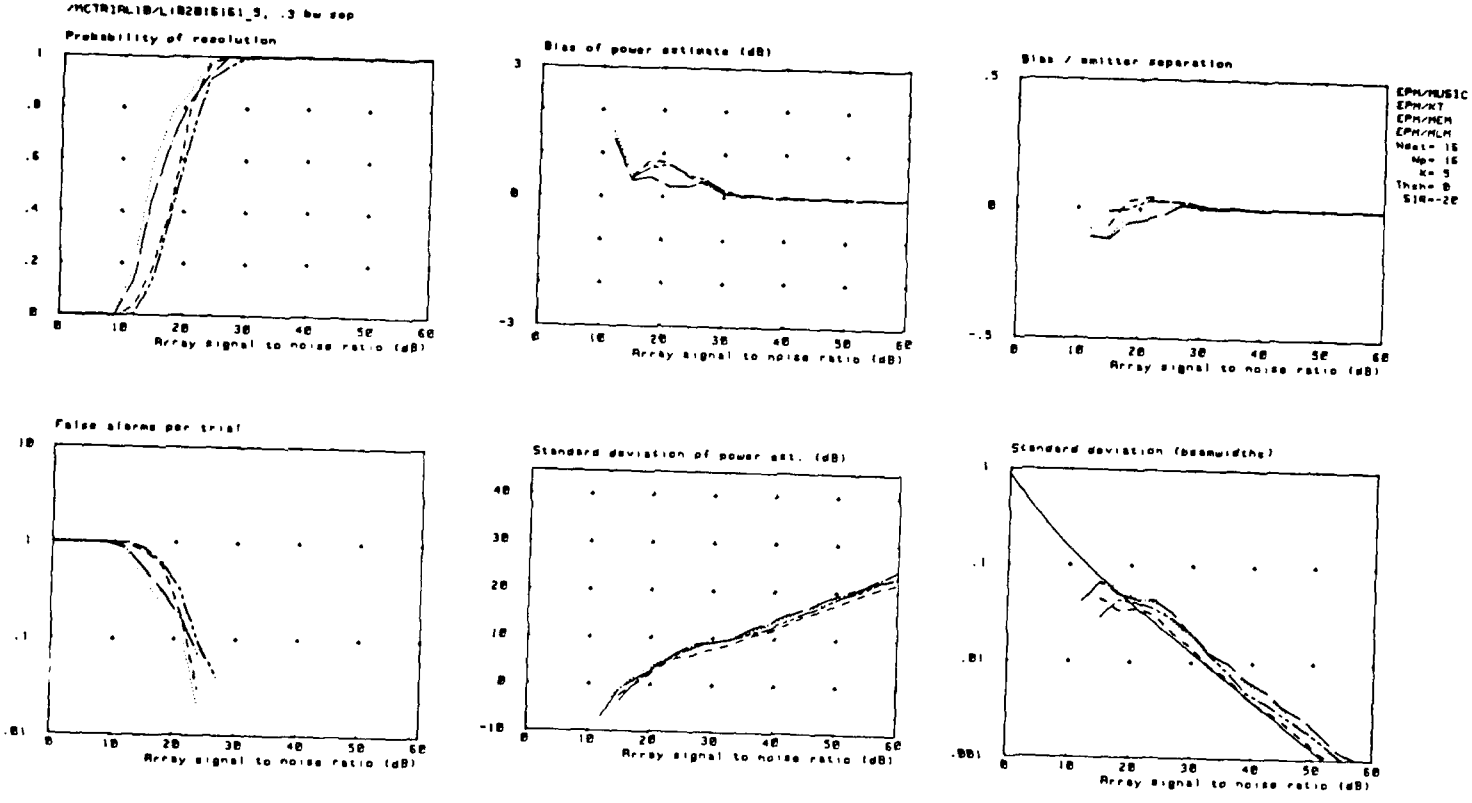
Probability of resolution
Array signal to noise ratio (dB)
Bias of power estimate (dB)
Array signal to noise ratio (dB)
Bias / emitter separation
Array signal to noise ratio (dB)
EPM/MUSIC
EPM/XT
EPM/MEM
EPM/MLM
False alarms per trial
Array signal to noise ratio (dB)
Standard deviation of power est. (dB)
Array signal to noise ratio (dB)
Standard deviation (beamwidths)
Array signal to noise ratio (dB)

Fig. A3.10

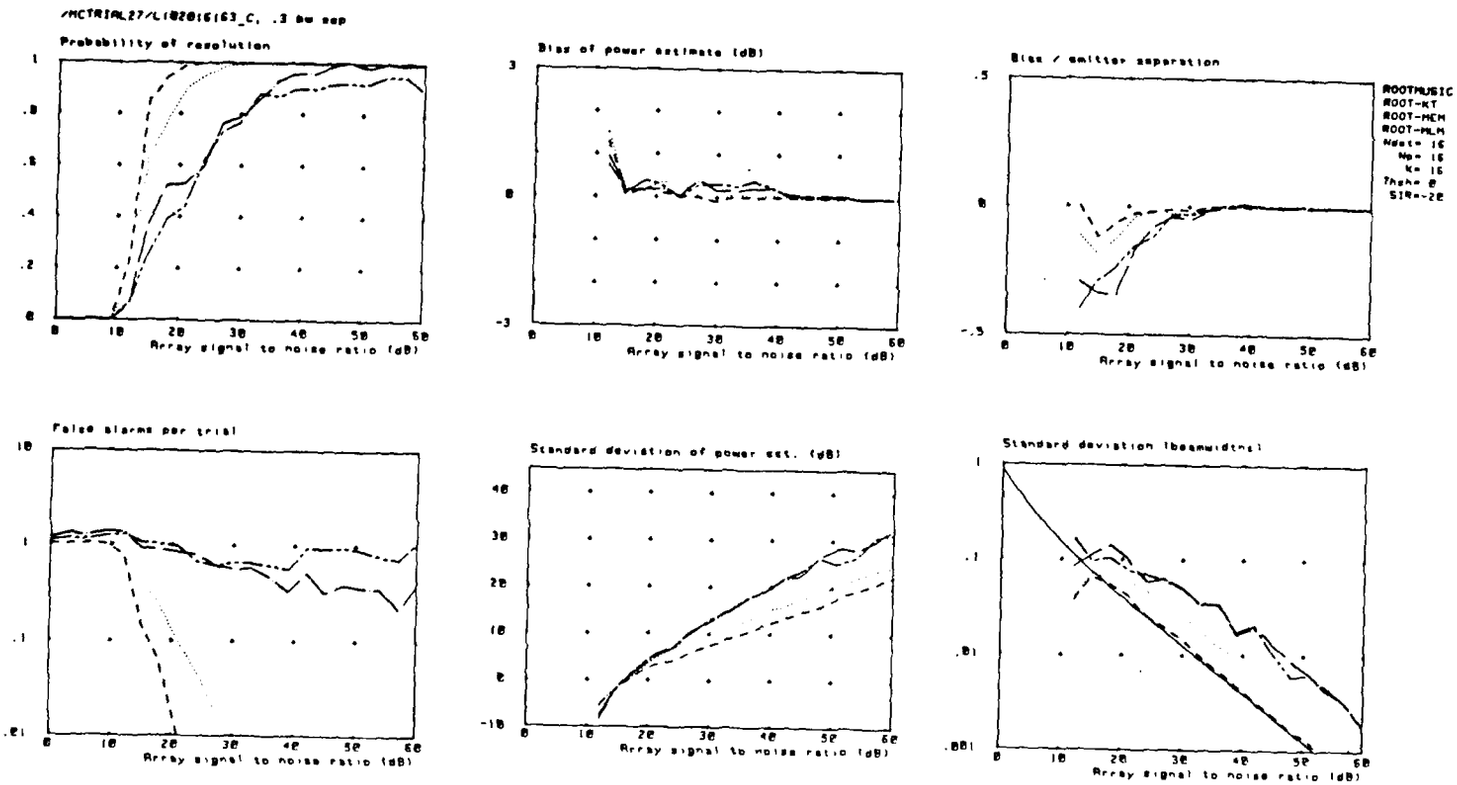
/MCTRIAL27/L18Z816163_C, .3 Bw sep
Probability of resolution
Bias of power estimate (dB)
Bias / emitter separation
ROOTMUSIC
ROOT-KT
ROOT-MEM
ROOT-MLM
False alarms per trial
Standard deviation of power est. (dB)
Standard deviation (beamwidths)
Array signal to noise ratio (dB)

Fig. A3.11

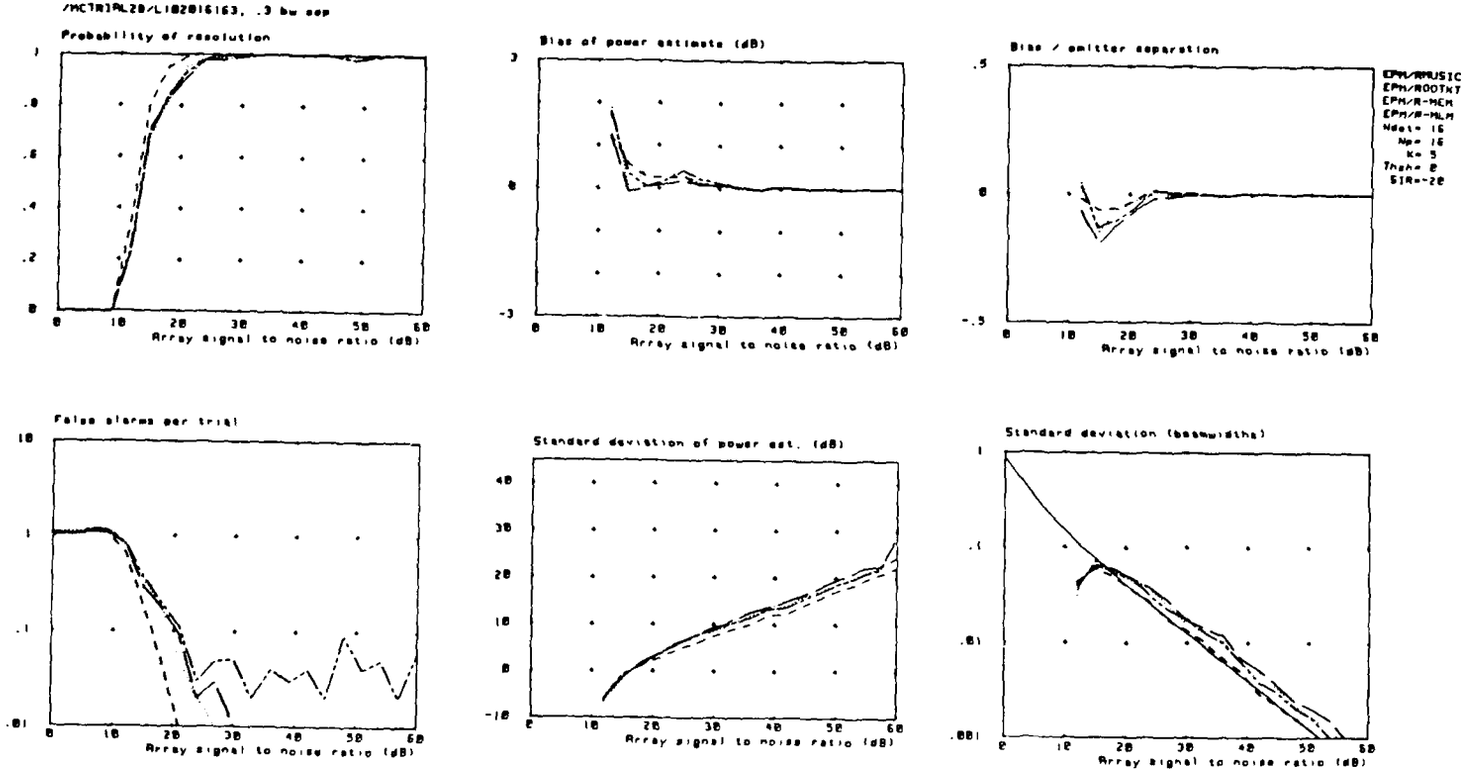
/MCTR1RL28/LI02816163, .3 bw sep
Probability of resolution
Array signal to noise ratio (dB)
Bias of power estimate (dB)
Array signal to noise ratio (dB)
Bias / emitter separation
Array signal to noise ratio (dB)
EPM/MMUSIC
EPM/ROOTMT
EPM/R-MEM
EPM/R-MLM
Ndata= 16
Npm= 16
K= 5
Thsh= 0
SIR=-20
False alarms per trial
Array signal to noise ratio (dB)
Standard deviation of power est. (dB)
Array signal to noise ratio (dB)
Standard deviation (beamwidths)
Array signal to noise ratio (dB)

Fig. A3.12

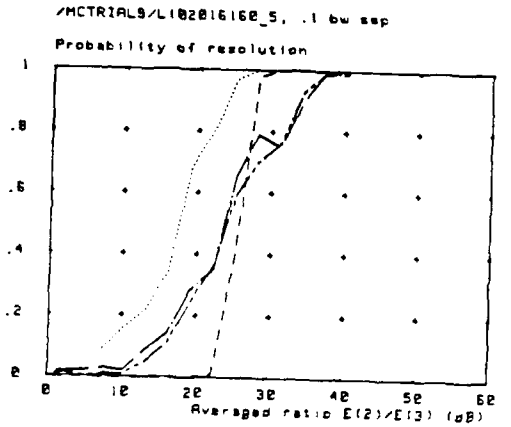

Fig. A3.13

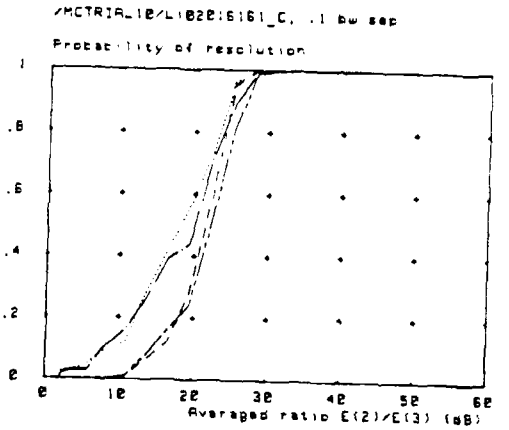

Fig. A3.14

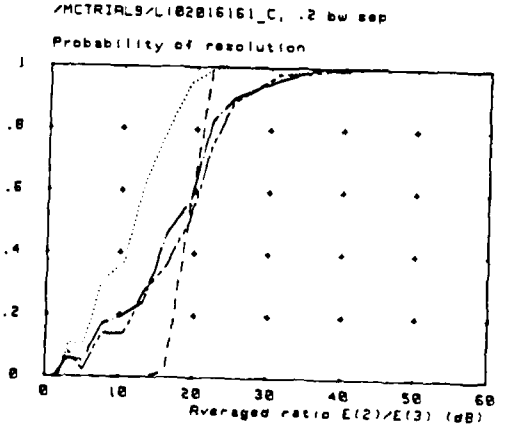

Fig. A3.15

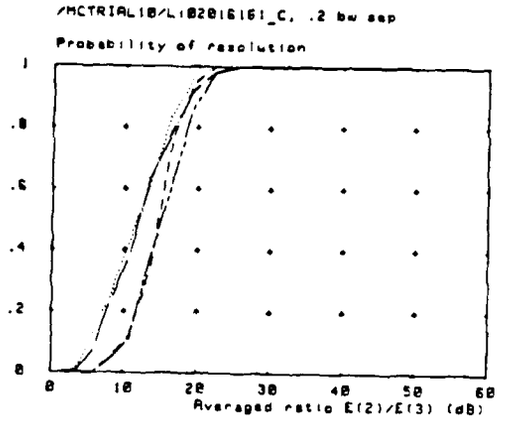

Fig. A3.16

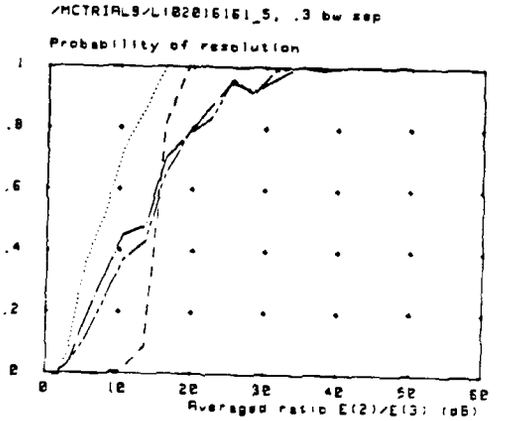

Fig. A3.17

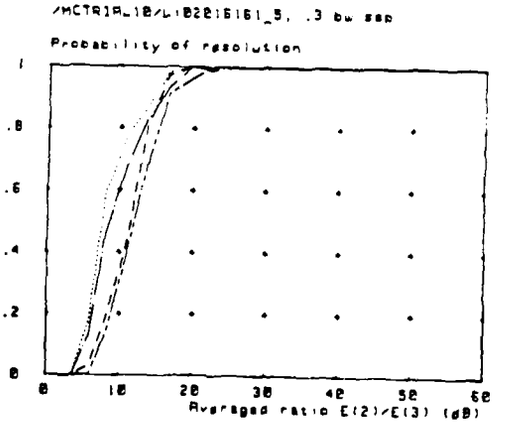

Fig. A3.18

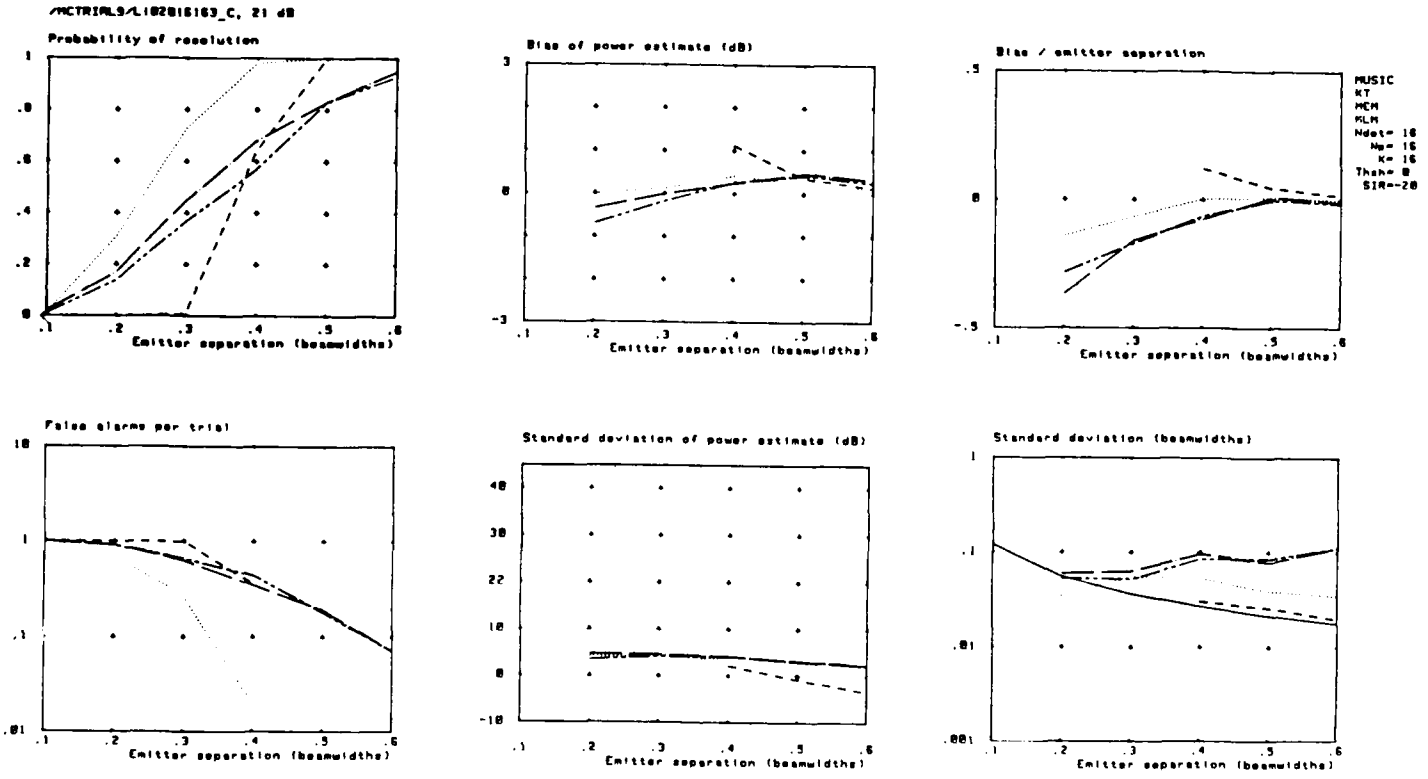
/MCTRIALS/L102816163_C, 21 dB
Probability of resolution
Emitter separation (beamwidths)
Bias of power estimate (dB)
Emitter separation (beamwidths)
Bias / emitter separation
Emitter separation (beamwidths)
MUSIC
KT
MCM
MLM
Ndet= 16
Ns= 16
K= 16
Thsh= 0
SIR=-20
False alarms per trial
Emitter separation (beamwidths)
Standard deviation of power estimate (dB)
Emitter separation (beamwidths)
Standard deviation (beamwidths)
Emitter separation (beamwidths)

Fig. A3.19

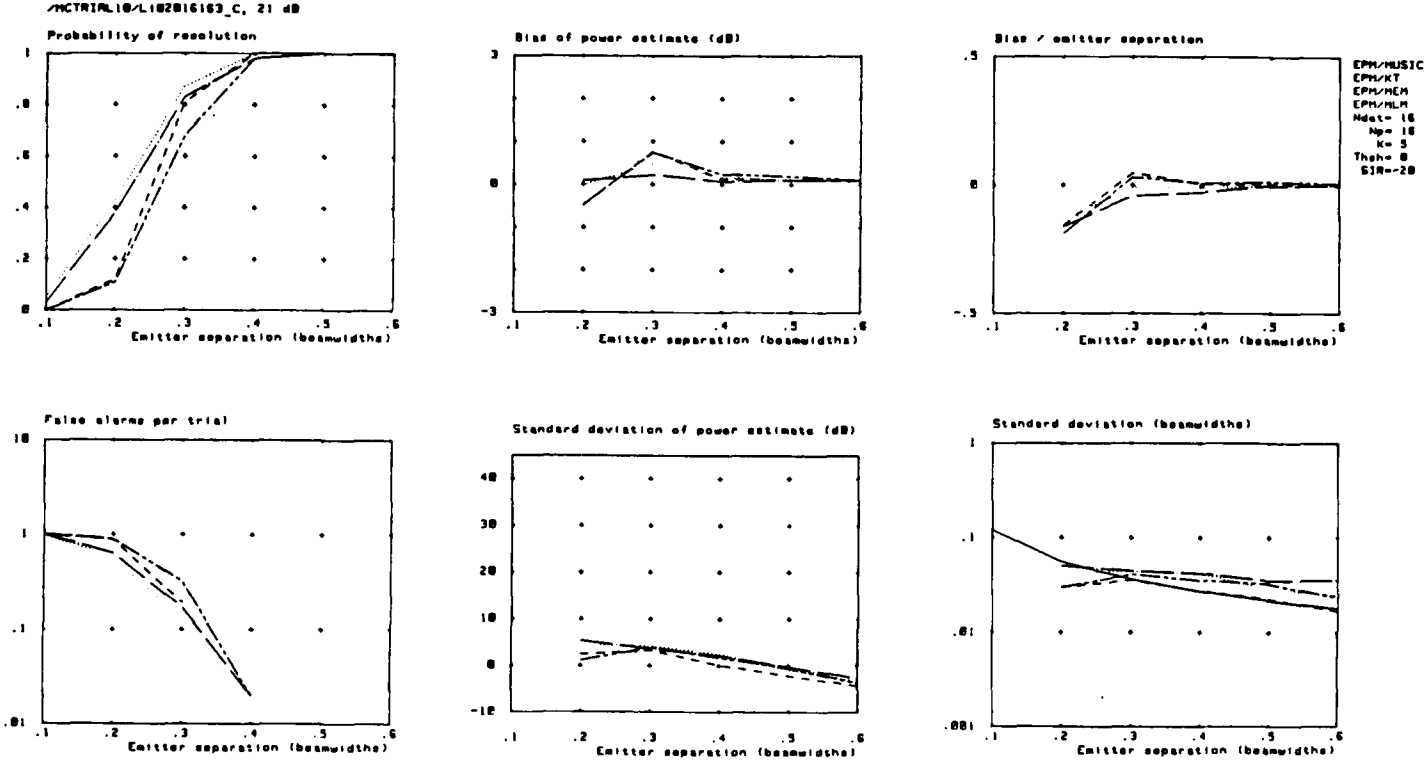
/MCTRIAL10/L10Z016103_C, 21 dB
Probability of resolution
Emitter separation (beamwidths)
Bias of power estimate (dB)
Emitter separation (beamwidths)
Bias / emitter separation
Emitter separation (beamwidths)
EPM/MUSIC
EPM/KT
EPM/MEM
EPM/MLM
Ndet= 16
Np= 16
K= 5
Thsh= 0
SIR=-20
False alarms per trial
Emitter separation (beamwidths)
Standard deviation of power estimate (dB)
Emitter separation (beamwidths)
Standard deviation (beamwidths)
Emitter separation (beamwidths)

Fig. A3.20

APPENDIX 4. MONTE CARLO RESULTS: ARRAY CALIBRATION ERRORS

Contained in this appendix are a number of results relating to the problem described in section 5.2.5. Data from a 16 element 0.5 wavelength spaced linear array, receiving signals from two far-field random phase point sources, has been simulated and analysed by a variety of high discrimination algorithms and their EPM pre-processed counterparts. The calibration of the array is assumed by the algorithms to correspond to uniform amplitude and phase weighting across the elements, but in fact has been perturbed by randomly distributed errors chosen from independent rectangular distributions. Amplitude errors at each element are between ±10%, and phase errors are between ±1%. Assumed and actual weights are as follows:

Element	assumed amplitude	assumed phase (rads)	perturbed amplitude	perturbed phase (rads)
1	1.0	0.0	0.917188	-1.204603×10^{-2}
2	1.0	0.0	0.978620	4.648638×10^{-2}
3	1.0	0.0	1.072075	-1.910583×10^{-2}
4	1.0	0.0	0.934826	1.410884×10^{-2}
5	1.0	0.0	0.999926	-2.143270×10^{-2}
6	1.0	0.0	1.092877	-0.472322×10^{-2}
7	1.0	0.0	1.057702	0.350052×10^{-2}
8	1.0	0.0	1.036057	0.536220×10^{-2}
9	1.0	0.0	1.034596	3.968480×10^{-2}
10	1.0	0.0	0.935603	4.797734×10^{-2}
11	1.0	0.0	0.954129	3.087766×10^{-2}
12	1.0	0.0	0.951808	2.046928×10^{-2}
13	1.0	0.0	0.936404	-3.966099×10^{-2}
14	1.0	0.0	0.901499	-5.989737×10^{-2}
15	1.0	0.0	0.994882	-1.169561×10^{-2}
16	1.0	0.0	0.952047	3.292482×10^{-2}

Results, in terms of probability of resolution, false alarm rate, and bias and variance of the resolved angle and power estimates, are plotted as a function of ASNR. Each set of plots corresponds to a particular group of algorithms as follows:

A:	MUSIC -----	B:	EPM(k=5)/MUSIC
	KT ·····		EPM(k=5)/KT
	MEM -·-·-·-		EPM(k=5)/MEM
	MLM —·—·—		EPM(k=5)/MLM
C:	ROOT-MUSIC	D:	EPM(k=5)/ROOT-MUSIC
	ROOT-KT		EPM(k=5)/ROOT-KT
	ROOT-MEM		EPM(k=5)/ROOT-MEM
	ROOT-MLM		EPM(k=5)/ROOT-MLM

The results as a function of ASNR are plotted as follows:

Figure	Methods	Number of snapshots	Location of signals (beamwidths from boresight)
A4.1	A	16	0, C.1
A4.2	B		
A4.3	C		
A4.4	D		

A4.5	A	16	0, 0.2
A4.6	B		
A4.7	A	16	0, 0.3
A4.8	B		

A common feature in the results from all algorithms is a bias in the angular estimates. The magnitude (and possibly even the sense) of any such bias is likely to depend in practice on the precise nature of the calibration errors. The present results can only be considered as preliminary.

It is interesting to note that, in the cases of MUSIC and KT and the EPM equivalents, the variance of the angle estimate is slightly below the Cramér Rao bound. This is because the bound is only valid for unbiased estimates of the unperturbed problem.

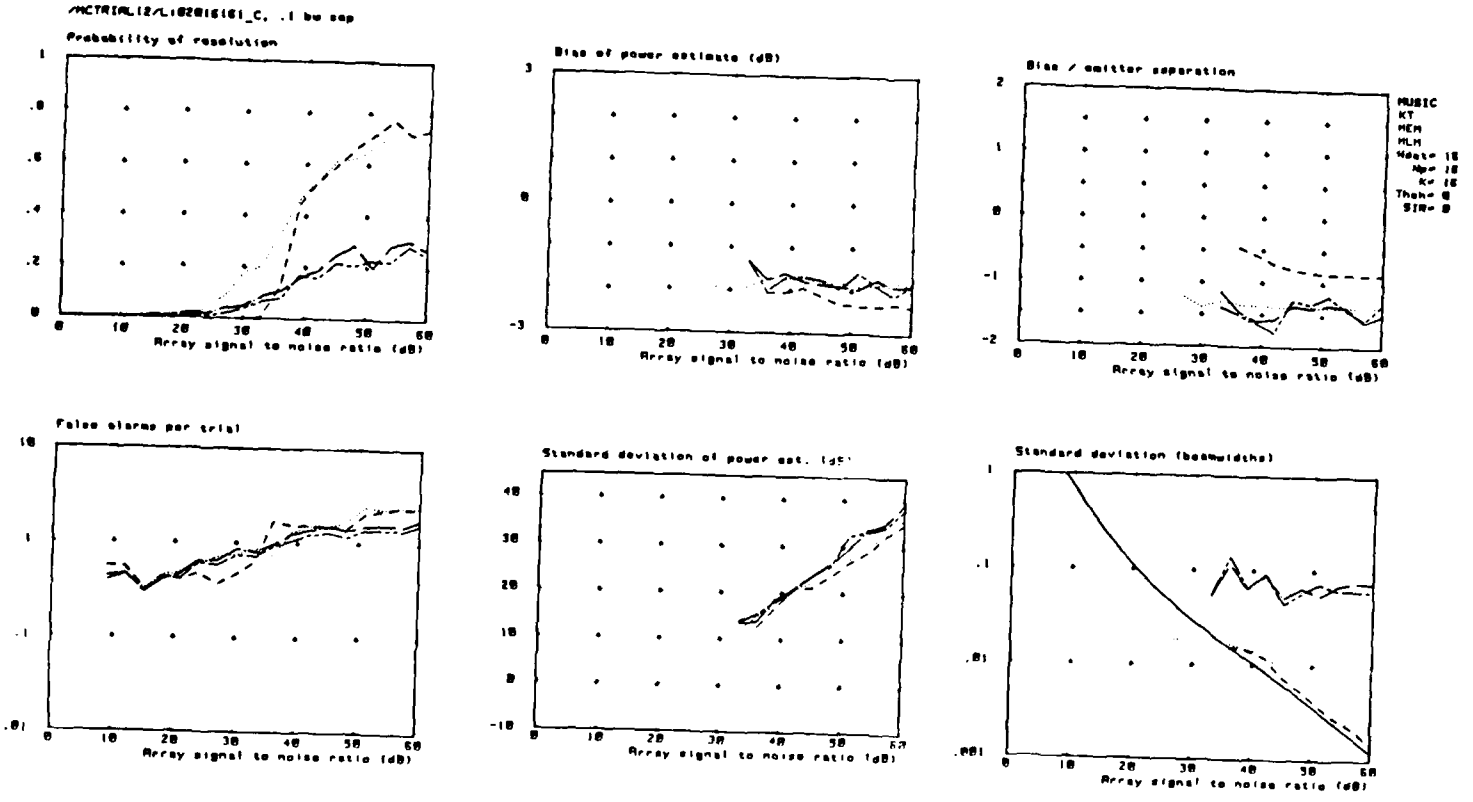
Probability of resolution
Bias of power estimate (dB)
Bias / emitter separation
MUSIC
KT
MEM
MLM
False alarms per trial
Standard deviation of power est. (dB)
Standard deviation (beamwidths)
Array signal to noise ratio (dB)

Fig. A4.1

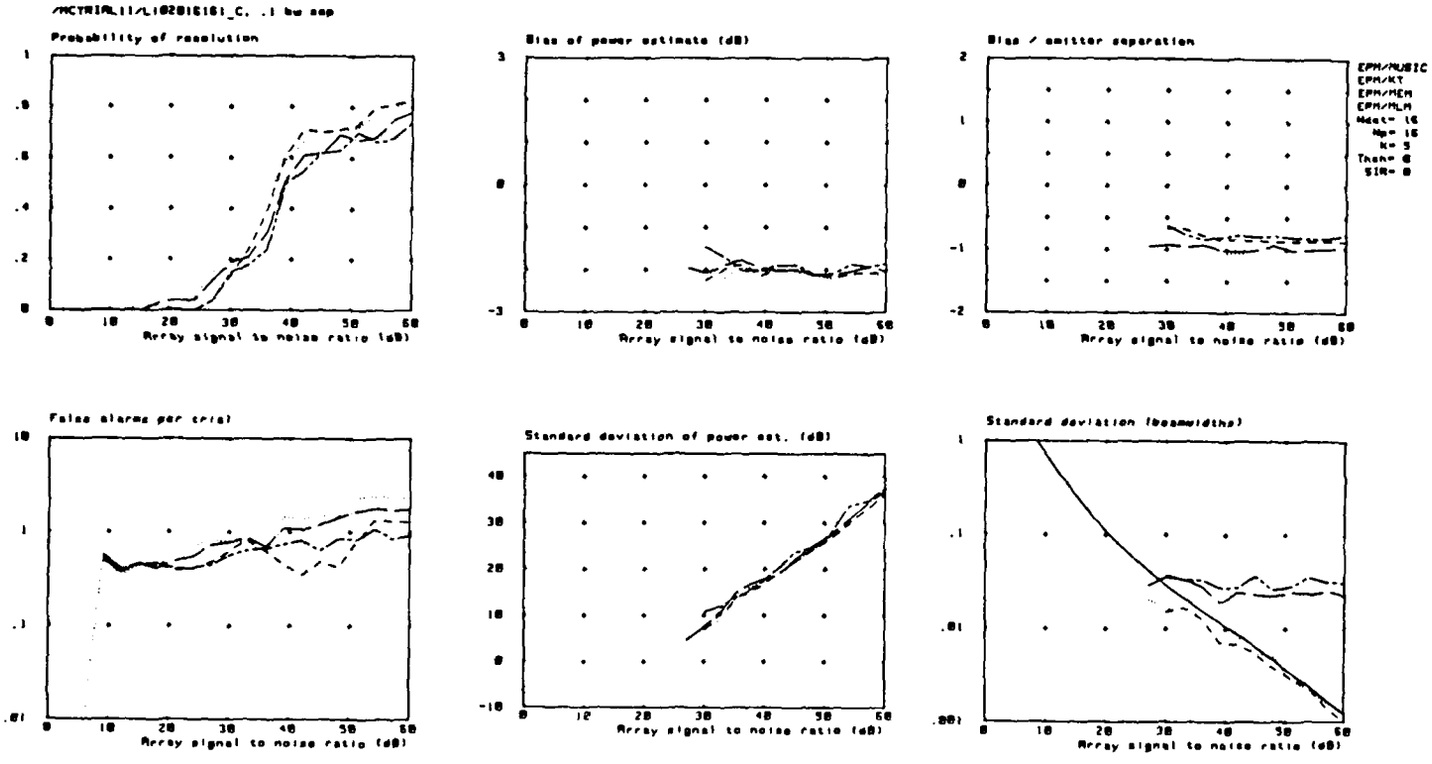
Probability of resolution
Bias of power estimate (dB)
Bias / emitter separation
EPM/MUSIC
EPM/KT
EPM/MEM
EPM/MLM
Array signal to noise ratio (dB)
False alarms per trial
Standard deviation of power est. (dB)
Standard deviation (beamwidths)

Fig. A4.2

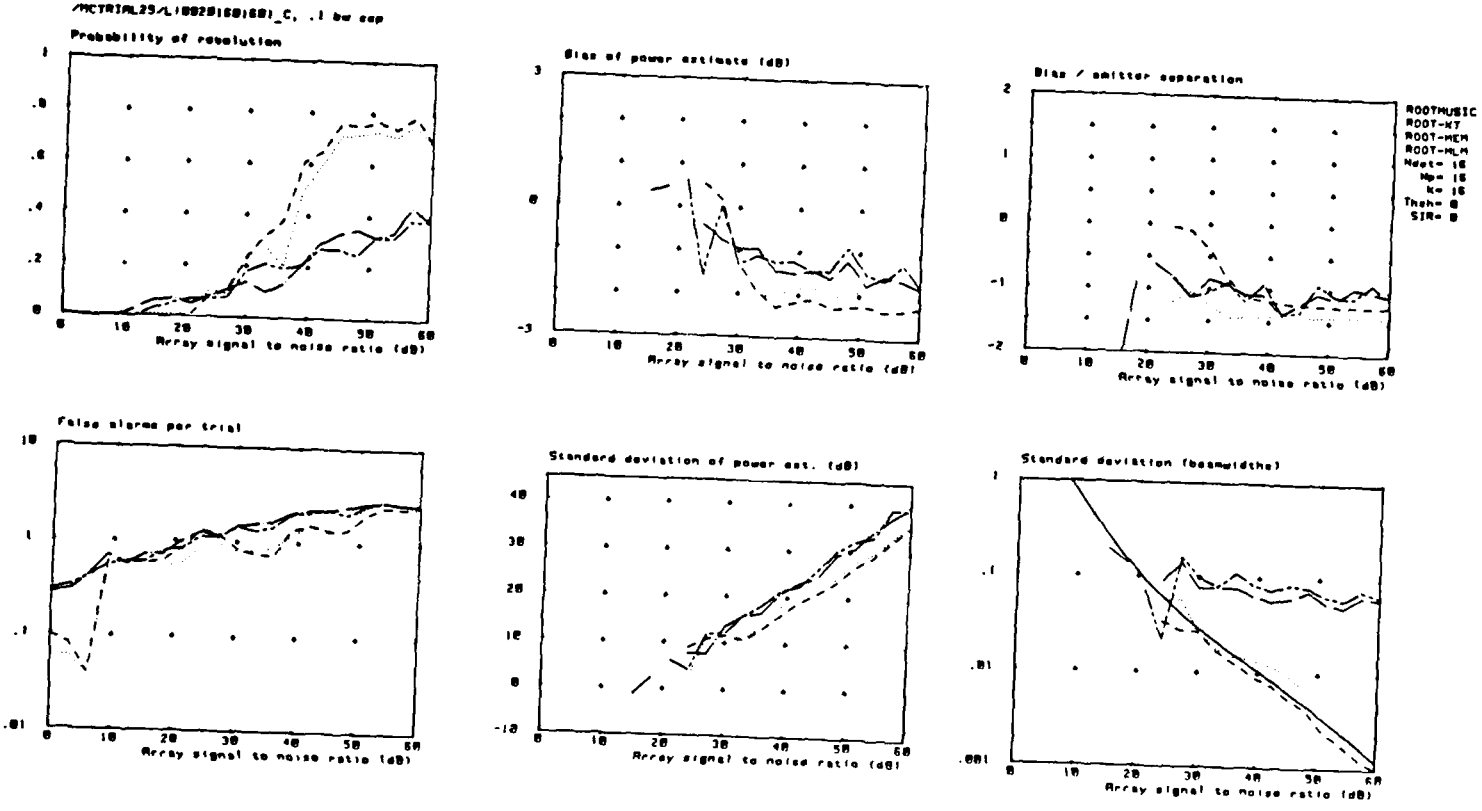
Probability of resolution
Array signal to noise ratio (dB)
Bias of power estimate (dB)
Array signal to noise ratio (dB)
Bias / emitter separation
Array signal to noise ratio (dB)
ROOTMUSIC
ROOT-NT
ROOT-MEM
ROOT-MLM
False alarms per trial
Array signal to noise ratio (dB)
Standard deviation of power est. (dB)
Array signal to noise ratio (dB)
Standard deviation (beamwidths)
Array signal to noise ratio (dB)

Fig. A4.3

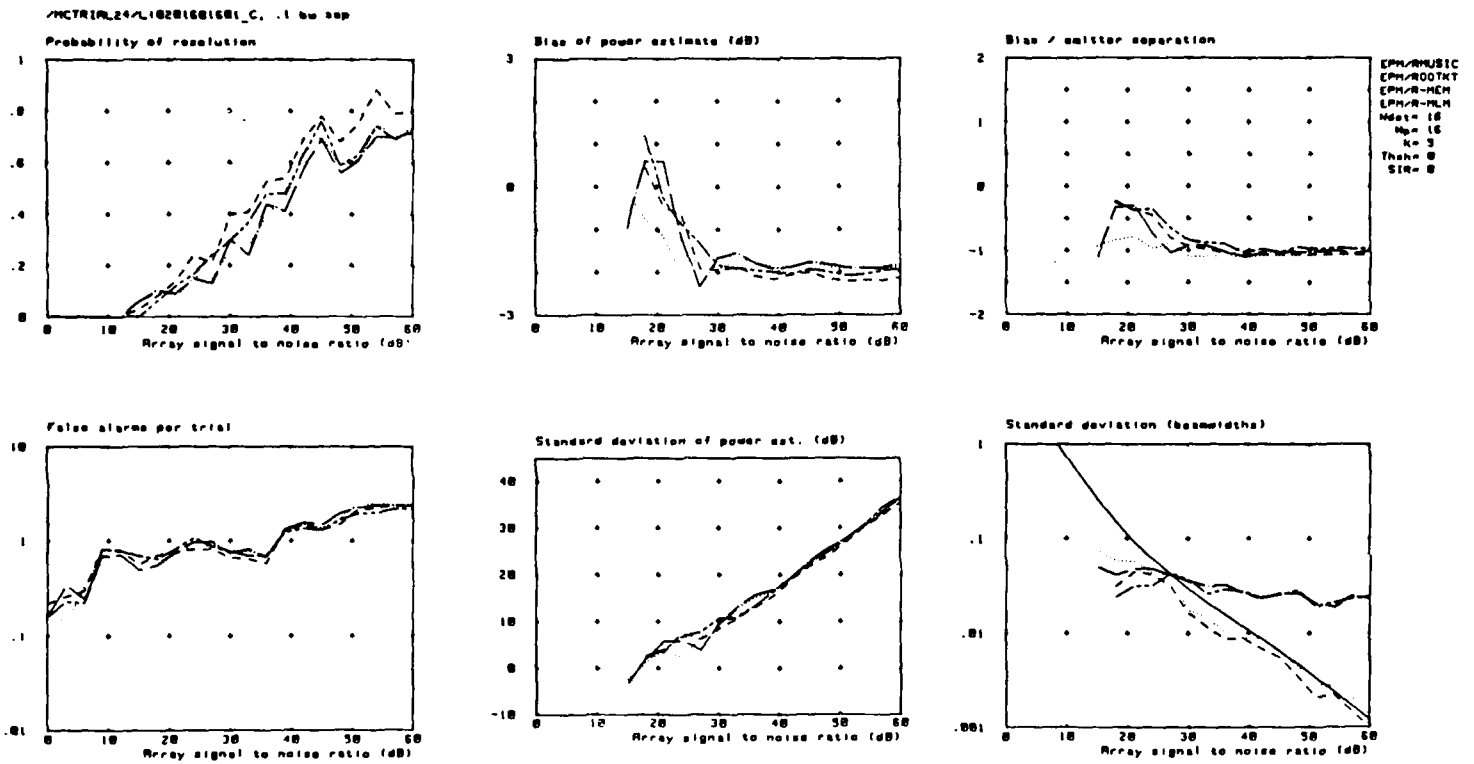
Probability of resolution
Array signal to noise ratio (dB)
Bias of power estimate (dB)
Array signal to noise ratio (dB)
Bias / emitter separation
Array signal to noise ratio (dB)
EPM/RMUSIC
EPM/ROOTKT
EPM/R-MEM
EPM/R-MLM
False alarms per trial
Array signal to noise ratio (dB)
Standard deviation of power est. (dB)
Array signal to noise ratio (dB)
Standard deviation (beamwidths)
Array signal to noise ratio (dB)

Fig. A4.4

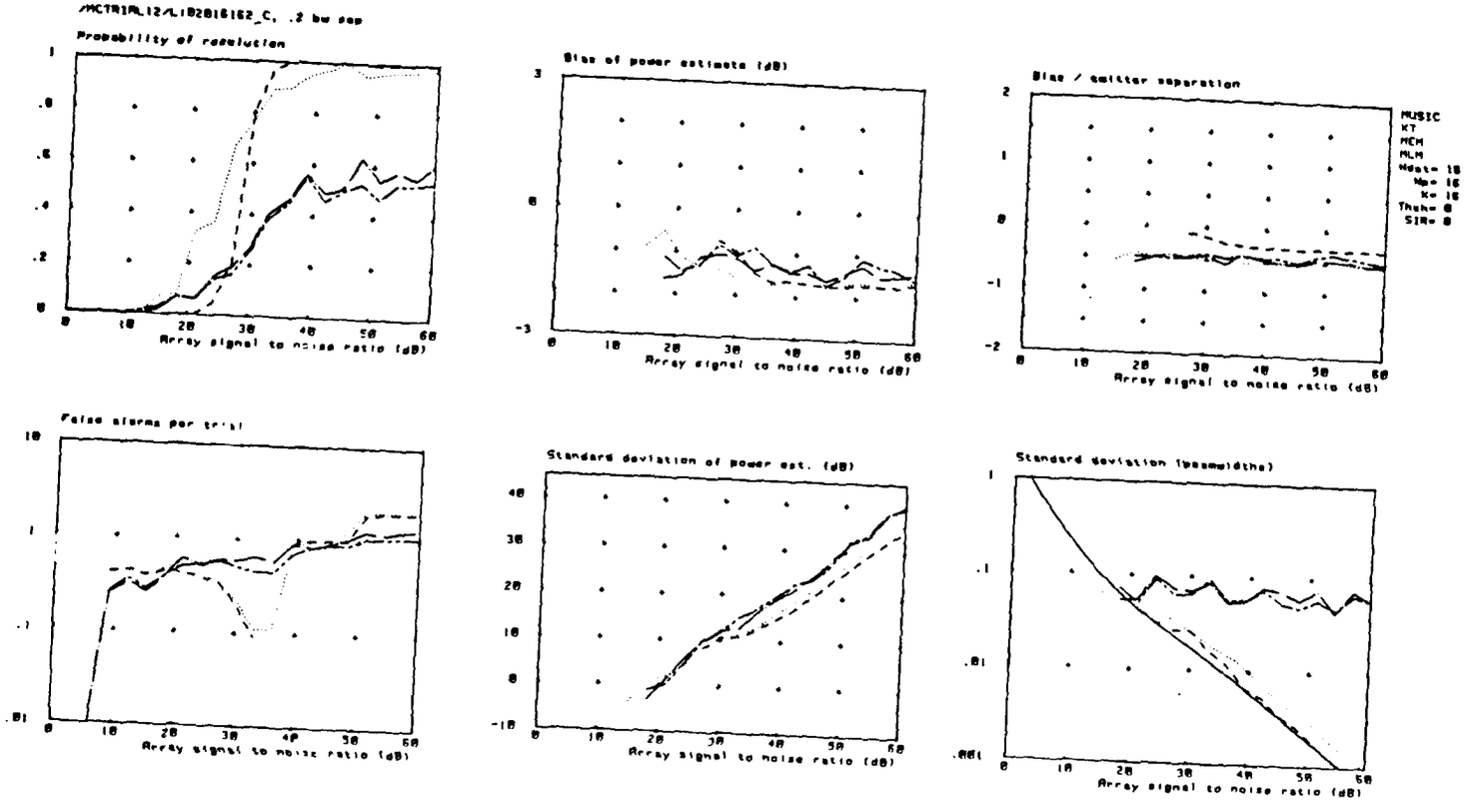
Probability of resolution
Array signal to noise ratio (dB)
Bias of power estimate (dB)
Array signal to noise ratio (dB)
Bias / splitter separation
MUSIC
KT
MEM
MLM
Array signal to noise ratio (dB)
False alarms per trial
Array signal to noise ratio (dB)
Standard deviation of Power est. (dB)
Array signal to noise ratio (dB)
Standard deviation (beamwidths)
Array signal to noise ratio (dB)

Fig. A4.5

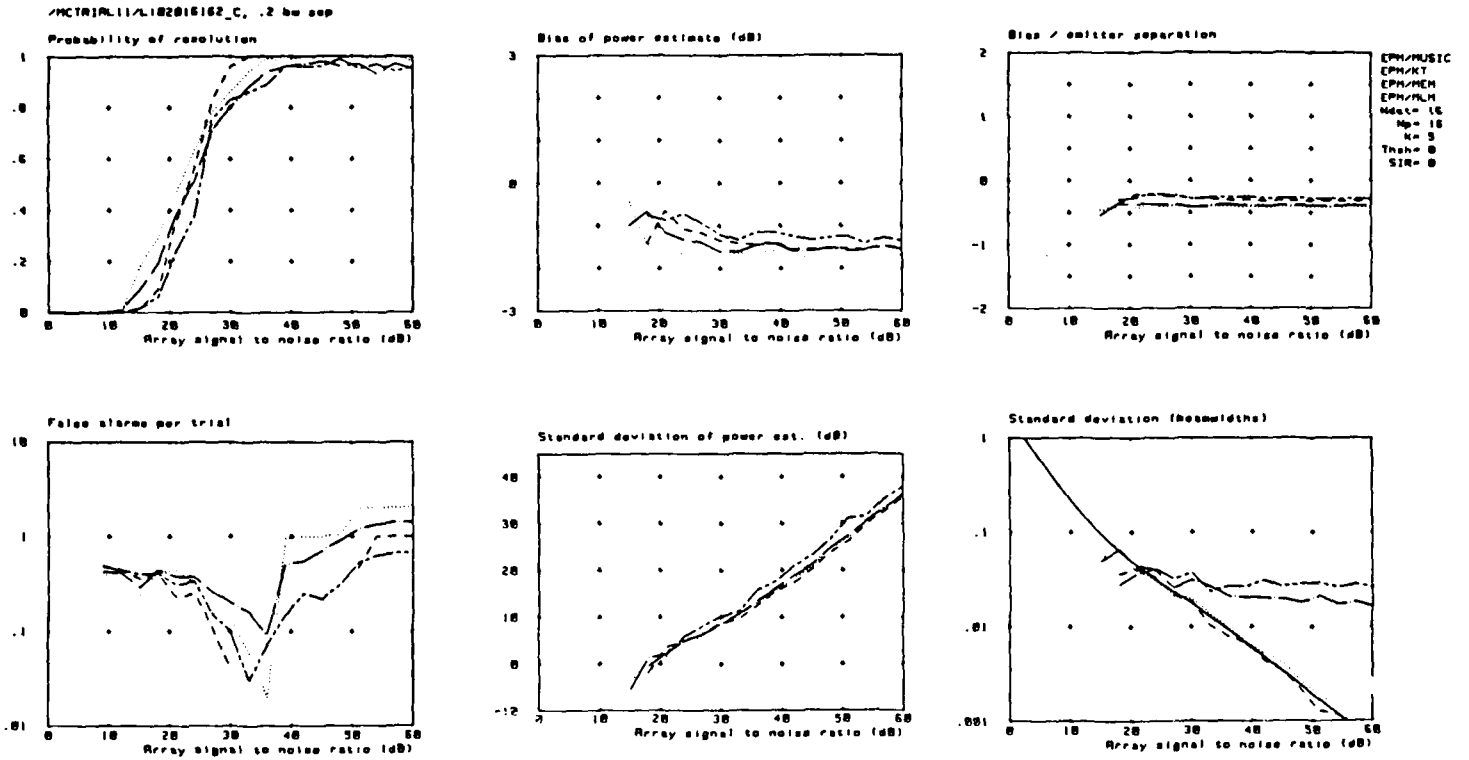
/MCTRIAL.11/L102016162_C, .2 bw sep
Probability of resolution
Bias of power estimate (dB)
Bias / emitter separation
EPH/MUSIC
EPH/RT
EPH/MEM
EPH/RLM
Array signal to noise ratio (dB)
False alarms per trial
Standard deviation of power est. (dB)
Standard deviation (Beamwidths)

Fig. A4.6

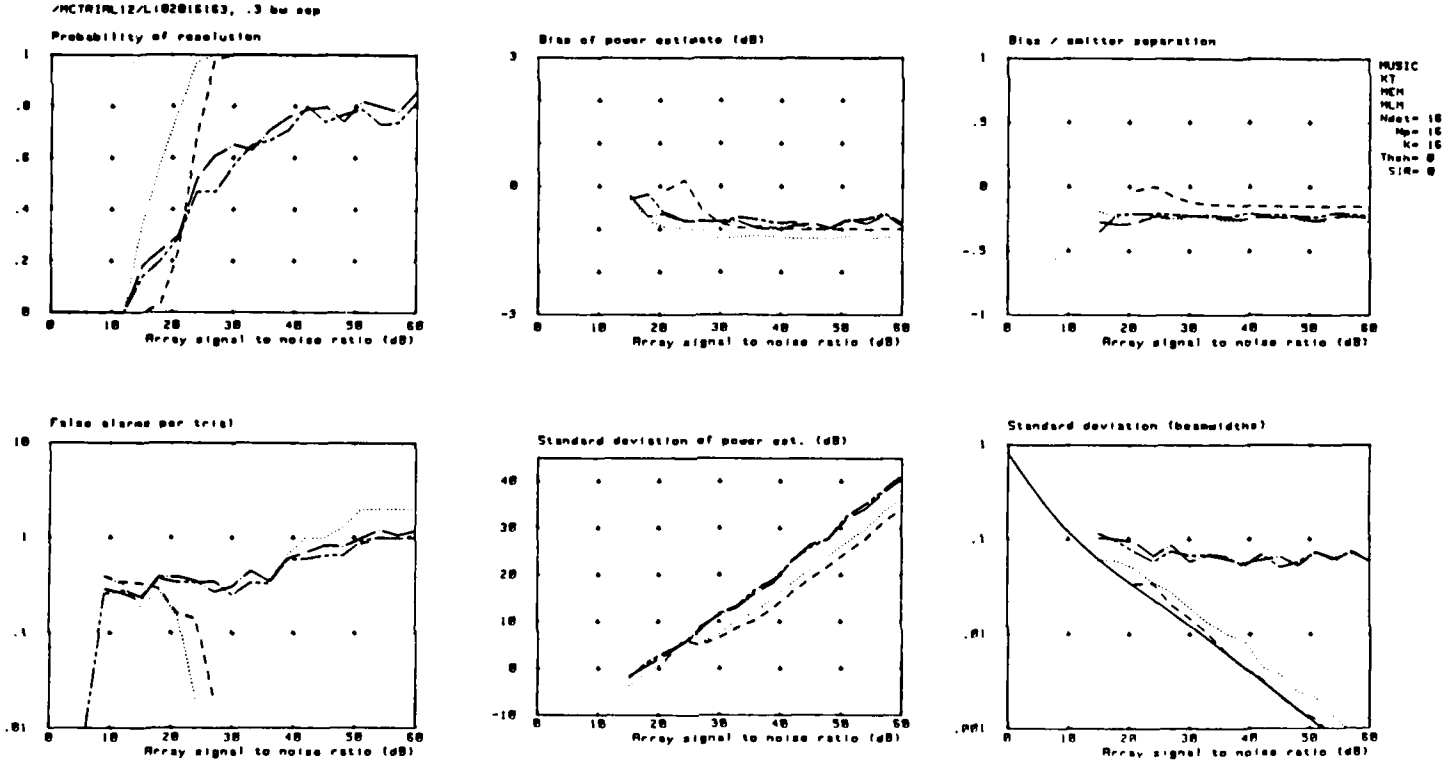
/MCTRIAL12/L102016163, .3 bw sep
Probability of resolution
Bias of power estimate (dB)
Bias / emitter separation
MUSIC
KT
MEM
MLM
False alarms per trial
Standard deviation of power est. (dB)
Standard deviation (beamwidths)
Array signal to noise ratio (dB)

Fig. A4.7

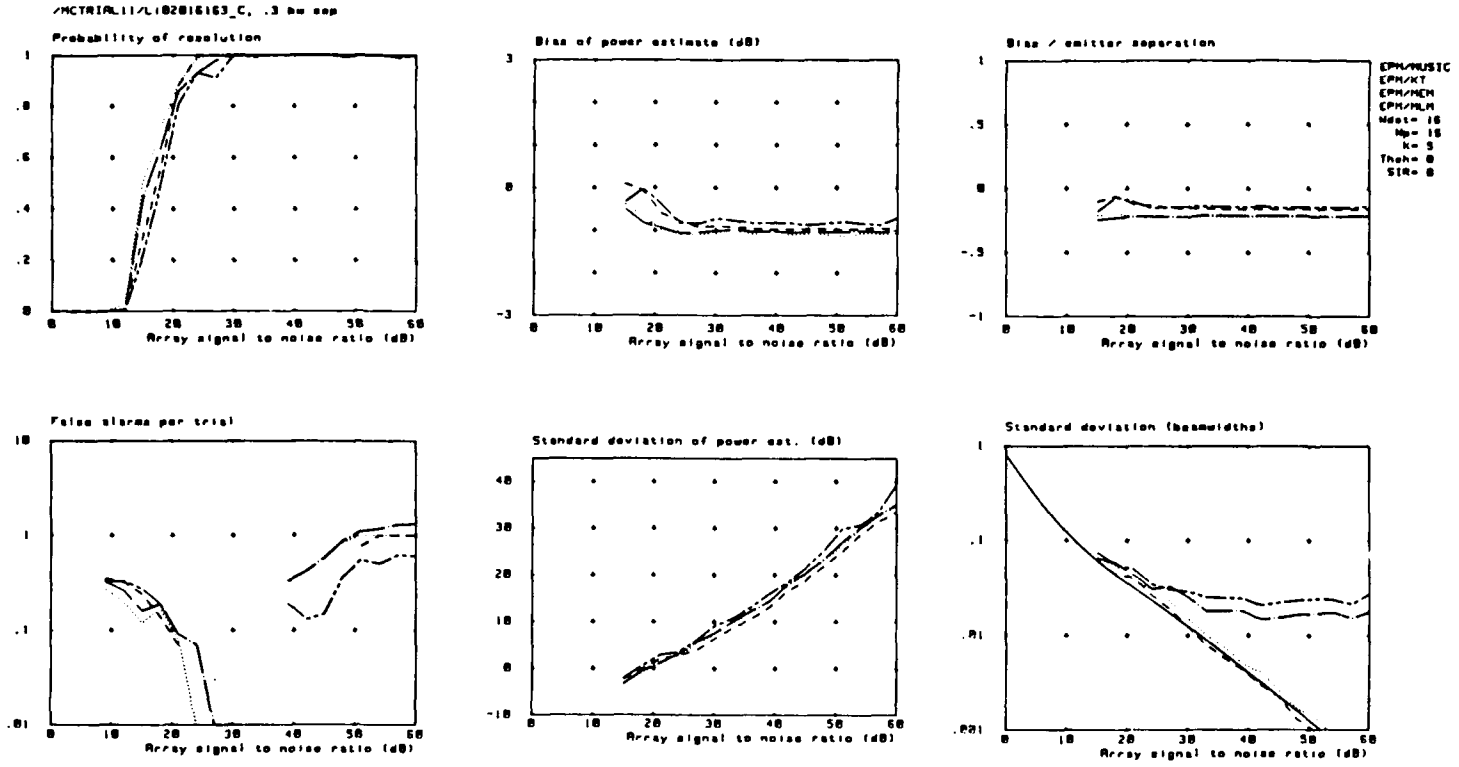
/MCTRIAL11/L18281S163_C, .3 bw sep
Probability of resolution
Array signal to noise ratio (dB)
Bias of power estimate (dB)
Array signal to noise ratio (dB)
Bias / emitter separation
Array signal to noise ratio (dB)
EPM/MUSIC
EPM/XT
EPM/MEM
EPM/MLM
Ndat= 16
Np= 16
K= 5
Thsh= 0
SIR= 0
False alarms per trial
Array signal to noise ratio (dB)
Standard deviation of power est. (dB)
Array signal to noise ratio (dB)
Standard deviation (beamwidths)
Array signal to noise ratio (dB)

Fig. A4.8

APPENDIX 5. TIME DOMAIN CROSS CORRELATIONS FOR MONTE CARLO TRIALS

In section A1.2, brief mention was made of the residual time domain correlation of the two random phase signals employed in the Monte Carlo trials. Clearly, there will be a difference in the correlations, both between the signals and the background noise, in the results based on 16 snapshots of data and those based on only 5 snapshots. To investigate the time domain decorrelation between the signals we have repeatedly generated pairs of 32, 16 and 5 snapshot sequences of random phase signals, and measured the distribution of the magnitudes of their cross correlation coefficients, ρ, where

$$|\rho|^2 = |\underline{x}^H \underline{y}|^2 / \{(\underline{x}^H \underline{x})(\underline{y}^H \underline{y})\} \quad . \tag{A5.1}$$

and $\underline{x}$ and $\underline{y}$ denote the two time series.

Fig. A5.1 is a histogram showing the distribution of ρ, as obtained over 2000 trials for the 16 snapshot case, and Fig. A5.2 is the equivalent histogram for the 5 snapshot case. We note that for 16 snapshots, the cross correlation coefficients fall below 0.6, and that the distribution peaks at approximately 0.2. For 5 snapshots, on the other hand, the graph includes the possibility of almost perfectly correlated signals, and features a very broad distribution, peaking at around 0.4. For comparison with these results, Fig. A5.3 gives a distribution for ρ obtained from pairs of 128 snapshot time series. Corresponding to the further decrease in the average cross correlation coefficient in this case, we should expect a further decrease in the array signal to noise ratio (and ratio of second to third eigenvalue) required for resolution. This is demonstrated by the results of Fig. 5.4, which show the performance of EPM(k=5)/MUSIC, /KT, /MEM, and /MLM operating on 128 snapshots of data from a 16 element linear array, as in Appendix 1.

The broad distributions of cross correlation coefficients observed here, and the known sensitivity of the particular algorithms investigated to the assumption of uncorrelated signals, calls into question the validity of the Monte Carlo results, based as they are on only 100 trials at each ASNR. This is particularly important for the results based on only 5 snapshots. This matter is investigated in Appendix 6.

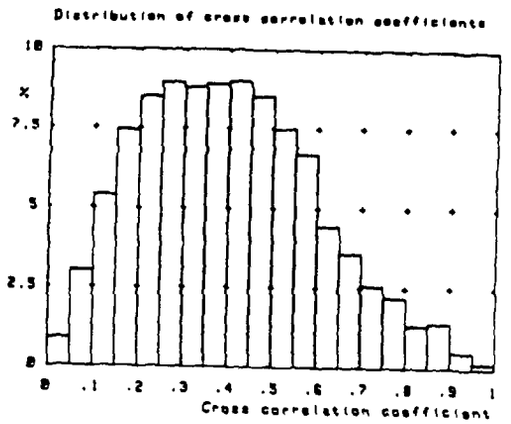

Fig. A5.1

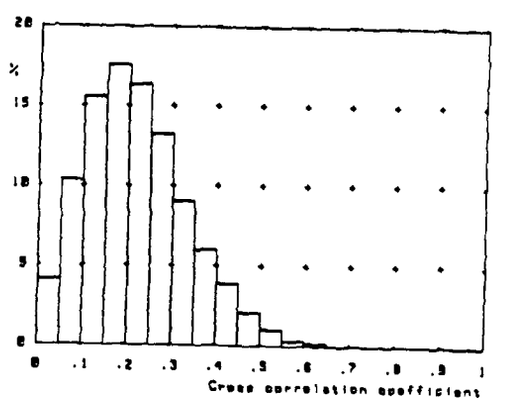

Fig. A5.2

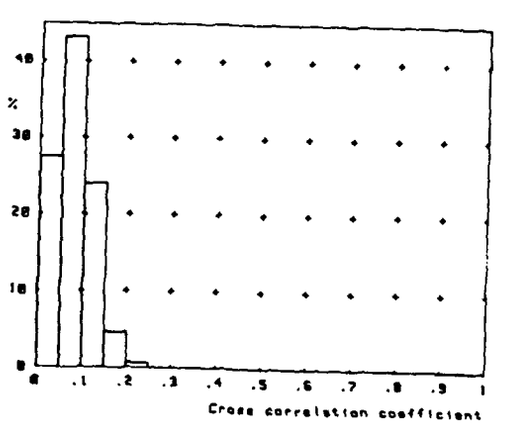

Fig. A5.3

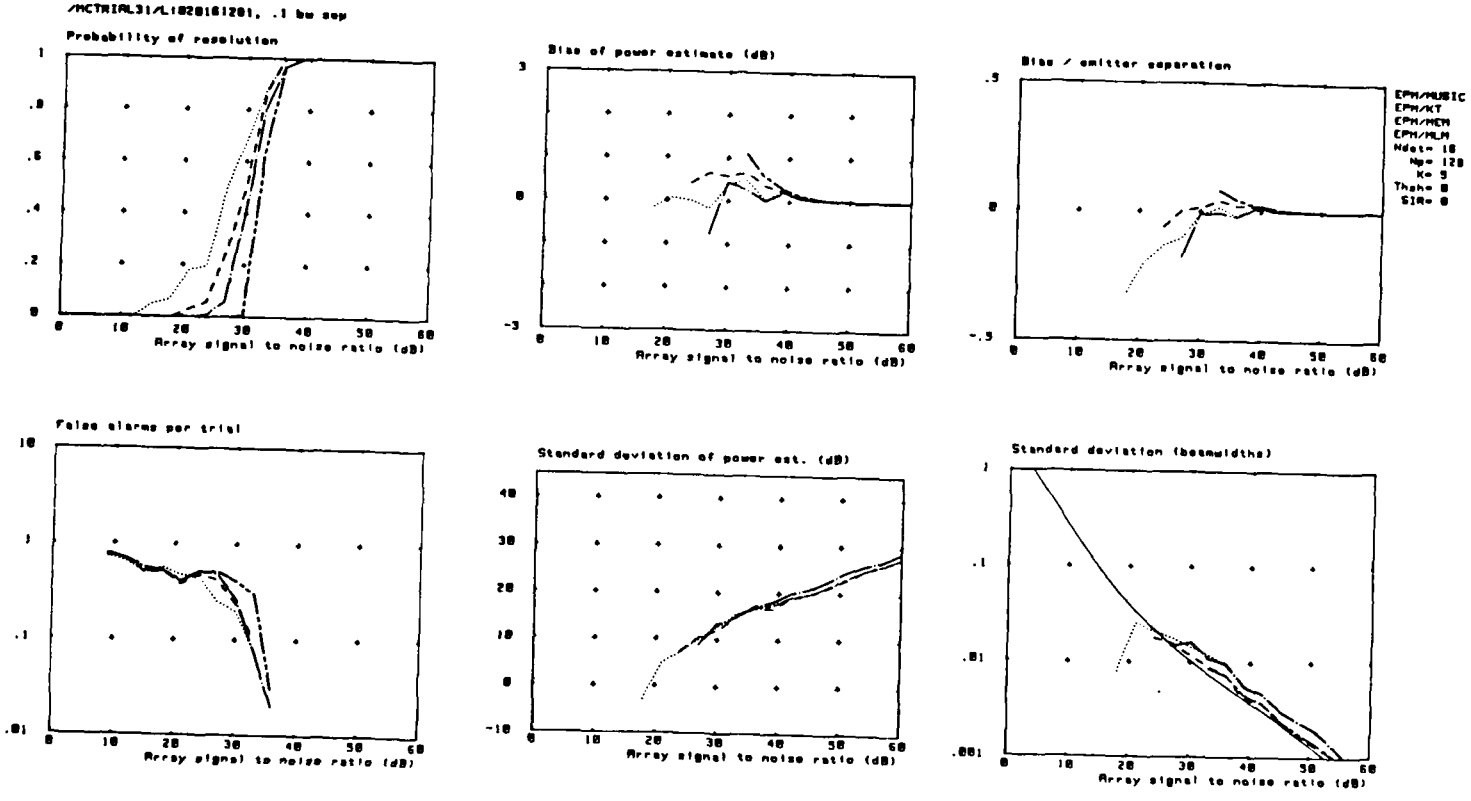
/MCTRIAL31/L18281281, .1 bw sep
Probability of resolution
Array signal to noise ratio (dB)
Bias of power estimate (dB)
Array signal to noise ratio (dB)
Bias / emitter separation
Array signal to noise ratio (dB)
EPH/MUSIC
EPH/KT
EPH/MEM
EPH/MLM
Ndata= 18
Npw 128
Xc= 5
Theta= 0
SIR= 0
False alarms per trial
Array signal to noise ratio (dB)
Standard deviation of power est. (dB)
Array signal to noise ratio (dB)
Standard deviation (beamwidths)
Array signal to noise ratio (dB)

Fig. A5.4

APPENDIX 6. CONSISTENCY OF MONTE CARLO RESULTS

The variability of the signal time domain cross correlation coefficients, and the sensitivity of the algorithms to the assumption of uncorrelatedness (discussed in section A1.2 and in Appendix 5) calls into question the consistency of our Monte Carlo analyses, based as they are on only 100 trials. In order to investigate this, a small number of experiments have been repeated, and the results compared with those of the earlier trials. The results are presented here by superimposing the two sets of curves obtained from a number of such instances. The results are typical of those observed. The algorithms used are as follows:

A:	MUSIC -----	B:	EPM(k=5)/MUSIC
	KT ·····		EPM(k=5)/KT
	MEM -·-·-·-		EPM(k=5)/MEM
	MLM —·—·—		EPM(k=5)/MLM

The results are plotted as follows:

Figure	Methods	Number of snapshots	Location of signals (beamwidths from boresight)
A6.1	A	16	0, 0.1
A6.2	B		
A6.3	A	5	0, 0.1
A6.4	B		

The probability of resolution curves have been re-plotted as a function of E(2)/E(3) (where E(2) and E(3) are the averaged second and third largest eigenvalues of the sample covariance matrix) as follows:

Figure	Methods	Number of snapshots	Location of signals (beamwidths from boresight)
A6.5	A	16	0, 0.1
A6.6	B		
A6.7	A	5	0, 0.1
A6.8	B		

Comparing the twin sets of results in each figure, we conclude that, for the purposes of this report, the Monte Carlo data is more than sufficiently consistent, even for the 5 snapshot case. In particular, curves corresponding to different algorithms are seen to retain their shapes and relative positions along the ASNR axis, and false alarm rates, biases and variances remain consistent. In addition, the probability of resolution reaches 100% at approximately the same values ASNR (and eigenvalue ratio) in each of the two sets of trials.

As a further check on the validity of our results, an additional set of experiments has been carried out, in which perfect time domain decorrelation of the two signals has been achieved over 5 snapshots by using regularly sampled sinusoidal waveforms. The algorithms used were as in group B. Fig. A6.9 shows the corresponding plots of the performance measures for this situation (two equal powered signals located at 0 and 0.1 beamwidths from boresight). In order to directly compare these results with those previously obtained

from the random phase signals, Monte Carlo results from both experiments have been plotted together in Fig. 6.10. Figs 6.11 and 6.12 are the corresponding plots of probability of resolution as a function of second to third eigenvalue ratio.

It can be clearly seen from Figs. 6.9 to 6.12 that the results for uncorrelated signals are remarkably similar to those for experiments involving a wide distribution of cross correlation coefficients (Fig.A5.1). Only false alarm rate differs significantly, being lower for the fully decorrelated signals. Such similarity indicates that the variation of performance measures with respect to the number of snapshots is largely a result of changing the cross correlation between the signals and the noise background, an element which we have not been able to control. Thus, for a small number of snapshots, the limiting factor in performance when using SVD based algorithms, for a given angular separation, is cross correlation between the noise and the signals.

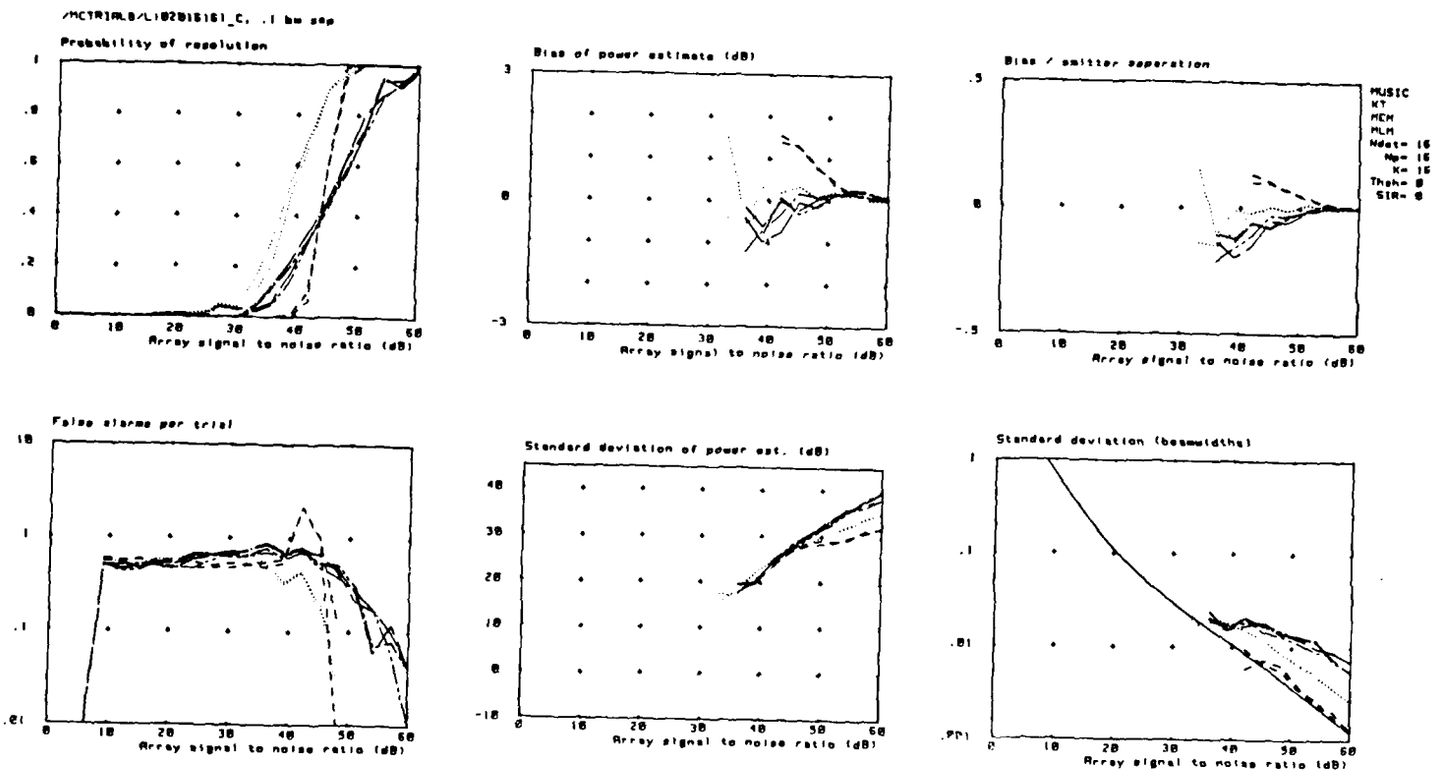
Probability of resolution
Array signal to noise ratio (dB)
Bias of power estimate (dB)
Array signal to noise ratio (dB)
Bias / emitter separation
Array signal to noise ratio (dB)
MUSIC
KT
MEM
MLM
False alarms per trial
Array signal to noise ratio (dB)
Standard deviation of power est. (dB)
Array signal to noise ratio (dB)
Standard deviation (beamwidths)
Array signal to noise ratio (dB)

Fig. A6.1

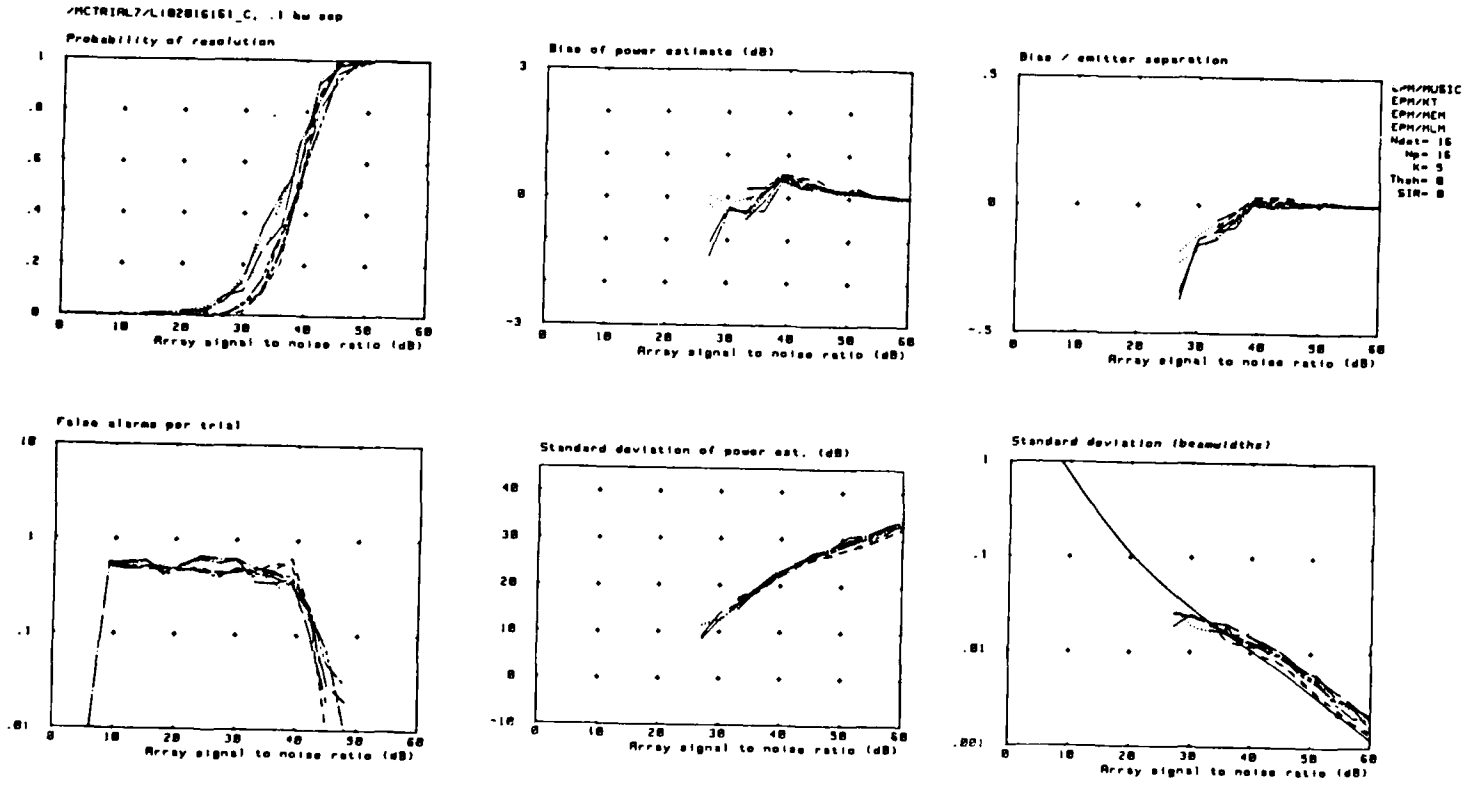
/MCTRIAL7/L102816161_C, .1 bw sep
Probability of resolution
Array signal to noise ratio (dB)
Bias of power estimate (dB)
Array signal to noise ratio (dB)
Bias / emitter separation
EPM/MUSIC
EPM/RT
EPM/MEM
EPM/MLM
Array signal to noise ratio (dB)
False alarms per trial
Array signal to noise ratio (dB)
Standard deviation of power est. (dB)
Array signal to noise ratio (dB)
Standard deviation (beamwidths)
Array signal to noise ratio (dB)

Fig. A6.2

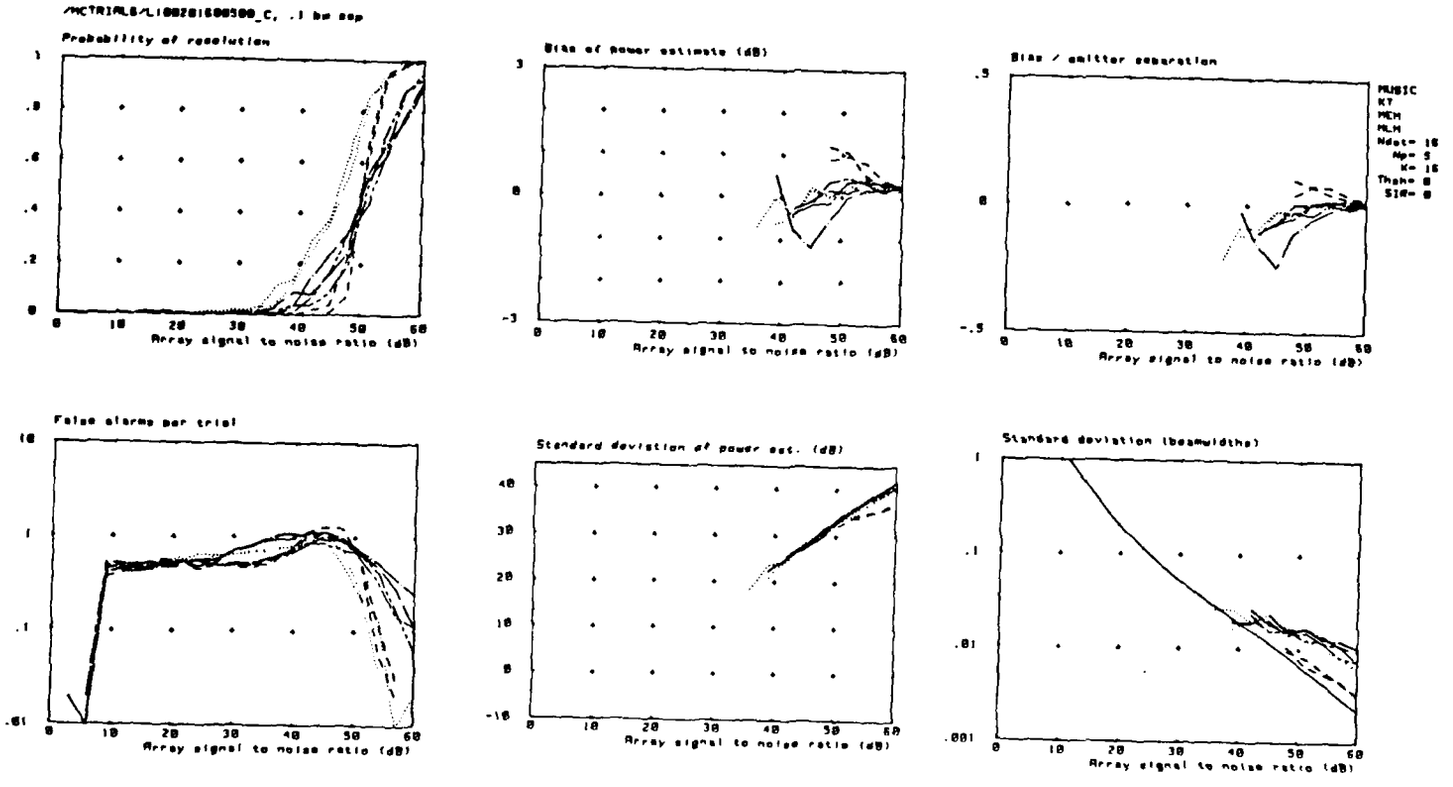
Probability of resolution
Array signal to noise ratio (dB)
Bias of power estimate (dB)
Array signal to noise ratio (dB)
Bias / emitter separation
Array signal to noise ratio (dB)
MUSIC
KT
MEM
MLM
False alarms per trial
Array signal to noise ratio (dB)
Standard deviation of power est. (dB)
Array signal to noise ratio (dB)
Standard deviation (beamwidths)
Array signal to noise ratio (dB)

Fig. A6.3

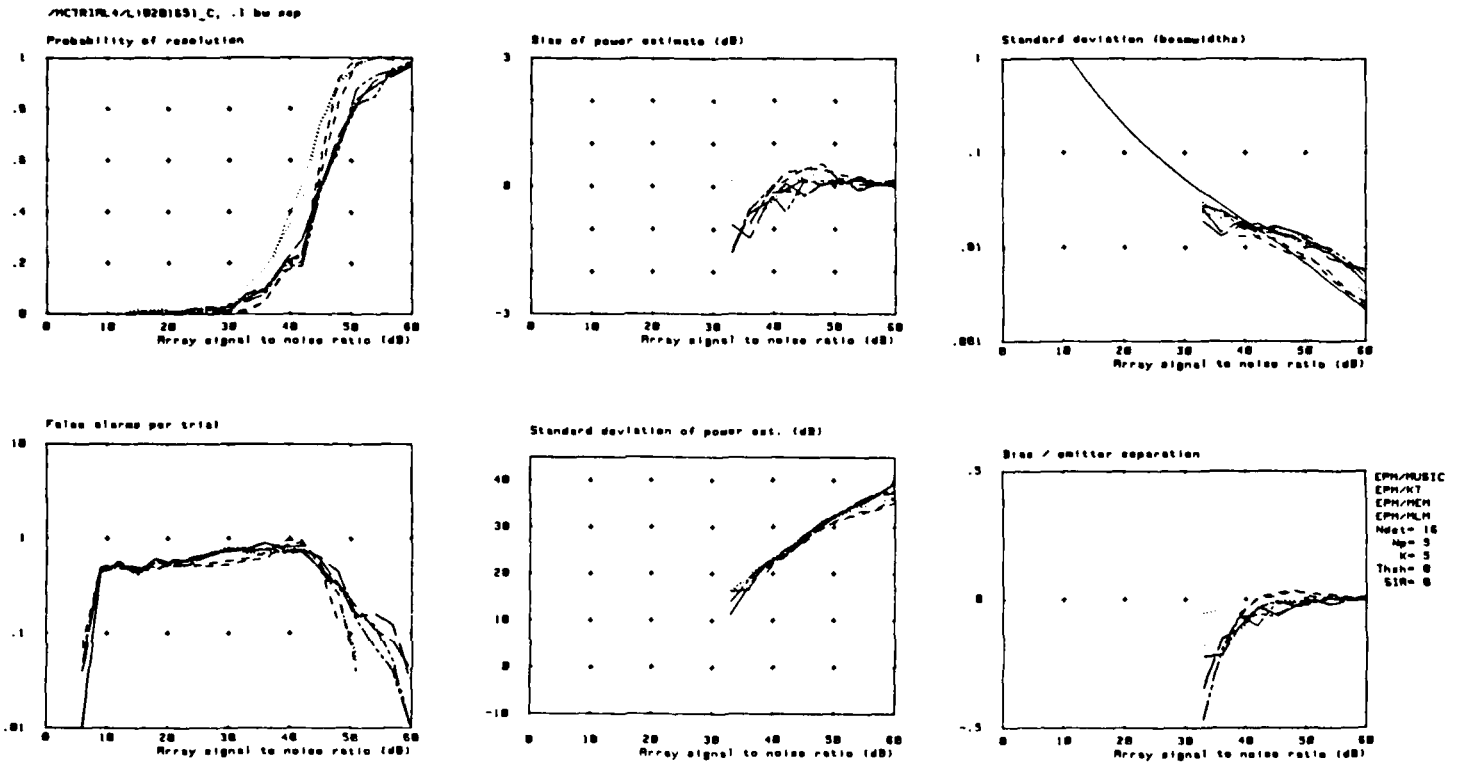
Probability of resolution
Bias of power estimate (dB)
Standard deviation (beamwidths)
False alarms per trial
Standard deviation of power est. (dB)
Bias / emitter separation
Array signal to noise ratio (dB)
EPM/MUSIC
EPM/NT
EPM/MEM
EPM/MLM
Ndat= 16
Np= 5
K= 5
Thsh= 0
SIR= 0

Fig. A6.4

Fig. A6.5

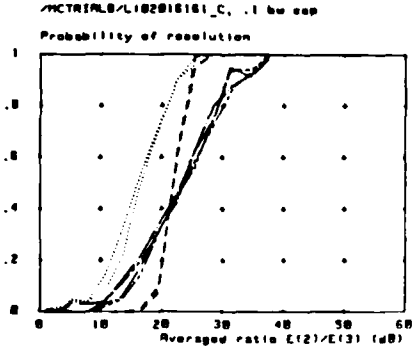

Fig. A6.6

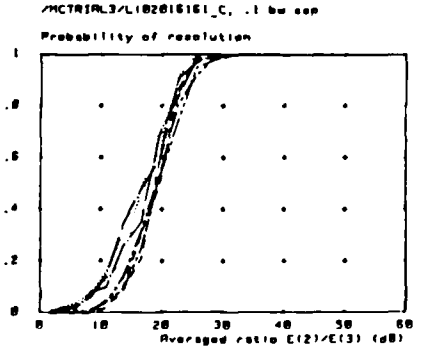

Fig. A6.7

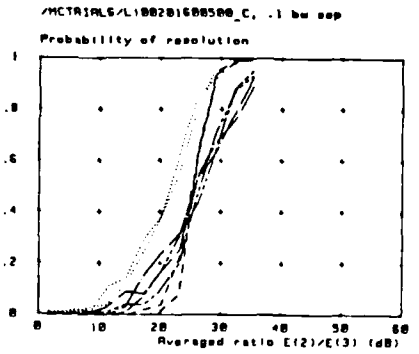

Fig. A6.8

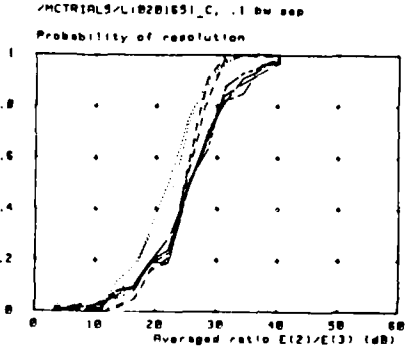

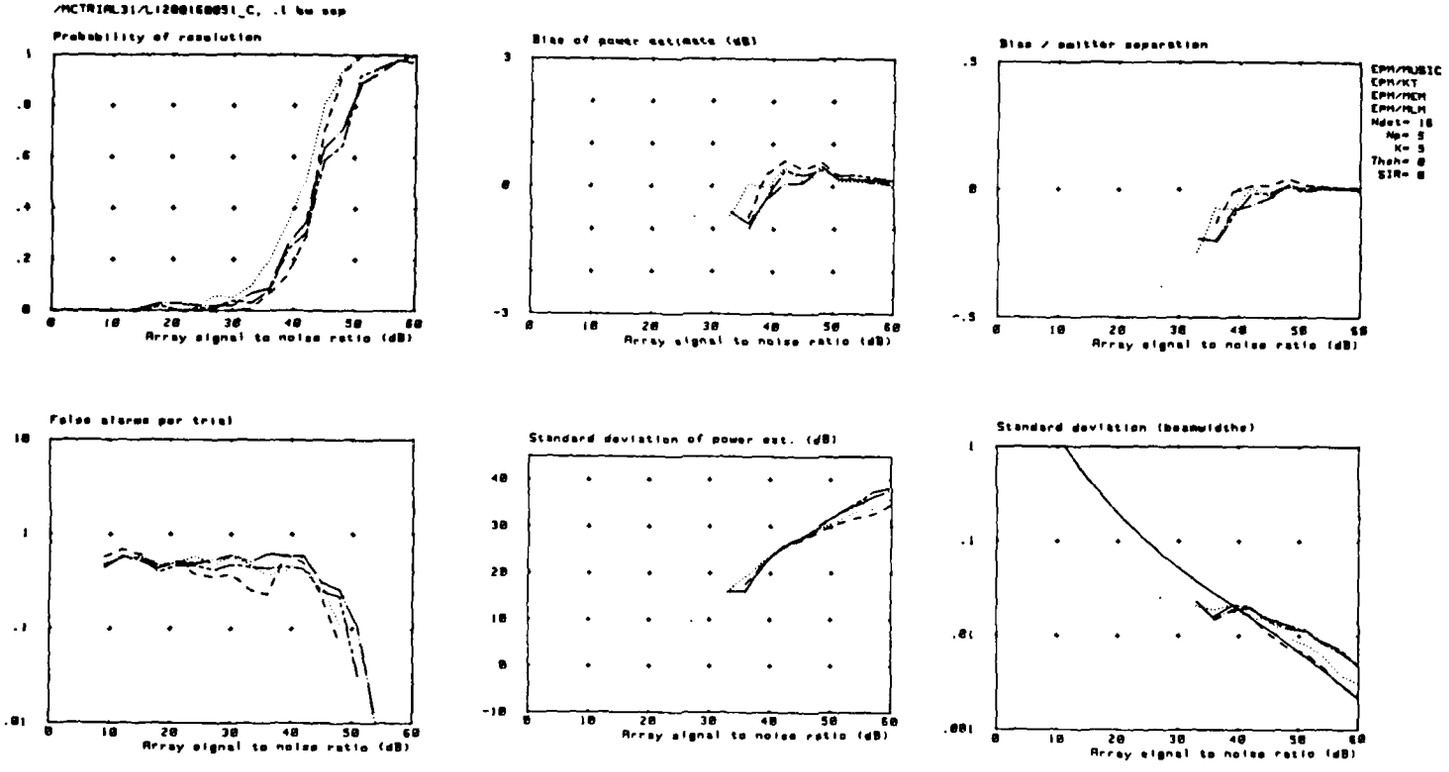
Probability of resolution
Array signal to noise ratio (dB)
Bias of power estimate (dB)
Array signal to noise ratio (dB)
Bias / emitter separation
EPM/MUSIC
EPM/KT
EPM/MEM
EPM/MLM
Ndet= 10
Np= 5
K= 5
Thsh= 0
SIR= 0
Array signal to noise ratio (dB)
False alarms per trial
Array signal to noise ratio (dB)
Standard deviation of power est. (dB)
Array signal to noise ratio (dB)
Standard deviation (beamwidths)
Array signal to noise ratio (dB)

Fig. A6.9

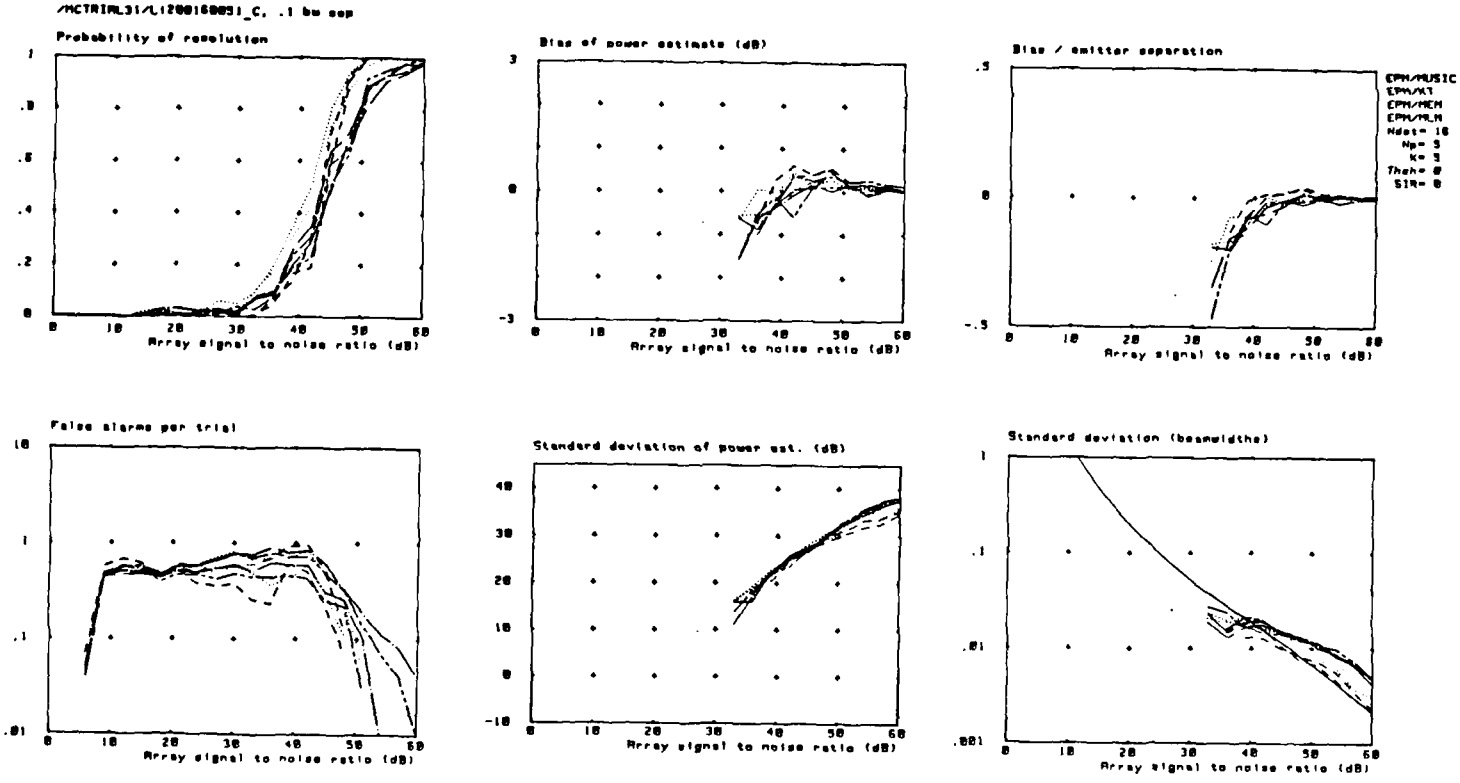
Probability of resolution
Array signal to noise ratio (dB)
Bias of power estimate (dB)
Array signal to noise ratio (dB)
Bias / emitter separation
EPM/MUSIC
EPM/MEM
EPM/MLM
Array signal to noise ratio (dB)
False alarms per trial
Array signal to noise ratio (dB)
Standard deviation of power est. (dB)
Array signal to noise ratio (dB)
Standard deviation (beamwidths)
Array signal to noise ratio (dB)

Fig. A6.10

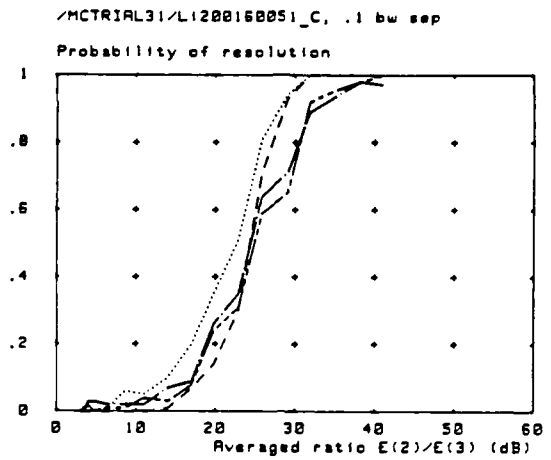

Fig. A6.11

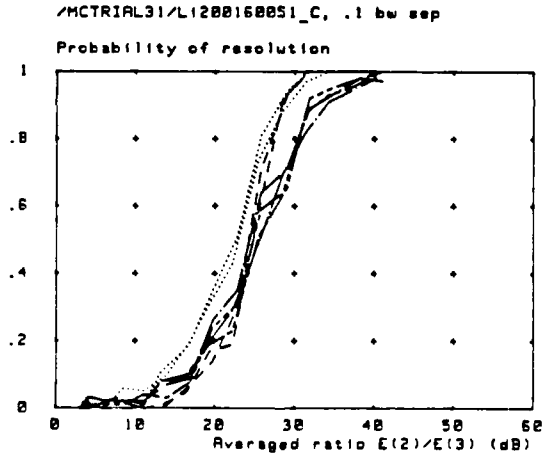

Fig. A6.12

APPENDIX 7. RELATIONSHIP BETWEEN ASNR AND E(2)/E(3)

In section A1.2, re-plotting of the Monte Carlo results as a function of eigenvalue ratio was justified on the basis that resolution of two targets would intuitively seem to depend on the ratio of second to third eigenvalue (E(2)/E(3)) of the sample covariance estimate. However, our results suggested that, even for signals which were uncorrelated in the time domain, spatial domain correlation (the cross correlation of the signal steering vectors) was still important, and that simplification of the presentation might not be possible. Nevertheless, if we examine the relationship between the ASNR and the ratio E(2)/E(3), as a function of emitter separation, some progress can be made.

Figs. A7.1 to A7.4 show curves relating the average measured eigenvalue ratio, E(2)/E(3), to the ASNR for emitter separations ranging from 0.1 to 0.6 beamwidths. Δ corresponds to the separation of the parallel portions of the curves along the E(2)/E(3) axis. For un-processed data (A), and EPM(k=5) pre-processed data (B), the results are arranged as follows:

Figure	Methods	Number of snapshots	Location of signals (beamwidths from boresight)
A7.1 A7.2	A B	16	0, 0.1 to 0.6
A7.3 A7.4	A B	5	0, 0.1 to 0.6

We see that the curves in each set converge to a constant eigenvalue ratio at low ASNR as the second eigenvalue is limited by noise. Note that the ratio is greater than 0dB as a result of non-whiteness in the noise arising from the limited time and space apertures. At higher ASNR, the curves form a parallel set. The shift, Δ, along the eigenvalue ratio axis, depends on angular separation. Taking the curves of Fig. 7.2, and referencing Δ to zero for a separation of 0.1 beamwidths, Fig. 7.5 shows a set of EPM(k=5)/MUSIC probability of resolution curves (corresponding to the separations 0.1, 0.2, 0.3, 0.4, 0.5, and 0.6 beamwidths) plotted as a function of E(2)/E(3) + Δ. Fig. 7.6 shows a similar set of curves for EPM(k=5)/KT. In both cases the signal to noise threshold for detection has been deactivated. It seems clear from these results that, as E(2)/E(3) + Δ increases, the probability of resolution curves converge to approximately the same line. The same is true of curves measured for all the algorithms investigated in this report.

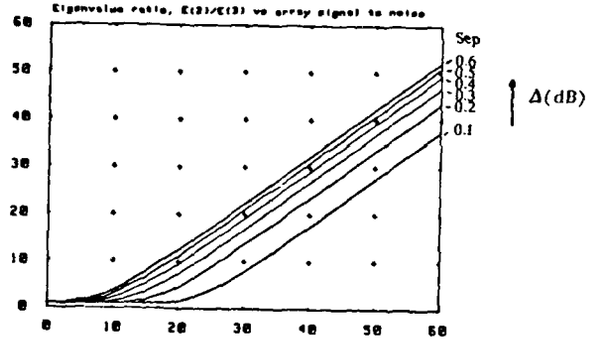

Fig. A7.1

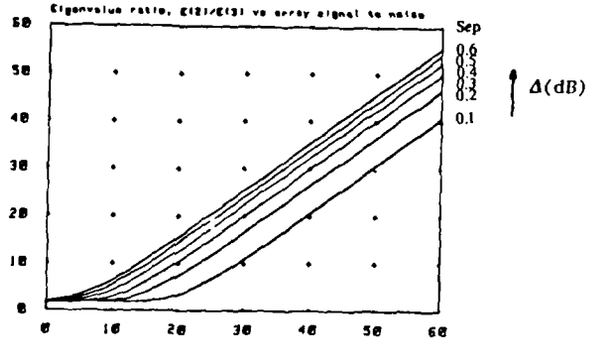

Fig. A7.2

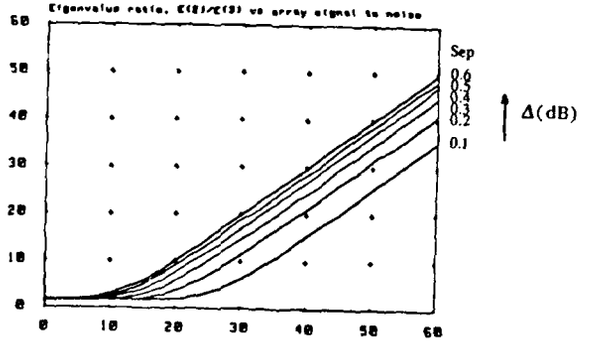

Fig. A7.3

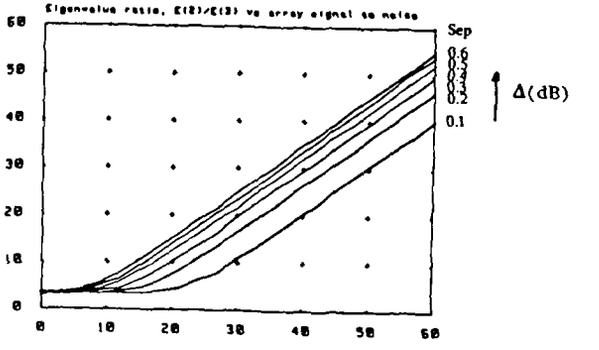

Fig. A7.4

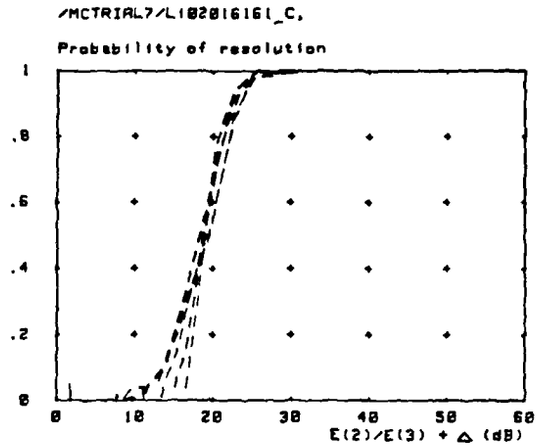

Fig. A7.5

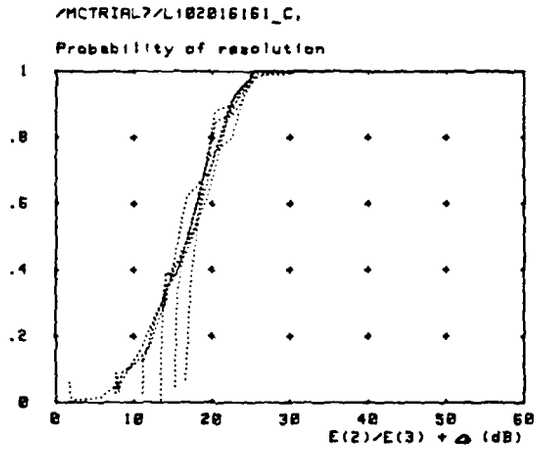

Fig. A7.6

DOCUMENT CONTROL SHEET

Overall security classification of sheet .....UNCLASSIFIED.....

(As far as possible this sheet should contain only unclassified information. If it is necessary to enter classified information, the box concerned must be marked to indicate the classification eg (R) (C) or (S))

1. DRIC Reference (if known)	2. Originator's Reference	3. Agency Reference	4. Report Security Classification
	MEMO 4083		U/C

5. Originator's Code (if known)	6. Originator (Corporate Author) Name and Location
7784000	ROYAL SIGNALS & RADAR ESTABLISHMENT ST ANDREWS ROAD, MALVERN, WORCS WR14 3PS

5a. Sponsoring Agency's Code (if known)	6a. Sponsoring Agency (Contract Authority) Name and Location

7. Title A MONTE CARLO PERFORMANCE ANALYSIS OF ACCELERATED SVD-BASED HIGH DISCRIMINATION ALGORITHMS

7a. Title in Foreign Language (in the case of translations)

7b. Presented at (for conference papers) Title, place and date of conference

8. Author 1 Surname, initials	9(a) Author 2	9(b) Authors 3,4...	10. Date	pp. ref.
MATHER J L			1988.07	136

11. Contract Number	12. Period	13. Project	14. Other Reference

15. Distribution statement

UNLIMITED

Descriptors (or keywords)

continue on separate piece of paper

Abstract High discrimination algorithms are increasingly being considered for the task of processing data from arrays of sensors and in the form of time series. Many such algorithms rely on singular value decomposition of a data matrix or eigen analysis of the corresponding covariance estimate, thereby imposing a heavy computational requirement. However, if data is oversampled, or if the solution vector may be constrained, in terms of its angular extent or frequency range for example, it is often possible to pre-process the data matrix in such a way to reduce its size. This may be carried out by means of a fixed matrix pre-multiplication, and can lead to a substantial acceleration of the subsequent analysis. The method is described, and its use exemplified in combination with a number of well-known high discrimination algorithms. A number of results from a Monte Carlo analysis are given which show that the new technique can lead to significantly improved parameter estimates being obtained from the high discrimination algorithms.